# CENTER FOR INFRASTRUCTURE ENGINEERING STUDIES

# DESTRUCTIVE AND NON-DESTRUCTIVE TESTING OF BRIDGE J857 PHELPS COUNTY, MISSOURI

VOLUME III
STRENGTHENING AND TESTING TO FAILURE OF BRIDGE PIERS

by

**Tarek Alkhrdaji**
**Antonio Nanni**
**Genda Chen**
University of Missouri-Rolla

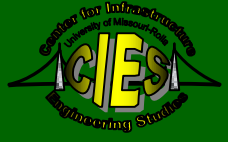

**CIES 99-08C**

## DISCLAIMER

The mission of CIES is to provide leadership in research and education for solving society's problems affecting the nation's infrastructure systems. CIES is the primary conduit for communication among those on the UMR campus interested in infrastructure studies and provides coordination for collaborative efforts. CIES activities include interdisciplinary research and development with projects tailored to address needs of federal agencies, state agencies, and private industry as well as technology transfer and continuing/distance education to the engineering community and industry.

Center for Infrastructure Engineering Studies (CIES)
University of Missouri-Rolla
223 Engineering Research Lab
1870 Miner Circle
Rolla, MO 65409-0710
Tel: (573) 341-6223; fax -6215
E-mail: cies@umr.edu
http://www.umr.edu/~cies

# DESTRUCTIVE AND NON-DESTRUCTIVE TESTING OF BRIDGE J857
# PHELPS COUNTY, MISSOURI
## VOLUME III
### STRENGTHENING AND TESTING TO FAILURE OF BRIDGE PIERS

## EXECUTIVE SUMMARY

Many of the existing reinforced concrete (RC) bridge piers constructed in the first half of this century were designed as gravity piers with minimal flexural reinforcement and no consideration to seismically induced lateral forces. When considered in earlier designs, the seismic lateral forces were typically low. The potential risk of failure of columns on these piers under a moderate earthquake is becoming a growing concern for the transportation management agencies. In addition, flexural strength deficiency in RC columns may arise from the loss of reinforcement due to corrosion, premature termination of the main reinforcement, or inadequate splicing. One method for retrofitting columns with flexural strength deficiencies consists of the addition of a RC or steel jackets. However, these systems may not be very practical due to undesirable section enlargement or construction constraints. Fiber Reinforced Polymers (FRP) have suitable mechanical properties for structural applications such as corrosion resistance and high strength-to-weight ratio. Although a properly designed FRP jacket can improve column compression strength, shear strength, and ductility, it may not sufficiently improve flexural capacity. Near-surface mounted (NSM) FRP rods is another technique that could be used to improve the flexural capacity of RC columns. This strengthening technique consists of FRP rods embedded in grooves made on the surface of the concrete and bonded in place with epoxy. To investigate the applicability and effectiveness of this technique, a research program was carried out in which bridge columns originally designed to carry gravity loads were upgraded and then tested to failure. Flexural strengthening was achieved by mounting carbon FRP (CFRP) rods on two opposite sides of the columns. In addition, the strengthened columns were wrapped with carbon and glass composites to satisfy seismic detailing requirements. The columns were tested to failure by applying lateral load cycles. The behavior of strengthened columns and their failure modes are discussed and conclusions are drawn. Test results indicate that the proposed strengthening is feasible and effective for improving the flexural capacity of RC columns. The capacity of the strengthened sections could be predicted using classical methods of analysis. Full investigation of the upgraded structure should be made to ensure that the deficiency is not shifted to other structural components.

The final report consists of three volumes. Volume I depicts the strengthening and testing to failure of the three bridge decks. Volume II focuses on the laboratory and field dynamic tests. Volume III presents the strengthening and testing to failure of the bridge piers.

# ACKNOWLEDGMENTS

Coordination and implementation of this research program were achieved by Tarek Alkhrdaji in partial fulfillment of the requirement for the degree of Doctor of Philosophy in Civil Engineering at the University of Missouri at Rolla (UMR). Technical support during field testing was provided by Jeff Bradshaw, BsEE, P.E. (UMR), and C. H. Cassil of the University of Missouri-Columbia (UMC). Steve Haug (UMR) provided the technical and editorial comments.

The research program was made possible with the financial support received from the Missouri Department of Transportation, Mid-America Transportation Center, University of Missouri-Rolla/University Transportation Center on Advanced Materials and NDT Technologies. Master Builders Technologies, Cleveland, OH, and Structural Preservation Systems, Baltimore, MD, provided and installed the FRP systems, respectively. Chester Bross Construction Company, Hannibal, MO, was the general contractor.

# TABLE OF CONTENTS

# LIST OF ILLUSTRATIONS

# LIST OF TABLES

# NOTATION

| | | |
|---|---|---|
| $a$ | = | Depth of equivalent compressive stress block (in.) |
| $A$ | = | Horizontal acceleration coefficient |
| $A_c$ | = | Area of concrete section (in.$^2$) |
| $A_f$ | = | Area of tensile FRP reinforcement (in.$^2$) |
| $A'_f$ | = | Area of compressive FRP reinforcement (in.$^2$) |
| $A_g$ | = | Gross area of concrete (in.$^2$) |
| $A_{ft}$ | = | Total area of NSM reinforcement (in.$^2$) |
| $A_s$ | = | Area of tensile steel reinforcement (in.$^2$) |
| $A'_s$ | = | Area of compressive steel reinforcement (in.$^2$) |
| $b$ | = | Width of the section (in.) |
| $c$ | = | Depth to the neutral axis (in.) |
| $C_s$ | = | Elastic seismic response coefficient |
| $d$ | = | Depth to tension steel reinforcement centroid (in.) |
| $d'$ | = | Depth to compression steel reinforcement centroid (in.) |
| $d_{bl}$ | = | Diameter of longitudinal reinforcement (in.) |
| $d_n$ | = | Depth to tension NSM reinforcement centroid (in.) |
| $d'_n$ | = | Depth to compression NSM reinforcement centroid (in.) |
| $D_e$ | = | Diameter of equivalent circle (in) |
| $E_c$ | = | Approximate elastic modulus of concrete in compression (psi) |
| $E_f$ | = | Elastic modulus of the FRP fiber material (psi) |
| $E_j$ | = | Elastic modulus of the FRP jacket (psi) |
| $E_s$ | = | Elastic modulus of reinforcing steel (psi) |
| $f'_c$ | = | Compressive strength of concrete (psi) |
| $f_f$ | = | Stress level developed in tension FRP reinforcement (psi) |
| $f'_f$ | = | Stress level developed in compression FRP reinforcement (psi) |
| $f_{ju}$ | = | Ultimate tensile strength of the composite jacket (psi) |
| $f_{fu}$ | = | Design strength of the FRP material (psi) |
| $f_{jd}$ | = | Jacket design strength (psi) |
| $f_s$ | = | Stress level in tension steel reinforcement (psi) |
| $f'_s$ | = | Stress level in compression steel reinforcement (psi) |
| $f_y$ | = | Yield strength of mild steel (psi) |
| $f_{yh}$ | = | Yield stress of transverse reinforcement (psi) |
| $g$ | = | Acceleration of gravity (in./sec$^2$) |
| $h_c$ | = | Core dimension of column (in.) |
| $I_g$ | = | Moment of inertia of the gross concrete section (in.$^4$) |
| $K$ | = | Column lateral stiffness (k/ft) |
| $L$ | = | Clear length of column (ft) |
| $M$ | = | Weight of deck (kips) |
| $M_a$ | = | Moment acting at the base of a column |
| $M_b$ | = | Moment acting at the top of a column |
| $M_n$ | = | Nominal moment capacity of a section |
| $N_u$ | = | Axial load (lb) |
| $P$ | = | Earthquake load (kips) |
| $P$ | = | Axial force on column (lb) |

$P_b$ = Axial column strength at balanced steel/concrete failure (lb)
$P_{bf}$ = Axial column strength at balanced NSM FRP/concrete failure (lb)
$P_{max}$ = Axial strength of RC column (lb)
R = Response modification factor
S = Site coefficient depends on soil type
T = Period of vibration (sec)
$t_j$ = Thickness of composite jacket (in.)
$t_{jd}$ = Composite jacket design strength (psi)
$v_c$ = Nominal concrete shear strength (psi)
$V_c$ = Nominal concrete shear capacity (lb)
W = Weight of deck (kips)
$\alpha_1$ = Multiplier on concrete strength to determine the equivalent concrete strength of an equivalent rectangular stress block
$\beta_1$ = Multiplier on c to determine the depth of an equivalent rectangular stress block
$\Delta$ = Lateral displacement at top of the column
$\varepsilon_c$ = Compressive strain level in the concrete (in./in.)
$\varepsilon'_c$ = Strain level in the concrete corresponding to the peak concrete stress, $f'_c$ (in./in.)
$\varepsilon_{cu}$ = Maximum usable compressive strain in the concrete = 0.003 (in./in.)
$\varepsilon_f$ = Strain level in tension FRP (in./in.)
$\varepsilon'_f$ = Strain level in compression FRP (in./in.)
$\varepsilon_{fu}$ = Ultimate strain of FRP material (in./in.)
$\varepsilon_s$ = Strain level in tension steel (in./in.)
$\varepsilon'_s$ = Strain level in compression steel (in./in.)
$\varepsilon_y$ = Strain level in the tension steel at yielding (in./in.)
$\rho_l$ = Ratio of longitudinal steel reinforcement
$\rho_{lf}$ = Ratio of longitudinal FRP reinforcement
$\rho_{nsm}$ = Ratio of NSM FRP reinforcement
$\rho_t$ = Volumetric ratio of transverse reinforcement
$\rho_{tf}$ = Volumetric ratio of transverse FRP reinforcement
$\omega$ = Frequency of vibration (rad/sec)

# 1. INTRODUCTION

## 1.1. GENERAL

Recent awareness of potential seismic events in regions of low to moderate seismicity have led to growing concerns of state DOT's for the safety and vulnerability of existing reinforced concrete (RC) bridges in which lateral force resistance and ductile behavior has not been incorporated in the original design. Due to relatively smaller magnitudes and frequency of occurrences, the seismic activities in eastern and central United States are not well defined. As a result, the degree of damage from a maximum credible earthquake in a region of low seismicity can be much higher than the damage induced from a maximum credible earthquake in a region of high seismicity (Whitman, 1987). In addition, aggressive environments (e.g., treatment with deicing salts or exposure to marine environment), may eventually lead to corrosion of the steel reinforcement, which can cause premature structural deterioration and loss of serviceability.

RC columns can be seismically deficient in shear and flexural strength, and flexural ductility. It is common to find minimal amount of axial and transverse reinforcement in columns designed for gravity loads only (gravity piers), especially for those constructed prior to 1970. However, such columns can be adequate to resist the earthquake induced shear forces due to the large cross sections. Inadequate flexural strength, on the other hand, may arise from the low seismic lateral forces that were typically considered in earlier designs. Inadequate flexural strength may also arise from the premature termination of the main reinforcement or inadequate splicing. One method for retrofitting columns with flexural strength deficiencies consists of the addition of a RC jacket. This method is also effective in improving the shear strength and the ductility of a column. However, it may not be very practical due to undesirable section enlargement or construction constraint.

Fiber Reinforced Polymer (FRP) composites have very good mechanical properties that make then suitable for structural applications (see Volume I, Section 1.5). Due to their corrosion resistance and high strength-to-weight ratio, these materials have a great potential for use in new construction as well as for the repair and rehabilitation of existing structures. One such application of FRPs involves retrofitting of RC columns by jacketing to increase their seismic resistance. Previous work on column jacketing with FRP has demonstrated its effectiveness in improving the shear capacity and flexural ductility of columns (Seible et al. 1995, Hakamada 1997, Macrae et al. 1997).

Due to their shape, rectangular sections are partially confined when subjected to axial load that is a significant portion of its axial capacity and the confining pressure is concentrated at the corners of the cross section. Previous research on rectangular columns confined with steel hoops consistently demonstrated improved ductility (Park et al., 1980, Sheikh et al. 1980, and Mander et al 1988). It is commonly assumed that the maximum stress reached by a confined concrete rectangular member is equal to the strength of the standard cylinder strength $f'_c$. Although there is evidence that rectangular hoops can increase the strength, the increase was not consistent and is conservatively ignored. Similar behavior was observed for rectangular columns jacketed with FRP composites (Seible et al 1995, Hakamada, 1997, and Macrae et al. 1997). In addition, jacketing with FRP can also prevent cover spalling; provide continuous lateral support to longitudinal reinforcement, and to enhance concrete deformation capacities, all of which are essential design requirement.

In an attempt to improve the flexural capacity of columns jacketed with FRP sheets, researchers have used steel plates with bolted connections accompanied by section enlargement at the base of the column (Hakamada, 1997). This method resulted in a slight improvement of the flexural capacity. However, such mechanical anchors, although effective in the laboratory, are not very practical for field application due to drawbacks such as stress concentration that can cause premature rupture of FRP. In addition, where carbon FRP is used, the likelihood of galvanic corrosion due to steel-carbon fiber contact is an additional concern.

Strengthening of RC members with near-surface mounted (referred to as NSM) FRP rods is another technique that could be used to improve the flexural capacity of columns. This strengthening technique consists of FRP rods embedded in grooves made on the surface of the concrete and bonded in place with epoxy. This technique was successfully used to upgrade Pier 12 at the Naval Station in San Diego, CA to meet demand of operational changes accompanied by higher vertical loads (Naval Facilities, 1998). The use of NSM rods could be more practical than externally bonded FRP laminates when the end anchorage of the FRP reinforcement is an essential design requirement, as in the case for the flexural strengthening of RC columns.

## 1.2. PROBLEM STATEMENT

Many reinforced concrete (RC) bridge piers, constructed in the first half of this century, were designed as gravity piers without considering seismically induced lateral forces. The columns of these piers have minimal flexural capacity and ductility. The potential risk of failure of these piers under a moderate earthquake is becoming a concern to transportation management agencies. In addition, loss of reinforcement due to corrosion may result in columns with deficiencies in flexural strength.

Since most of the existing gravity columns were designed to carry axial loads that consist only a small fraction of their axial load capacity (usually less that $0.1A_c f'_c$), the influence of FRP jacketing on their flexural capacity is minimal. This is because jacketing can only improve the flexural capacity through concrete confinement if failure is governed by concrete crushing (compression-controlled failure). In this case, a larger portion of the cross-sectional area is under compression and the mechanical properties of the concrete control the strength and ductility of the column.

Strengthening of columns for flexure using FRP sheets with the fibers aligned in the column direction is not practical due to anchorage requirement at the top and the base of the column. New techniques for the flexural retrofit of RC columns, especially for gravity piers, are therefore required. In addition, the database for performance of FRP strengthened RC members is based on laboratory tests, which are usually conducted on small-scale specimens that do not account for the variation of boundary conditions of a real structure. Full-scale field tests, on the other hand, can demonstrate the actual behavior of a structure and can lead to a better understanding of the performance of the system as a whole and therefore the strengthening design requirements.

## 1.3. OBJECTIVES

This part of the research program was tailored to demonstrate the feasibility and effectiveness of NSM rods for improving the flexural capacity of RC piers and investigate their possible modes of failure. Bridge J857, scheduled for demolition during the spring of 1999, was selected for this demonstration.

An upgrading technique of these piers utilizing NSM FRP rods and FRP jacketing is investigated. FRP Jackets are used to prevent cover spalling; provide continuous lateral support to longitudinal reinforcement, and, to less extent, enhance concrete deformation capacities, all of which are essential design requirement. Test results are intended to verify this approach and to bridge the gap between small-scale experiments and the full-scale behavior of FRP strengthened bridge columns for capacity verifications. It is intended to provide supporting full-scale testing data on the performance of typical RC gravity piers in central United States, a zone classified as a region of low-to-moderate seismic risk.

## 1.4. ANTICIPATED BENEFITS

FRP reinforcement could provide significant cost savings in repair/strengthening as well as corrosion problems. With the expertise, FRP experience, and testing capabilities of the research team, the contributions of the industrial partners, and the field demonstrations, the result of this project will provide a verification of the effectiveness of FRP strengthening systems for improving the flexural capacity of RC bridge piers. The test results presented in this document could provide the engineers with some preliminary data on the potential performance of typical gravity-load–designed RC columns before and after strengthening and the influence of the boundary conditions. These data could be used to develop design criteria based on a scientifically valid foundation. Standard specifications for design and construction and quality control tests for FRP repair/strengthening are necessary to allow general use in concrete highway structures.

## 1.5. SUMMARY OF RESEARCH PROGRAM

The research program aims at strengthening and testing to failure of the RC columns of bridge J857, located in Phelps County, Missouri, in order to investigate the effectiveness of near-surface mounted FRP rods for improving their flexural capacities. The bridge considered for this study (Bridge J857) was ideal for this demonstration since it represented typical conditions of several bridges in Missouri and the surrounding Mid-America states.

The original drawings of the bridge are given in Appendix A. The columns, which were originally designed to carry gravity loads, were upgraded using FRP composites and then tested to failure. The columns were upgraded to a concrete structure under seismic performance category (SPC) B. Three of the four columns were strengthened using different strengthening schemes. Flexural strengthening was achieved by installing near-surface mounted CFRP rods on two opposite sides (north and south) of the columns. The strengthened columns were wrapped with carbon and glass FRP composites to satisfy seismic detailing requirements. The columns were tested to failure by applying cyclic lateral loads to the pier cap beams. The behavior of strengthened columns, influence of different strengthening schemes and failure modes were compared and conclusions were drawn.

# 2. SEISMIC EVALUATION AND STRENGTHENING

## 2.1. GENERAL

The main focus of this part of the research program was to improve the flexural capacity of the RC columns, a major concern for gravity columns. In order to establish a level of strengthening and to relate the project to real life applications, the bridge was assessed for seismic vulnerability. Seismic assessment was carried out using a simplified approach based on a single degree of freedom vibration. Different strengthening levels were used for the columns to allow for investigating different aspects of their behavior. Flexural strengthening of the columns was achieved using near surface mounted carbon FRP rods. Composite jackets were applied to provide lateral support to the mounted rods to prevent bar buckling.

## 2.2. DESCRIPTION OF BRIDGE PIERS

### 2.2.1. Geometry

Bridge decks were supported on two abutments and two bents. Each bent consists of two columns connected at the top by a RC cap beam, as shown in Figure 2.1. The abutments and the bents were all at a 15-degree skew. The columns had a 2 ft × 2 ft (0.6 m× 0.6 m) square cross-section and were reinforced with four #6 (19 mm) deformed steel bars located at the corners of the cross section. The haunch of each column was reinforced with four #6 (19 mm) steel bars that extended 3 ft (0.9 m) into the column from the bottom of the haunch. The transverse reinforcement consisted of #2 (6 mm) steel ties spaced at 18 in. (457 mm) on centers. Each column was supported by a 4 ft by 4 ft by 2.5 ft (1.2 m × 1.2 m × 0.75 m) RC square spread footing. Figure 2.2 shows typical geometry and reinforcement details of a bridge column as given by the original plans.

**Figure 2.1.** Photo showing bridge columns.

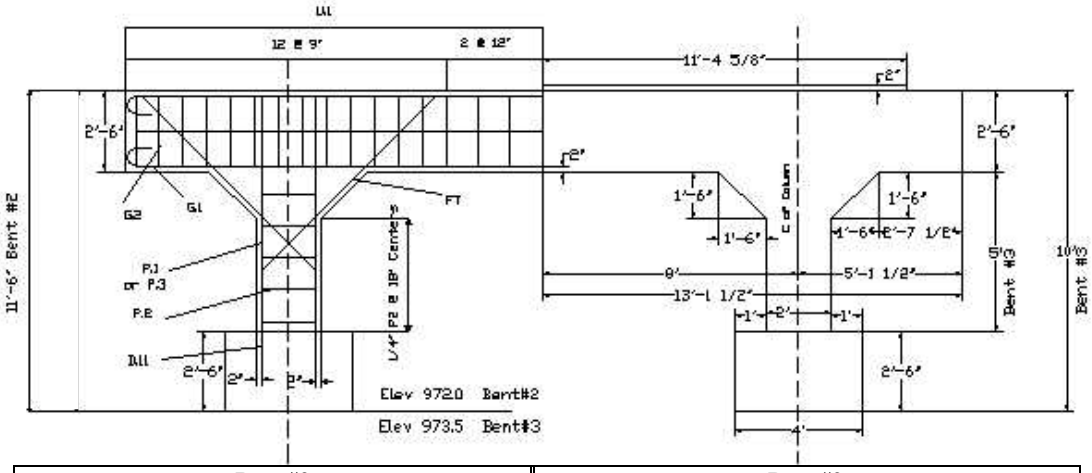


| Bent #2 | | | | | Bent #3 | | | | |
|---|---|---|---|---|---|---|---|---|---|
| No | Size | Length | Mark | Location | No | Size | Length | Mark | Location |
| 3 | ¾ | 6 : 3" | D.11 | Footing | 8 | ¾ | 6 : 3" | D.11 | Footing |
| 16 | ¾ | 8 : 6" | F.1 | Haunch | 16 | ¾ | 8 : 6" | F.1 | Haunch |
| 12 | 1 | 27 : 3" | G.1 | Beam | 12 | 1 | 27 : 3" | G.1 | Beam |
| 2 | ¾ | 25 : 3" | G.2 | Beam | 2 | ¾ | 25 : 3" | G.3 | Beam |
| 8 | ¾ | 8 : 4" | P.1 | Column | 6 | ¼ | 8 : 0" | P.2 | Column |
| 8 | ¼ | 8 : 0" | P.2 | Column | 8 | ¾ | 7 : 3" | P.3 | Column |
| 30 | ½ | 9 : 0" | U.1 | Beam | 30 | ½ | 9 : 0" | U.1 | Beam |

**Figure 2.2.** Original drawing of Bent 3 showing typical bent details.

According to the bridge plans, the clear length of the columns varied from 3.5 to 5.0 ft (1.1 to 1.5 m). Upon field inspection, it was found that the actual lengths of the columns varied from 6 to 12 ft (1.8-3.7 m). Figure 2.3 shows the measured length of each column and its designation. In general, the condition of the bridge was good and no major damage (e.g., corrosion of reinforcement, or concrete spalling) was observed.

### 2.2.2. Materials

The original plans of the bridge J857 did not provide any specifications for the materials used in bridge construction other than the concrete mix proportions (1:2:3½) and reinforcement schedule. The materials properties used in the preliminary analysis were based on the materials strength values recommended by MoDOT (MoDOT, 1996). Table 2.1 summarizes the material properties used for the preliminary investigation of bridge capacity.

## 2.3. ANALYSIS OF BRIDGE COLUMN

### 2.3.1. Flexural Capacity

Figure 2.4 shows the cross-sectional properties of a typical column. Each column carried an axial load of 100 kips (444 kN), resulted from the weight of the supported deck and the cap beam. Figure 2.5 illustrates the axial load-moment interaction for a bridge column. Based on this diagram, the nominal moment capacity of a bridge column subjected to an axial load of 100 kips, was determined to be 140 ft-k (190 kN-m). It should be noted that this capacity is for a section at the base of the column. The flexural capacity of a section at the top should be higher due to the additional reinforcement of the haunch. The cracking moment of the section was calculated in accordance with ACI 318-95 to be 72 ft-kips.

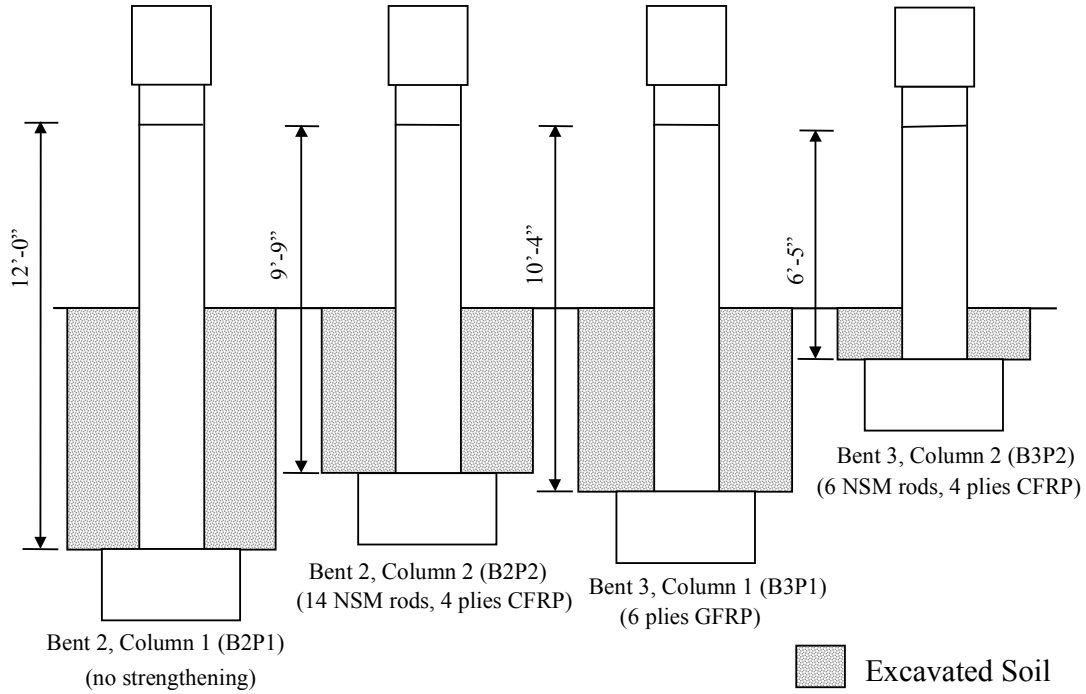


**Figure 2.3.** Clear length of the columns and excavation profile.

**Table 2.1.** Material Properties.

| $f'_c$ psi (MPa) | $E_c$ ksi (GPa) | $f_y$ psi (MPa) | $E_s$ ksi (GPa) |
|---|---|---|---|
| 2500 (17.2) | 2850 (19.5) | 33,000 (227) | 29,000 (200) |

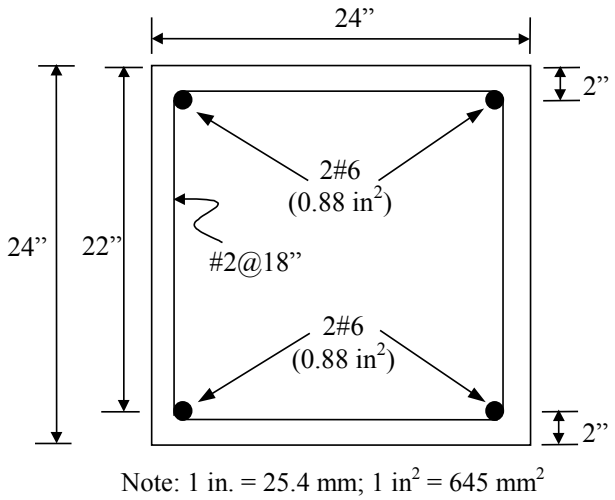


**Figure 2.4.** Typical cross-section properties of a bridge column.

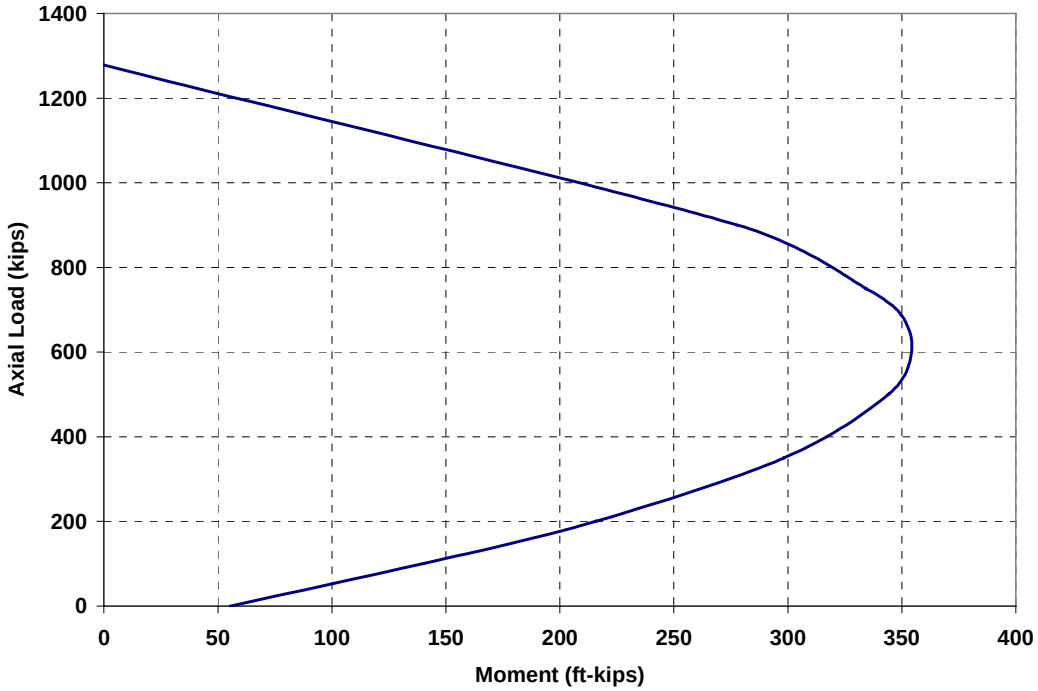


Note: 1 kip = 4.45 kN; 1 ft-kip = 1.36 kN-m

**Figure 2.5.** P-M diagram for a typical column section.

### 2.3.2. Shear Capacity

According to AASHTO (1996), the shear capacity provided by concrete, $V_c$, for members subjected to axial compression is computed as follows:

$$V_c = 2\left(1+\frac{N_u}{2000A_g}\right)\sqrt{f_c'}bd \qquad (2.1)$$

In which $N_u$ is the axial load acting on the member and $A_g$ is the gross area of the compression members and the ratio $N_u/A_g$ is expressed in pounds per square inch. Based on this equation, the shear capacity of the columns was 57 kips (253 kN).

## 2.4. LATERAL LOAD REQUIREMENT BASED ON SEISMIC EVALUATION

Seismic evaluation of the bridge piers was performed as if the bridge were located in Saint Louis County and therefore exposed to a higher risk of seismic event. This is because the later is closer to the New Madrid fault. Seismic evaluation was based on Division I-A, Seismic Design, of the Standard Specifications for Highway Bridges (AASHTO, 1996). Using these specifications, the peak horizontal acceleration coefficient, A, (expressed as percentage of the gravity, g) was determined as 0.1. Peak accelerations are based on 90 percent probability that they will not be exceeded in 50 years. The determined peak acceleration corresponds to a structure with Seismic Performance Category B. Seismic evaluation was achieved using a simplified approach based the single-mode response spectral method and using the, as given on plans, geometry of the columns. Figure 2.6 shows a schematic of the condition of bridge deck

supports as given in these plans. According to this configuration, both decks 2 and 3 had a shear key at bent 3. Therefore, this bent would be subjected to the highest lateral loads induced by an earthquake. Two cases of earthquake loading were investigated. In the first case, it was assumed that the roller supports had no friction while in the second, a friction factor greater than 0.4 was assumed at the roller supports.

CASE 1: Assuming no friction on the roller supports, the weight due to superstructure (decks 2 and 3), cap beam, and fifty percent of column weight was determined as 356 kips (1580 kN). Assuming that the columns on bent 3 are fixed at the footing, their stiffness K of the column is therefore:

$$K = 2 \times \frac{3E_c I_g}{L^3} \tag{2.2}$$

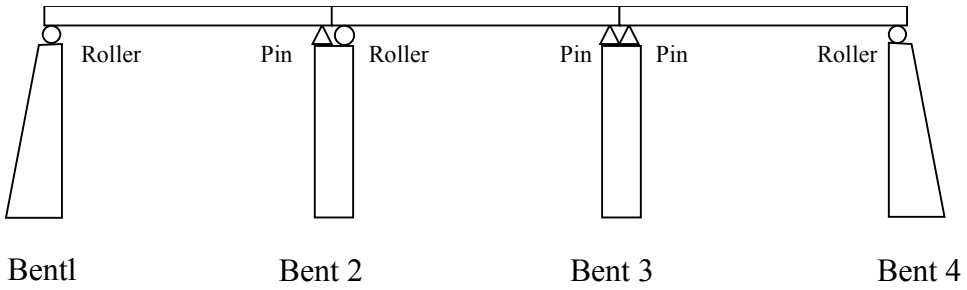


**Figure 2.6.** A schematic of the support conditions of the bridge decks.

In which $I_g$ is the moment of inertia of the column determined as follows:

$$I_g = \frac{bh^3}{12} = \frac{2^4}{12} = 1.333 \text{ ft}^4 \ (0.011 \text{ m}^4) \tag{2.3}$$

$$K = 2 \times \frac{3 * 1/9 * 29{,}000(\text{ksi}) * 12^2 * 1.333}{7.5^3} = 8797 \text{ k/ft} \ (128000 \text{ kN/m}) \tag{2.4}$$

The frequency ω and period T of vibration are calculated based on the estimated mass M and stiffness K as follows:

$$\omega = \sqrt{\frac{K}{M}} = \sqrt{\frac{8797 * 32}{356}} = 28.1 \text{ rad/sec} \tag{2.5}$$

$$T = \frac{2\pi}{\omega} = 0.223 \text{ sec} \tag{2.6}$$

Assuming a site coefficient S = 1.0 (rock), the elastic seismic response $C_s$ is determined as follows:

$$C_s = \frac{1.2AS}{T^{2/3}} = \frac{1.2 \times 0.1 \times 1}{.223^{2/3}} = 0.326 \qquad \text{should be} \le 2.5A = 0.25 \tag{2.7}$$

Therefore, $C_s$ is equal to 0.25. Using a response modification factor of R = 1.0, the total earthquake load on bent 3 is therefore:

$$P = \frac{C_s W}{R} = \frac{0.25 \times 356}{1.0} = 89 \text{ kips (395 kN)} \quad \text{(in longitudinal direction)} \qquad (2.8)$$

The shear force on each column is calculated by dividing the earthquake load by two, which yielded a lateral force of 44.5 kips (198 kN).

CASE 2: Assuming that the coefficient of friction at the roller supports was greater than 0.4, the three spans of the bridge are expected to move together. By inspection, the period of vibration will be slightly decreased and the effective weight is approximately 534 kips (2370 kN). The total earthquake load on bent #3 was therefore:

$$P = \frac{C_s W}{2} = \frac{0.25 \times 534}{2} = 67 \text{ kips (297 kN)} \qquad (2.9)$$

From which, the shear force per column is 33.5 kips (149 kN). Considering an approximate average value of the two cases, the seismically force for strengthening design purpose was taken as 40 kips (178 kN).

## 2.5. SUMMARY OF PIER EVALUATION

The estimated shear capacity of the columns of 57 kips (253 kN) is adequate to resist the seismically induced shear forces. The moment resulting from the considered lateral force was different for each column due to variation in their heights. These moments were 480, 390, 413, and 257 ft-k (650, 530, 560, and 350 kN-m) for columns B2P1, B2P2, B3P1, and B3P2, respectively. The columns were therefore adequate in resisting shear and deficient in flexure. To investigate the effectiveness of FRP composites for improving the flexural capacity of the columns, two of the bridge columns were strengthened with near surface mounted carbon FRP (CFRP) rods. The columns were then jacketed to meet detailing requirement. A third column was jacketed with glass FRP (GFRP) jacket to investigate its influence on the ductility under low axial load while the fourth column was used as a benchmark.

## 2.6. MATERIALS FOR STRENGTHENING DESIGN

Detailed description of the proposed strengthening systems (e.g., NSM and surface bonded sheets) and their components is provided in Volume I of this document. The rods considered for near surface mounted application were $^7/_{16}$ in. (11 mm) diameter CFRP rods with surface roughened by sandblasting to improve their bond properties.

Previous research on FRP reinforcing rods indicated that CFRP rods have a lower compressive strength than the tensile strength and is subject to significant variation (Wu 1990, Kobayashi and Fujisaki 1995, and Japan Society of Civil Engineers 1997). In addition, the compressive modulus of elasticity of FRP reinforcing bars appears to be smaller than the tensile modulus (Mallick 1988 and Ehsani 1993). Accordingly, it was recommended that the contribution of compression FRP bars be ignored in design calculations (Almusallam et al. 1997 and ACI 440H 1999). The mechanical properties of the CFRP rods and CFRP and GFRP fiber sheets considered for strengthening application are given in Table 2.2.

**Table 2.2.** Mechanical Properties of FRP Reinforcement.

| FRP Type | Dimension† in. (mm) | Design Strength ksi (MPa) | Design Strain in./in. or mm/mm | Tensile Modulus ksi (GPa) |
|---|---|---|---|---|
| Glass sheets* | 0.0139 (0.353) | 220 (1520) | 0.0210 | 10,500 (72) |
| Carbon sheets* | 0.0065 (0.165) | 550 (3800) | 0.0170 | 33,000 (228) |
| Carbon rods** | $^{7}/_{16}$ (11) | 144 (993) | 0.0084 | 17,200 (119) |

† Sheet thickness or bar diameter * Fiber properties ** Composite rod properties

## 2.7. FLEXURAL STRENGTHENING REQUIREMENTS

Due to the nature of seismic forces, the addition of strengthening reinforcement should be achieved in a symmetric manner. That is, reinforcement should be provided on the two opposite sides of the column that are perpendicular to the considered direction of seismic force. The design of near-surface mounted FRP strengthening is achieved by trial and error in which an amount of FRP reinforcement is assumed and the ultimate capacity is calculated utilizing force equilibrium, strain compatibility, and the constitutive laws of the materials. Strengthening design of NSM rods is described in Appendix A.

Two columns were considered for flexural strengthening using NSM reinforcement: B2P2 and B3P2. Moment capacities were determined without accounting for compression FRP reinforcement and considering an axial load of 100 kips (445 kN). The columns were strengthened to two different levels that would result in two different modes of failure: concrete crushing and FRP rupture, in the same respective order. The strengthening design called for 7 CFRP rods and 3 CFRP rods mounted on either of two opposite sides of column B2P2 and B3P2, respectively. Summary of the shear and flexural capacity requirements for the bridge columns along with the upgraded capacities are given in Table 2.3.

**Table 2.3.** Current and Upgraded Flexural Capacities of Bridge Columns.

| Current Capacity | | Required Capacity Based on SPC B | | | Upgraded Capacity | |
|---|---|---|---|---|---|---|
| Shear kips (kN) | Flexure ft-k (kN-m) | Shear kips (kN) | Flexure ft-k (kN-m) | | Flexural ft-k (kN-m) | |
| | | | B2P2 | B3P2 | B2P2 | B3P2 |
| 57 (253) | 140 (190) | 40 (178) | 390 (530) | 257 (350) | 393 (533) | 254 (344) |
| | | | | Capacity Improvement | 185% | 84% |

## 2.8. FRP JACKETING

FRP jacketing could be used for RC columns to enhance their shear strength, confine the concrete at plastic hinge and lap splice regions, and to provide lateral support for longitudinal reinforcement. However, the effectiveness of composite jacketing to enhance the different aspect of RC column performance may vary depending on column geometry. In addition, column strengthening with NSM FRP rod for flexural capacity enhancement results in different column behavior and thus requires different approach for FRP jack design.

### 2.8.1. Shear Strength Enhancement

Investigation of the shear strength of bridge columns based on conservative material properties indicated that the columns had adequate shear strength, therefore no shear strength enhancement was needed.

### 2.8.2. Plastic Hinge Confinement

Confinement of column concrete is required in locations where plastic hinges are likely to occur to increase the concrete ultimate compressive strain and with it the inelastic rotation capacity. Based on experimental results of circular and rectangular columns jacketed with FRP composites, Seible and Innamorato (1995) concluded that the effectiveness of confining rectangular columns with composite jackets decreases significantly since only corner forces are generated during the dilation of column flexural hinge. Accordingly, for rectangular columns with side aspect ratio of 1.5 or less, a jacket thickness of twice the one calculated for an equivalent circular jacket was recommended. The aspect ratio limit was set to reflect the scope of the experimental program. The required composite jacket thickness for flexural hinge confinement of rectangular columns is expressed as follows:

$$t_j = \frac{D_e f'_c}{2.25 f_{ju}} \left[ 0.5 + 1.25 \frac{P}{f'_c A_g} \right] + 0.13(\rho_l - 0.01) \qquad (2.10)$$

In which:
$A_g$ = gross area of the column section
$D_e$ = diameter of equivalent circle
$f_{ju}$ = ultimate tensile strength of the composite jacket
P = column axial load
$\rho_l$ = ratio of longitudinal steel reinforcement
The equivalent column diameter $D_e$ is expressed as follows:

$$D_e = \frac{b^2}{a} + \frac{a^2}{b} \qquad (2.11)$$

For rectangular column side dimensions A and B where A is the larger column side, a and b were defined as follows:

$$\begin{aligned} a &= k\, b \\ b &= \sqrt{\left(\frac{A}{2k}\right)^2 + \left(\frac{B}{2}\right)^2} \\ k &= \left(\frac{A}{B}\right)^{\frac{2}{3}} \end{aligned} \qquad (2.12)$$

Considering the small amount of steel reinforcement (0.3%) of bridge columns and due to linear elastic stress-strain behavior of NSM CFRP rods, it is unlikely for a plastic hinge to occur in the strengthened columns. In addition, the predicted failure mode of the strengthened columns was governed by CFRP rod rupture and with a concrete strain at failure below the ultimate

concrete strain of 0.003 in./in. (or mm/mm). (see Appendix A). Therefore, minimal lateral dilation of concrete is expected at failure of these columns. For this application, FRP jackets would have minimal contribution to the strength and ductility of the strengthened columns. An unstrengthened column was jacketed with glass FRP to investigate the influence of the composite jacket on its ductility and failure mode. The calculated thickness of glass FRP jacket was 0.09 in. (2.3 mm). Considering GFRP fiber sheet thickness of 0.0139 in. (0.35 mm), the required number of plies was determined to be 6. It should be noted that for the current application the ratio of longitudinal steel reinforcement $\rho_l$ was 0.003, which was less than the 0.001 given in the second term of the jacket thickness equation. Therefore this term was ignored when calculating the jacket thickness.

### 2.8.3. Lap Splice Confinement

Lap splice debonding occurs in the form of failure planes in the cover concrete along the longitudinal column bar perimeter. To prevent this failure mode, sufficient lateral pressure onto the splice region is required to prevent the relative slip of the concrete prisms (Priestly et al., 1992). Such clamping force can only be provided by convex jacket curvature. Accordingly, Seible and Innamorato (1995) concluded that FRP jacketing is not effective for rectangular columns to prevent lap splice debonding. For these cases, a circular or oval jacket with appropriate concrete bolsters needs to be provided.

### 2.8.4. Lateral Support of Longitudinal Reinforcement

To prevent column bar buckling in the plastic hinge region the volumetric transverse reinforcement ratio $\rho_t$ for rectangular columns was given by Seible and Innamorato (1995) as follows:

$$\rho_t = \frac{0.0052\rho_l D_e}{d_{bl}} \frac{f_y}{f_{yh}} \tag{2.13}$$

In which, $\rho_l$ is ratio of longitudinal reinforcement, $d_{bl}$ is the diameter of longitudinal reinforcement, $f_y$ is the yield stress of longitudinal reinforcement, and $f_{yh}$ is the yield stress of transverse reinforcement. Experimental results of shear tests of FRP jacketed columns indicated that the ultimate strain of FRP composites couldn't be attained in jacketing situations (Priestly et al., 1993). This behavior was related to the excessive cracking at higher dilation levels that causes loss of aggregate interlock and therefore degradation of the lateral stiffness prior to attaining jacket strength. Accordingly, a strain limit of 0.004 in./in. (or mm/mm) was proposed for FRP composite jackets (Priestly et al., 1996). Similar limit can be set for calculation of the lateral support requirement to ensure stability of the longitudinal bars. Composite jacket design strength $f_{jd}$ was defined in term of the jacket modulus $E_j$ as follows:

$$f_{jd} = 0.004E_j \tag{2.14}$$

Substituting $f_{jd}$ for $f_{yh}$ and the volumetric transverse FRP reinforcement ratio $\rho_{tf}$ defined as:

$$\rho_{tf} = \frac{4t_j}{D_e} \tag{2.15}$$

For $\rho_t$ in Equation (2.13), the required composite jacket thickness to prevent longitudinal steel bar buckling could be defined as follows:

$$t_j = \frac{\rho_l D_e^2}{3 d_{bl}} \frac{f_y}{E_j} \tag{2.16}$$

Using the same approach, the required jacket thickness to prevent NSM FRP rod buckling is expressed as follows:

$$t_j = \frac{\rho_{lf} D_e^2}{3 d_{bl}} \frac{f_{fu}}{E_j} \tag{2.17}$$

Using bridge column section geometry and design material properties, the sum of the required CFRP fiber thickness to prevent column steel and NSM reinforcement buckling was calculated as 0.0178 in. (0.45 mm). Considering CFRP fiber sheet thickness of 0.0065 in. (0.165 mm), the required number of plies was 3. However, due to the novelty of the strengthening system it was decided to jacket the strengthened columns with 4 plies rather than 3 plies of CFRP.

In summary, two columns were strengthened for flexure using near-surface mounted carbon FRP rods. Column B2P2 was strengthened with 14 NSM rods, mounted on two opposite sides, seven on each side. Column B3P2 was strengthened with six NSM rods, three on each side. The rods were fully anchored (approximately 15 in.) into the footing of each column. The two columns were also jacketed with 4-ply CFRP jackets. A third column B3P1 was externally jacketed with six plies of glass FRP sheets. The fourth column B2P1 was left unstrengthened as a benchmark. Figure 2.7 illustrates strengthening schemes of bridge columns.

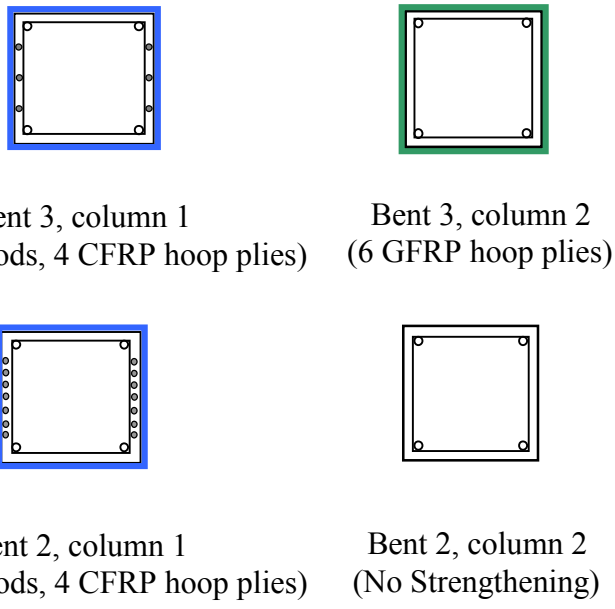


**Figure 2.7.** Strengthening schemes of bridge columns.

## 2.9. FRP INSTALLATION

Prior to the installation of the FRP, the soil around the columns was excavated to the level of the footing. Visual examination of the soil excavated around columns B2P1 and B2P2 revealed that it consisted of a mixture of gravelly sand, coarse gravel, and fragments of highly weathered rocks. At columns B3P1 and B3P2, the soil consisted of gravelly sand, cobbles and rock boulders. Softer soil was encountered around the footing, indicating the possibility of a backfill prior to the construction of the footing. Column B3P2 had the shallowest foundation that was cast into the bedrock.

### 2.9.1. Installation of NSM CFRP Rods

The test configuration was such that lateral movement of the columns was allowed at the top while restrained at the base by the footing. Accordingly, the NSM rods were only anchored to the footing.

The NSM FRP rods were embedded in ¾ in. (19 mm) deep, and $^{9}/_{16}$ in. (14 mm) wide grooves cut onto the sides of the columns along their axis. To anchor the rods, 16-in (400-mm) deep holes, aligned with the grooves, were drilled into the footings. To install an FRP rod, the groove and the hole were initially filled halfway with a viscous epoxy grout. The FRP rod was then installed in the hole, placed into the groove, and lightly pressed. This action forced the adhesive to flow around the rod and cover the sides of the groove. The FRP rod was held in place using wooden wedges. The groove was then filled with the same adhesive and the surface was leveled. Some of the FRP rods were instrumented with strain gages prior to installation. Photos showing the grooves and the drilled holes are shown in Figures 2.8 and 2.9.

**Figure 2.8.** Grooves on the side of column B2P2.

**Figure 2.9.** Drilled holes at the base of column B2P2 for anchorage of CFRP rods.

### 2.9.2. Installation of FRP Sheets

Three of the four columns were jacketed with FRP composites. The jackets covered the entire length of the columns with the fiber direction perpendicular to the column axis. The corners of the columns were rounded to prevent stress concentrations. The jacketed columns were sandblasted to remove any loose material and laitance and provide an open pore structure. The FRP plies were applied with six inches (150-mm) of end overlap. The end overlaps of the successive plies were staggered around the column to avoid creating a weak zone.

Due to variation in column lengths, the number of lifts of CFRP sheets required to cover the entire column was different. The number of lifts for B2P2, B3P2, and B3P2 were 6, 6 ¼, and 4 lifts, respectively, as shown in Figure 2.10. The bottom lift was applied after the rest of the lifts were installed and allowed to cure, as shown in Figure 2.11. This was done to prevent damaging the strain gages wires. The bottom lift was applied after the wires were extended such that they exit between the first and the second lifts from the bottom of the column, as shown in Figure 2.12. A photo showing a general view of the bridge after strengthening is given in Figure 2.13.

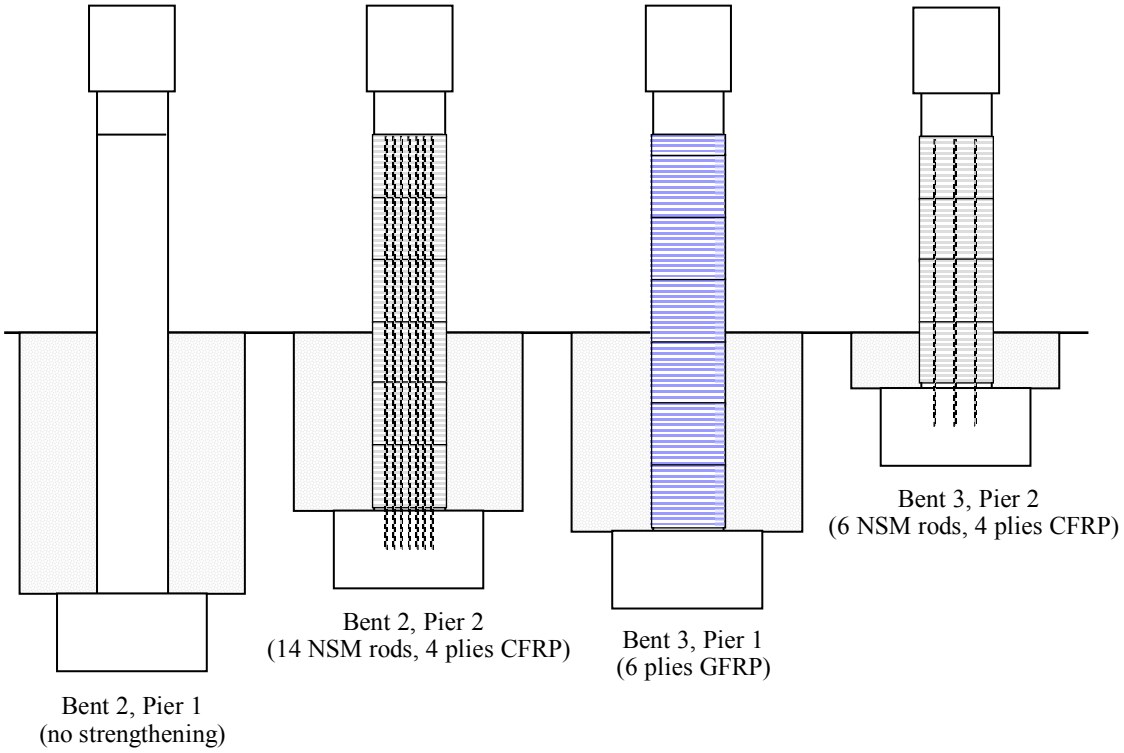


**Figure 2.10.** Strengthening schemes of bridge columns.

**Figure 2.11.** Applying the bottom lift of the jacket.

**Figure 2.12.** Strain gage wires.

**Figure 2.13.** Photo showing the bridge after strengthening.

# 3. TEST SET UP AND INSTRUMENTATION

## 3.1. GENERAL

To account for the unknown boundary conditions of the piers, the test setup was designed to apply loads significantly higher than the lateral load capacity of the columns. The test setup was assembled using the test setup components used for the destructive testing of the bridge decks. Details of these components are given in Chapter 4 of Volume 1 of this document.

## 3.2. LOADING CONFIGURATION

The test setup was designed such that it could induce reversed loading cycles in which the columns were allowed to displace laterally at the top. To allow for the relative movement of the cap beam and the topping deck, a 10-inch (250-mm) strip of the deck was saw-cut along the entire deck and removed, as shown in Figure 3.1. The central portions (about 42 in. or 1 m) of the cap beams were also saw-cut, as shown in Figure 3.2. After saw cutting, the concrete was removed by knocking it down from the top with a backhoe bucket while the backhoe was located next to the bridge. Figure 3.3 shows the bridge deck and a cap beam after removing the concrete.

A schematic of the test setup is shown in Figure 3.4. The same setup configuration was used to test the columns on the two piers of the bridge. The loading system comprised of an electric pump, three hydraulic jacks, and control valves. Three hydraulic jacks were used to induce the cyclic loading cycles. Two of the hydraulic jacks (end jacks) were used to induce pull-in force while the third jack (middle jack) was inserted in the cut potion of the cap beam and used to induce the push-out force. Each jack had a 200 kips (90 tonnes) capacity and 18 in. (457 mm) stroke. The end jacks were connected to the electric pump in parallel to achieve equal pressure while the middle jack was connected directly to the electric pump. End and middle jacks were used alternately to create reversed static lateral loading cycles.

To apply the pull-in force, a reaction frame was constructed such that it confined the cap beam. The frame consisted of two spreader beams, four distribution beams, and high strength steel rods and accessories. These were the same spreader beams used to test the bridge decks. Each spreader beam was made of two standard W14×90 steel shapes. To avoid damaging the spreader beam due to concentrated load, distribution beams were used to distribute the load across the width of each spreader beam. Details of the spreader and distribution beams are given in Volume I. To erect the setup frame, each spreader beam was lifted to place with the backhoe and was held in place by chaining it to the bridge parapet walls using steel chains. The distribution beams were attached to the spreader beams using C-clamps. A scaffold was then erected on one end of cap beam and the two jacks were placed on the scaffold against the spreader beam. Wooden blocks were stacked under the jacks to raise them to the desired level. The end jacks were approximately spaced at 3.5 ft (1 m) apart. The jacks were chained to the parapet wall as an additional safety measure. The assembly of the beams and the jacks on both ends of the cap beam are shown in Figures 3.4 and 3.5. The complete test setup is shown in Figure 3.6.

The high strength steel rods were passed through the jacks, distribution beams, and the spreader beams and were anchored on both ends with steel plates and nuts (see Figure 3.7). The rods were used to transfer the load from one end of the cap beam to the other.

For the push-out loading cycles, the middle jack was inserted in the cut portion of the cap beam and was held in place using a simple holding frame consisted of a steel plate, threaded rods, and steel channels. Details of this frame are shown in Figure 3.8. To ensure uniform stress distribution, two 24 x 24 in. (600 x 600 mm) pieces of plywood were attached to the cut surfaces of the cap beam. Figure 3.9 shows the placement of the middle jack. Figure 3.10 shows the assembled setup for a bridge pier testing. With this configuration, the lateral loads were applied by reacting against the adjacent column in the pier. Once the weaker column at the bent is failed, the reaction force required to fail the second column was achieved using a diagonal brace made of 10-inch (250 mm) diameter, 3/8 inch (16 mm) thick, standard steel pipe. The brace was placed against the failed column and reacted against a RC footing that was cast into the bedrock of the creek. The diagonal brace was installed after removing the setup frame. Details of the bracing system are shown in Figure 3.11.

### 3.3. REDUCTION OF DECK-PIER CAP FRICTION

The maximum lateral loads to fail the columns of the bent 2 exceeded in magnitude the predicted loads. To minimize friction between the cap beam and the deck, the bridge decks resting on bent 3 were jacked up prior to testing and lubricated steel plates were inserted between the cap beam and the topping decks. The decks on each side of the bent were jacked up using two hydraulic jacks that were elevated using 4 x 4 x 48 in. (0.2 x 0.2 x 1.2 m) wooden blocks (cribbing), as shown in Figure 3.12. After the decks were jacked and a clearance of 1 to 1.5 in (25 to 40 mm) was achieved, the bituminous sheets between the deck and the cap beam were removed and a number of steel plates assemblies were inserted in the gap. Each assembly was made of two 8 x 20 x $^{3}/_{8}$ in (200 x 500 x 9 mm) steel plates with heavy-duty grease in between. A clear space of 6 in. (150 mm) was maintained between the assemblies to allow for the relative movement of the plates. Figure 3.13 shows a photo of the inserted steel plates assemblies.

**Figure 3.1.** Cutting the bridge deck.

**Figure 3.2.** Cutting the cap beam.

**Figure 3.3.** The bridge deck and a cap beam after cutting and removing concrete.

(a) Front view of the assembly

(b) Side view of the assembly

**Figure 3.4.** Confining frame assembly at one end of cap beam.

(a) Front view

(b) Side view

**Figure 3.5.** Confining frame assembly at the other end of cap beam.

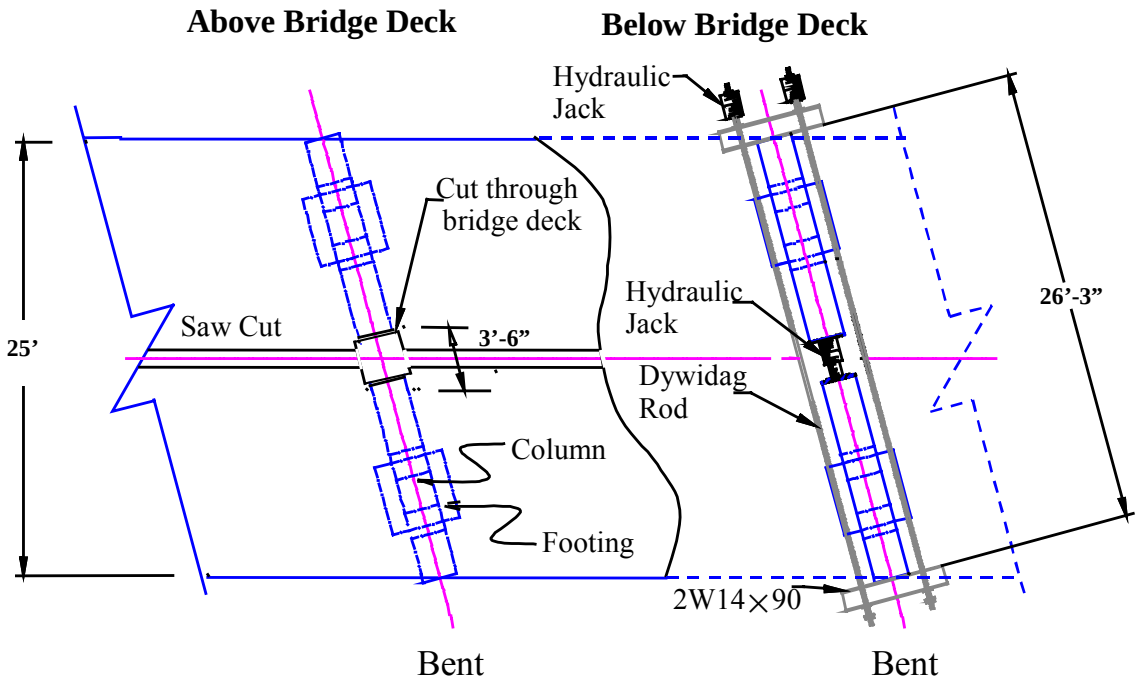


Note: 1 in. = 25 mm; 1 ft = 0.305 m

**Figure 3.6.** Schematic of the test setup.


**Figure 3.7.** Dywidag rods and accessories.

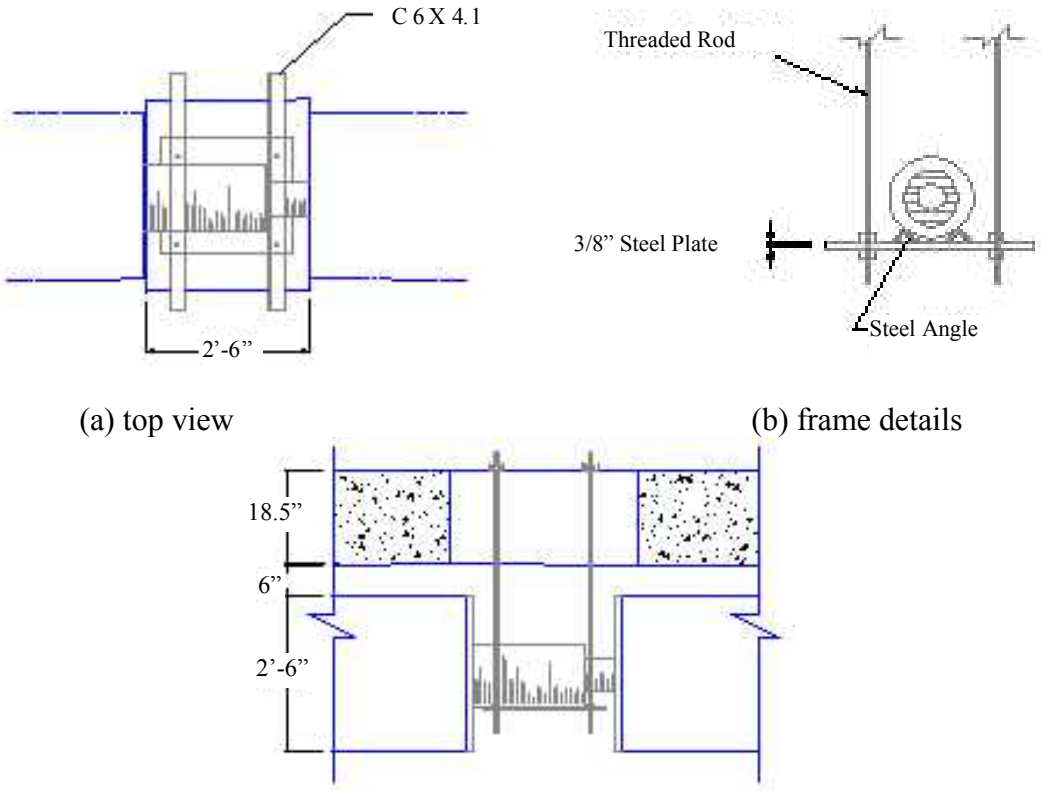


(a) top view (b) frame details

(c) side view

**Figure 3.8.** Details of holding frame for the middle jack.

**Figure 3.9.** Placing the middle jack.

**Figure 3.10.** Photo showing piers test setup.

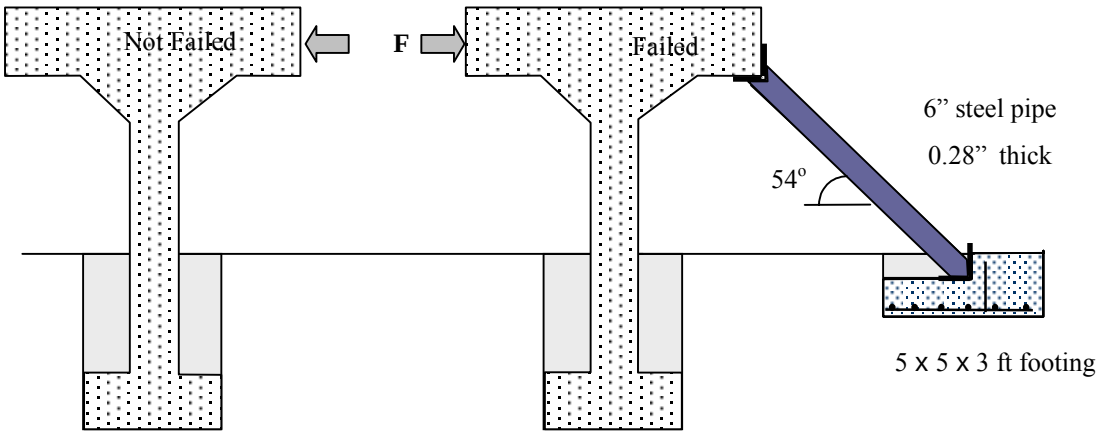


**Figure 3.11.** Details of the columns bracing system.

**Figure 3.12.** Set up for jacking the decks.

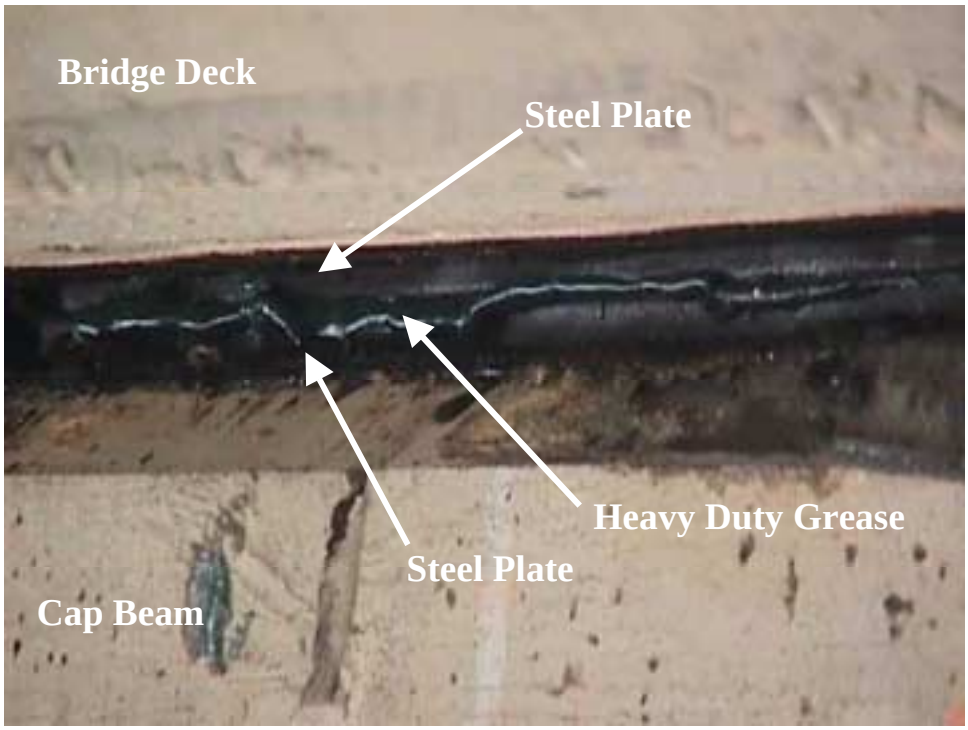


**Figure 3.13.** Steel plates assembly to reduce deck/cap beam friction.

## 3.4. INSTRUMENTATION

Instrumentation of the bridge columns included strain gages to measure reinforcement strains, LVDTs to measure displacement, inclinometers to measure rotation, and a load cell to measure the applied load.

### 3.4.1. Strain Measurement

Strain measurements were achieved using electric strain gages type EA-06-250BG-120 manufactured by Vishay Measurement Group, Inc., Micro Measurement Division, Raleigh, North Carolina. The strain gages were attached to the steel and FRP reinforcement. The number of strain gages on CFRP rods for columns B2P2 and B3P2 was 18 (9 on each side). The number of strain gages on the FRP jacket was 6 (3 on each side). The layout of the strain gages for the strengthened columns is given in Appendix B. No strain gages were attached to the unstrengthened column. The stain gages on the CFRP rods were concentrated in the anchored zone of the rods to investigate anchorage performance. The strain gages were attached to the CFRP rods prior to their installation.

To attach the strain gages to the steel reinforcement, the concrete cover was chipped away about 5 in. (125 mm) from the surface of the footings and the steel reinforcement was exposed. The surface of the steel bars was smooth polished using a high-speed rotary tool. The strain gages were then bonded to the steel reinforcement and were coated using a product supplied by their manufacturer to provide them with environmental and mechanical protections. Finally, the chipped corners of the column were filled with epoxy paste. Three strain gages were attached to the steel reinforcement of each of the strengthened columns. Strain gages were also installed on the FRP jackets.

After the columns were strengthened, the four sides of the columns were covered with plywood and the excavated areas around the four columns were backfilled with soil to prevent ponding of creek water. When the columns were excavated again, it was found that a number of the strain gages were corrupted. Most of these strain gages were installed on the reinforcement under the jacket and could not be replaced. However, a number of the strain gages were still functional and gave sufficient information on the strain of the reinforcement. In the figures of Appendix B, the gages circled are the ones remain functional at the time of the test.

### 3.4.2. Displacement Measurements

Two LVDTs were used to measure the lateral displacement at the top and mid-length of each column. To measure the relative displacement of the column at these two locations, the LVDTs were mounted on a steel tower that that was anchored to the footing. Therefore, the lateral displacements due to the rotation of the footing were not accounted for in the measurements. To ensure that the LVDTs would not be damaged, they were soft-mounted on the steel tower using magnets. Details of the steel tower are shown in Figure 3.14. Photos showing the mounted LVDTs are given in Figure 3.15.

### 3.4.3. Rotation Measurement

Three inclinometers were used to measure the rotation at the top, mid-height, and the footing of each column. The inclinometers used in this project have a range of $\pm$3 degrees. The top inclinometer was attached to the cap beam while the bottom inclinometer was attached to the surface of the footing. Figure 3.16 depicts a schematic of inclinometer locations. Figure 3.17 shows a photo of an inclinometer on the surface of the footing.

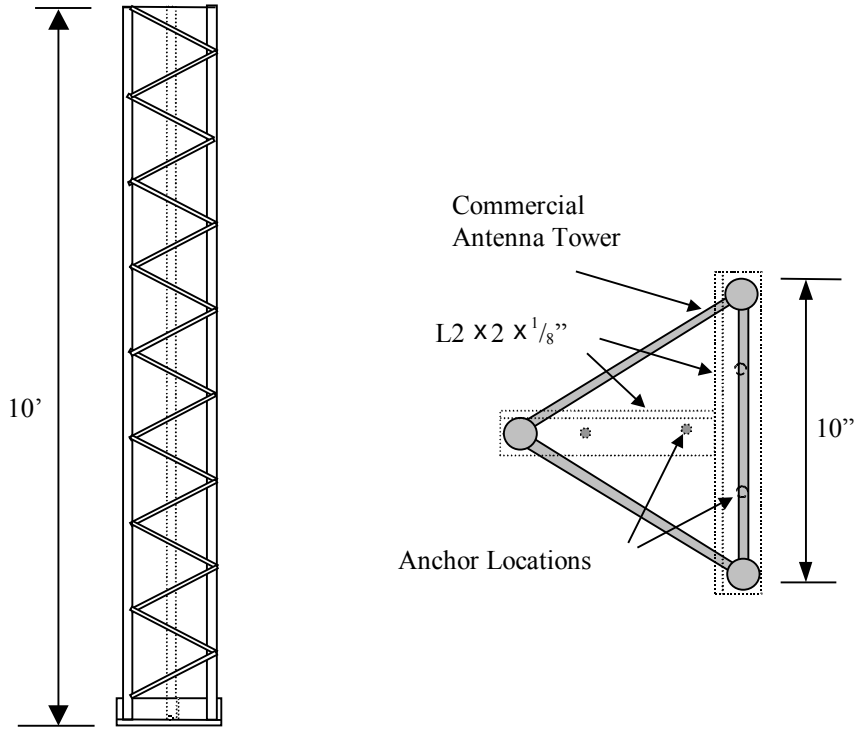


**Figure 3.14.** Details of the tower to hold the LVDTs.

(a) at the top of the column (b) at mid-height

**Figure 3.15.** Typical LVDTs locations.

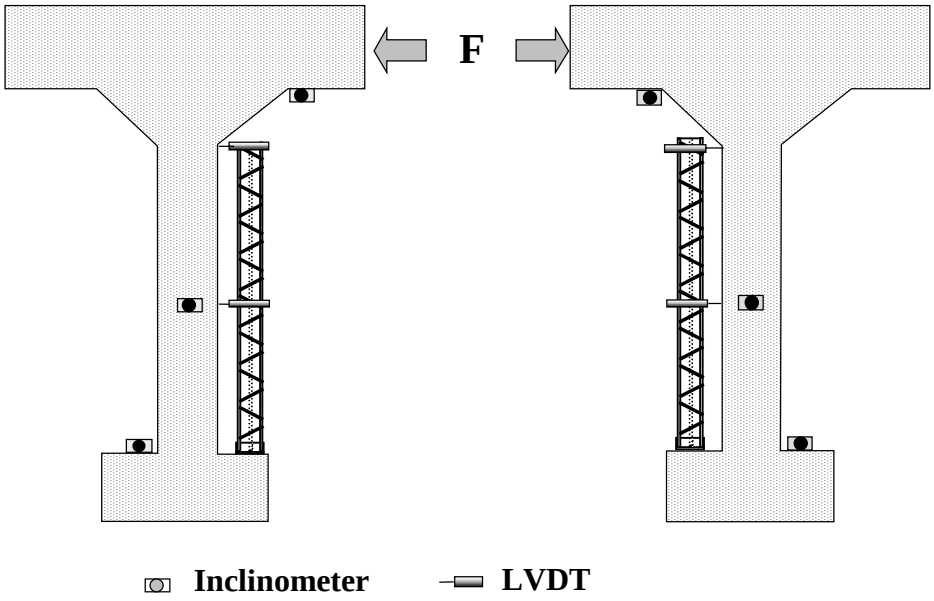


**Figure 3.16.** Typical locations of LVDTs and inclinometers for a bent test.

**Figure 3.17.** Inclinometer on the surface the footing.

### 3.4.4. Load Measurement

Load measurements were achieved using one 200-kips (90-Tonnes) capacity load cell. The load cell has a donut shape with a hollow core. For the pull-in loading condition, the load cell was placed between the hydraulic jack and the end plate and nut on the Dywidag rod. For the push-out loading condition, the load cell was placed between the hydraulic jack and the side of the cap beam.

### 3.4.5. Data Acquisition

Data was acquired using the data acquisition recreational vehicle housed at the University of Missouri-Columbia. The vehicle houses two computers with five connection boxes. Each connection box can accommodate 19 strain gages and 5 LVDT connections.

## 3.5. LOAD TEST PROTOCOL

The bridge columns were tested to failure by applying static lateral load cycles. Prior to testing, the LVDTs were adjusted and the strain gages were examined. As indicated previously, some of the strain gages did not work due to exposure to the harsh environment for over six months. Once the instrumentation was checked, initial readings were taken. For safety reasons, the first loading cycle was always a pull-in loading condition. When the desired lateral force was achieved, the system was unloaded and the hydraulic hoses were disconnected from the end jacks and connected to the middle jack. The end plate and nut of the steel rod housing the load cell were removed and the load cell was relocated between the middle jack and the side of the cap beam. A push-out load was then applied until the desired load level was achieved. These two loading cycles were repeated until the weaker column failed. The magnitude of the maximum load was increased the successive cycle based on the observations of the research team. To test the second column of the same bent, the confining frame was removed and the diagonal bracing was installed against the failed column, as shown in Figure 3.18. Load was applied in a single push-out cycle until failure of the second column was achieved.

Prior to the testing of the columns of bent 3, the bridge decks resting on the bent were jacked up using hydraulic jacks and lubricated steel plates were inserted between the cap beam and the deck slabs. This action was intended to eliminate some of the frictional forces at the top of the piers thus minimizing the superstructure/substructure interaction. The columns of bent 3 were tested in a similar fashion to that of bent 2.

**Figure 3.18.** Diagonal bracing of the failed column.

# 4. EXPERIMENTAL RESULTS

## 4.1. INTRODUCTION

The following sections present the experimental results obtained during testing to failure of the bridge columns. These include the measured load, lateral displacement, rotations, and reinforcement strains.

In general, the failure loads of tested columns were higher than expected. All the columns demonstrated a double-curvature behavior. Larger rotations and displacements were observed on the cap beams of the columns with inserted plates. Minimum interaction occurred between the bridge deck and the cap beam. As the cap beam rotated, it pushed the topping deck upward and the location of the vertical load from the weight of the deck shifted toward to the cut edge of the cap beam. This resulted in an additional moment at the top of the column caused by the eccentricity of the vertical load.

To simplify data interpretation, the applied load was assigned a positive sign for push-out loading condition and a negative sign for pull-in loading condition. Also, the outward displacement of the columns was positive while the inward displacement was negative. Similarly, outward rotation was positive and inward rotation was negative. The sign convention used hereafter is shown in Figure 4.1.

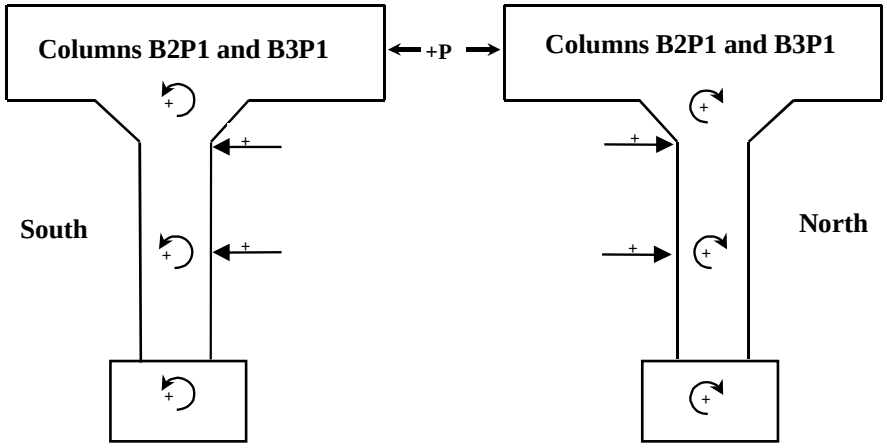


**Figure 4.1.** Sign convention.

## 4.2. BENT 2

The columns of this bent were tested in nine alternate pull/push loading cycles with the first being a pull-in loading cycle. In the first two cycles, the maximum applied load was 12.5 kips (55.6 kN). No significant column response was measured in this cycle. Cycle 5 was terminated prematurely to adjust some of the setup components. Accordingly, cycles 1, 2, and 5 are not reported herein. Table 4.1 gives the maximum loads achieved for the rest of the loading cycles.

Failure of column B2P1 occurred in cycle 8, after which the diagonal bracing was installed against it and a push-out load was applied until failure of column B2P2 was achieved. Only the response of Column B2P2 is reported for the last loading cycle.

**Table 4.1.** Description of the Loading Cycles for Bent 2.

| Cycle | Configuration | Max. Load Kips (kN) |
|---|---|---|
| 3 | pull-in | -20 (-89) |
| 4 | push-out | 17 (76) |
| 6 | pull-in | -60 (-267) |
| 7 | push-out | 80 (356) |
| 8 | pull-in | -59 (-262) |
| 9 | push-out | 81 (360) |

### 4.2.1. Test Results of Column B2P1

#### 4.2.1.1. Displacement and Rotation

Figures 4.2 and 4.3 show the measured displacement at the mid-height and top of the column. Figures 4.4 through 4.6 depict the measured rotation at the top, mid-height and the footing of the column. As shown in these figures, up to the second loading cycle, the column exhibited elastic behavior with no significant residual deformation. The column started to behave in a non-linear fashion at load cycle 6 when the load exceeded 25 kips (111 kN). The first crack was observed during load cycle 6 on the north side of the column at the column/footing intersection at approximately 30 kips (156 kN). As the load was increased, a second crack occurred on the south side of the column at a load level of 45 kips (200 kN). This was accompanied by a sudden increase in displacements and rotations. The crack was located about 2.9 ft (0.88 m) from the bottom of the haunch. Cracks occurring in this manner (at the bottom on the north side and at the top on the south side) indicated a double-curvature behavior of the column.

According to the original bridge plans, the steel reinforcement of the haunch extended into the column and was terminated approximately 3 ft (0.92 m) from the end of haunch. Accordingly, the upper 3 ft (0.92 m) portion of the column had twice the amount of reinforcement as that of the lower part of the column. This may explain why the crack on the south side occurred at this location, which corresponded to the location of haunch reinforcement termination. When the load was approximately 60 kips (267 kN), the column started to undergo continuous deformation under constant load. The measured increase in rotation at column mid-height and at the top was similar in magnitude while the rotation measured at the footing was relatively small. This behavior indicated that a plastic hinge had formed at the base of the column. This mode of failure was expected since the amount of steel reinforcement at the base of the column was half that at the top. When the load was removed, the column attained its initial position due to the high axial load. Very small residual rotations and displacements were observed when the load was removed. The load was then applied in a push-out condition. Similar to the behavior of cycle 6, a crack was detected at the level of the footing at approximately 50 kips (222 kN). A second crack was detected at 65 kips (289 kN) on the south side of the column. The crack was located 4 ft (1.2 m) from the end of the haunch, as shown in Figure 4.7. The loads measured at column cracking during loading cycle 7 were higher than those measured in loading cycle 6 for comparable cracks.

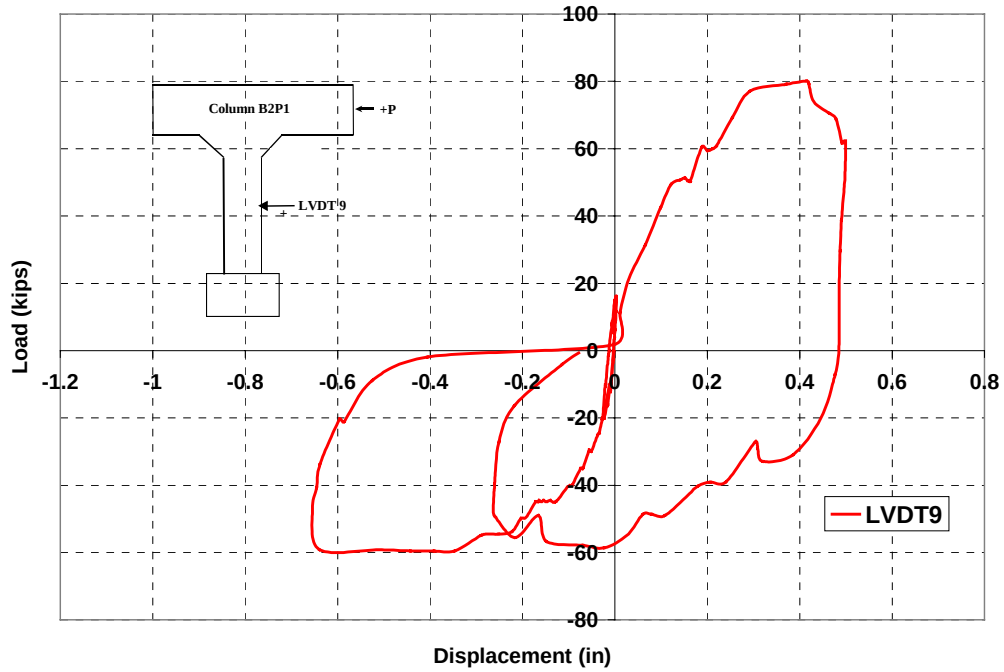


Note: 1 kip = 4.45 kN; 1 in = 25.4 mm

**Figure 4.2.** Displacement at mid-height of Column B2P1.

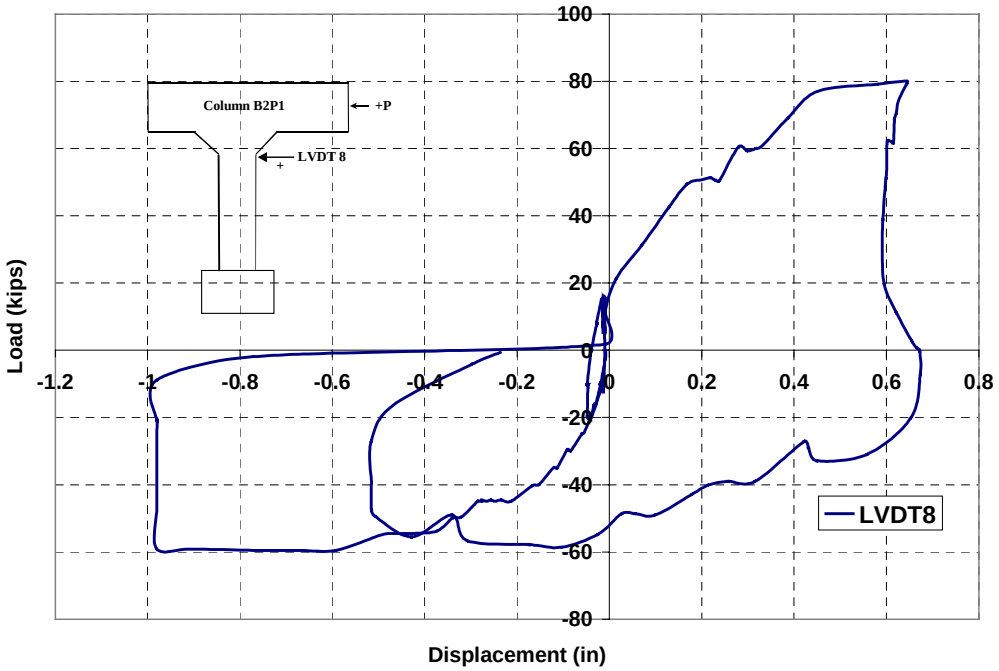


Note: 1 kip = 4.45 kN; 1 in = 25.4 mm

**Figure 4.3.** Displacement at top of Column B2P1.

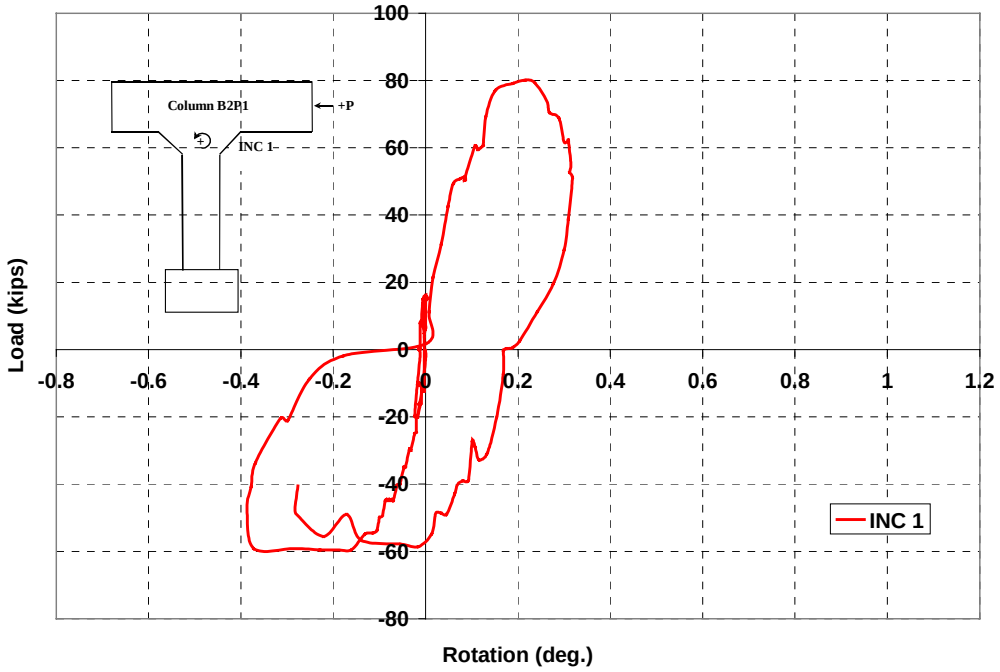


Note: 1 kip = 4.45 kN; 1 in = 25.4 mm

**Figure 4.4.** Measured rotation at the top of Column B2P1.

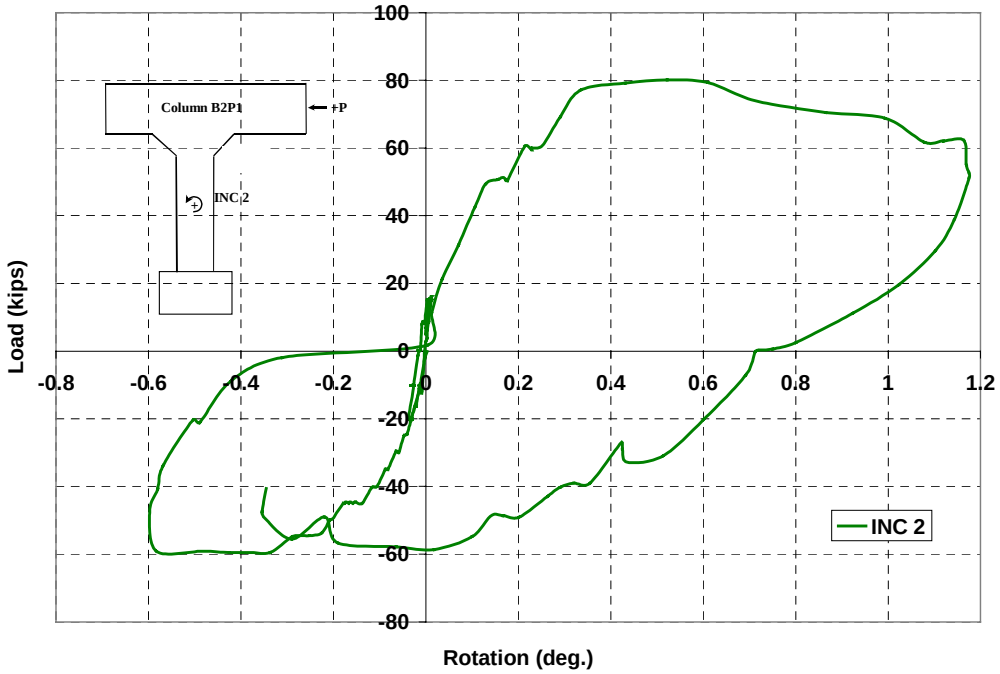


Note: 1 kip = 4.45 kN; 1 in = 25.4 mm

**Figure 4.5.** Measured rotation at mid-height of Column B2P1.

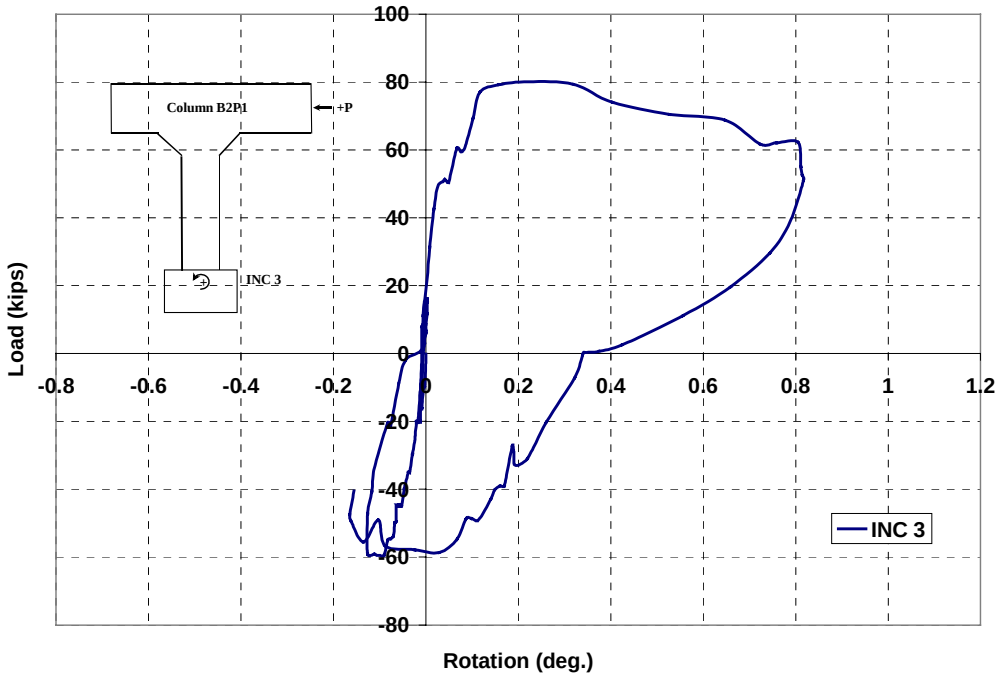


Note: 1 kip = 4.45 kN

**Figure 4.6.** Measured rotation at the footing of Column B2P1.

(a) general view (b) side view showing crack extension

**Figure 4.7.** Crack on Column B2P1.

The load was increased gradually until it reached 80 kips (356 kN) where the top crack started to widen significantly and the column started to undergo continuous deformation. Similar behavior was observed at the base of the column. The continuous rotation of the footing under constant load indicated that the soil under the footing had failed. A final pull-in load cycle was applied. The load could not be increased beyond 59 kips (262 kN).

#### 4.2.1.2. Reinforcement Strain

No strain data were available for the unstrengthened column.

### 4.2.2. Test Results of Column B2P2

#### 4.2.2.1. Displacement and Rotation

Figures 4.8 and 4.9 show the measured displacement at the mid-height and the top of column B2P2, respectively. Figures 4.10 through 4.12 provide the measured rotations at the top, mid-height, and the base of the column, respectively. During the first six loading cycles, the measured displacements of column B2P2 were smaller than those measured on of column B2P1. The behavior of column B2P2 was elastic up to load cycle 8 with no major stiffness reduction. Cracks could not be detected on this column due to the composite jacket.

It should be noted that the clear length of this column (9.75 ft or 3 m) was smaller than that of B2P1 (12 ft or 3.7 m). Accordingly, at any load level, the moments due to the applied load was expected to be smaller than those achieved in column B2P1.

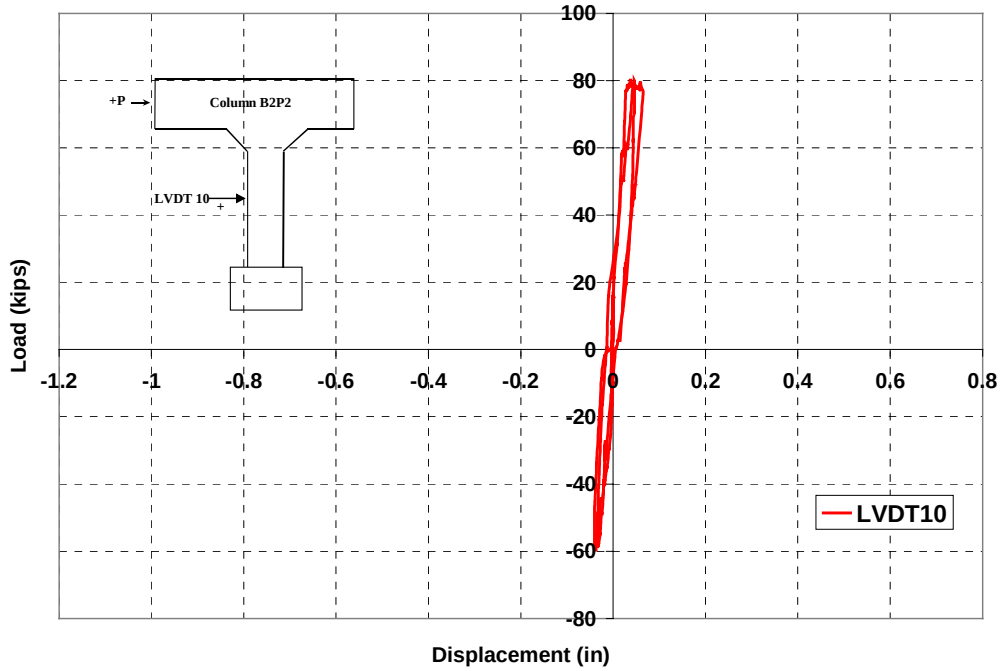


Note: 1 kip = 4.45 kN; 1 in = 25.4 mm

**Figure 4.8.** Displacement at mid-height of Column B2P2.

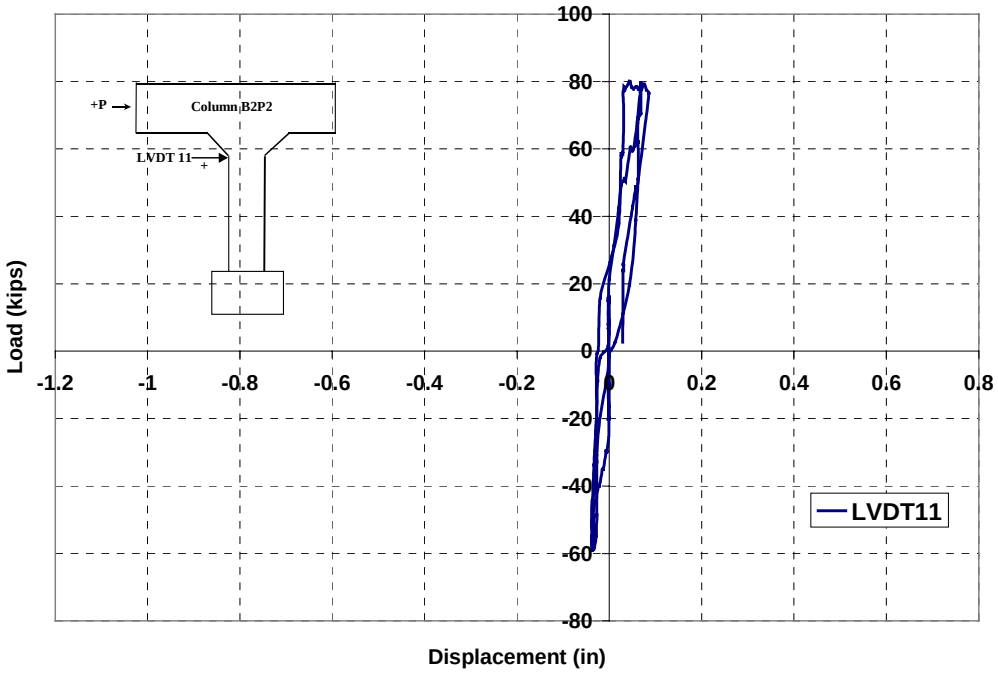


Note: 1 kip = 4.45 kN; 1 in = 25.4 mm

**Figure 4.9.** Displacement at top of Column B2P2.

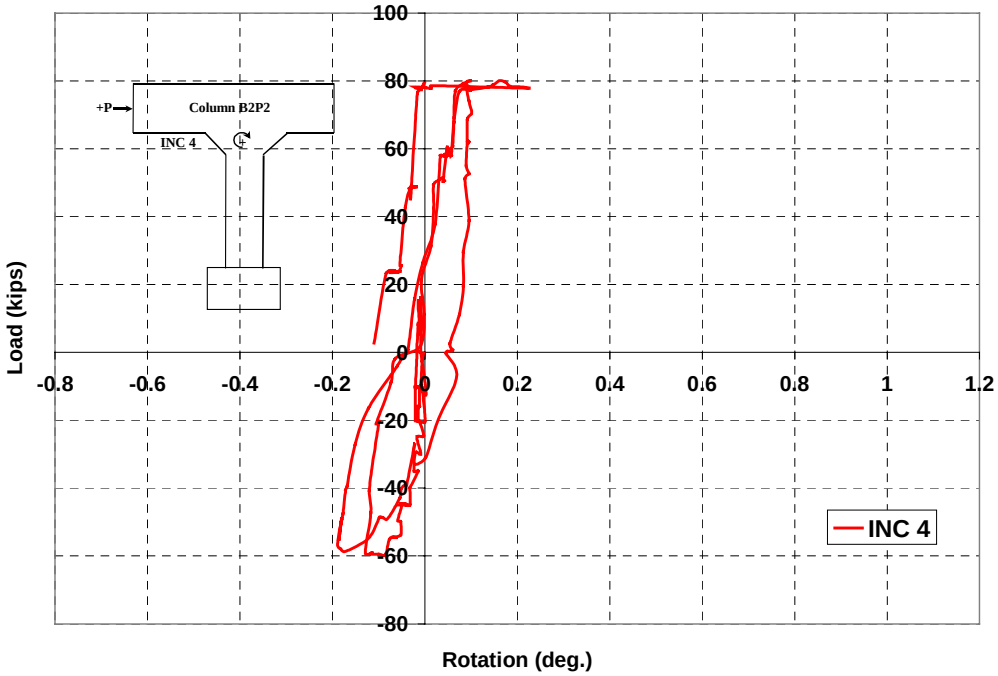


Note: 1 kip = 4.45 kN

**Figure 4.10.** Measured rotation at the top of Column B2P2.

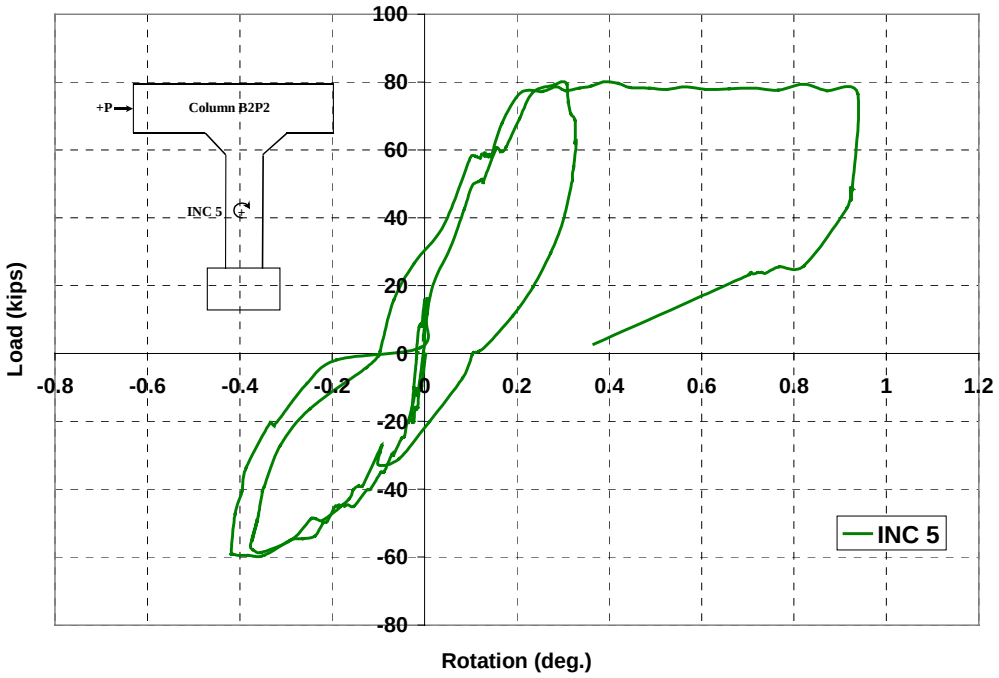


Note: 1 kip = 4.45 kN

**Figure 4.11.** Measured rotation at mid-height of Column B2P2.

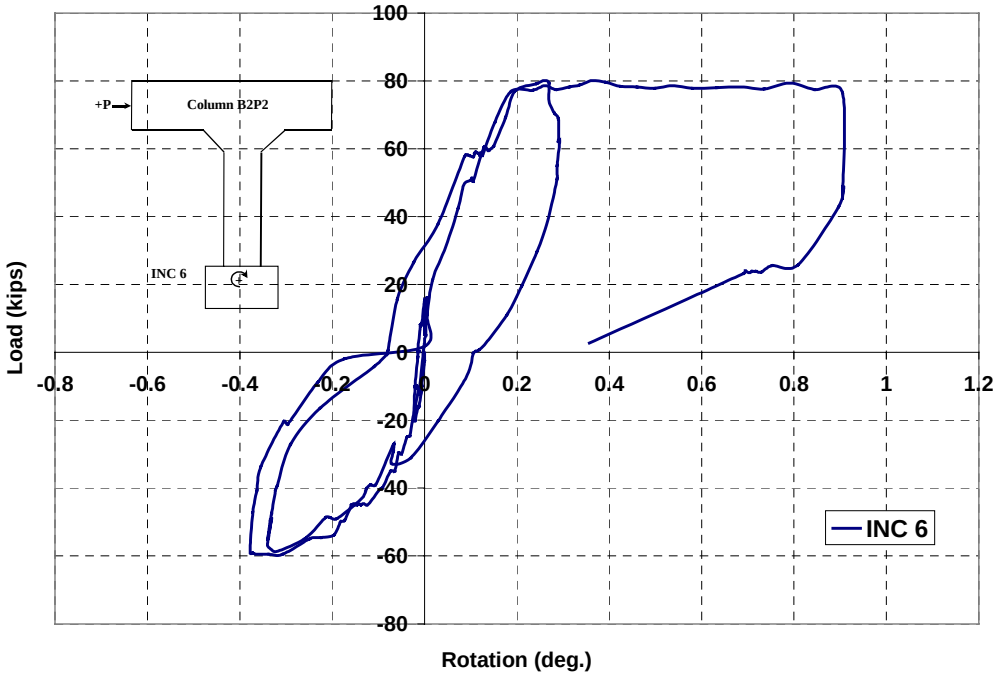


Note: 1 kip = 4.45 kN

**Figure 4.12.** Measured rotation at the footing of Column B2P2.

After failure of column B2P1, the diagonal bracing was installed against it and load was applied again in a push-out condition until failure of column B2P2 was achieved. Failure of column B2P2 was initiated by a crack that occurred at the end of the haunch approximately 3 inches above the location where the mounted rods were terminated, as shown in Figure 4.13. When the crack occurred, the rotation of the cap beam reduced significantly and the whole column went through a continuous rotation with no increase in load carrying capacity. The measured rotation at failure at the top was much smaller than those measured at mid-height and on the footing, which were almost identical. This indicated that a plastic hinge formed at the top of the column. In addition, the continuous rotation of the footing at failure indicated that the soil had failed. The maximum load measured at failure was 81 kips (360 kN).

#### 4.2.2.2. Reinforcement Strain

Figures 4.14 and 4.15 report the measured strains on the north and south sides of column B2P2 during the last three loading cycles. As shown in these figures, the strain gages on the two opposite sides of the column measured opposite strains. The measured tensile strains were significantly higher than the compressive strains indicating that cracks had formed at the base of the column. At loading cycle 7 (push-out), the maximum applied load was 80 kips (356 kN) and the maximum measured tensile and compressive strains were 2103 and –224 με, respectively. Higher residual strains were measured on the north side after the column was unloaded. In loading cycle 9, only column B2P2 was loaded and the failure load of 81 kips (360 kN) was similar to that of column B2P1 (cycle 7). The maximum tensile and compressive strains at load cycle 9 were 1325 and –440 με, respectively. These strains were smaller than those measured in cycle 7. This could be related to the softening of the soil due to cyclic loading that reduced its rotational stiffness and resulted in moment redistribution. The measured strains at failure became constant due to the plastic behavior of the soil.

**Figure 4.13.** Crack at failure of column B2P2.

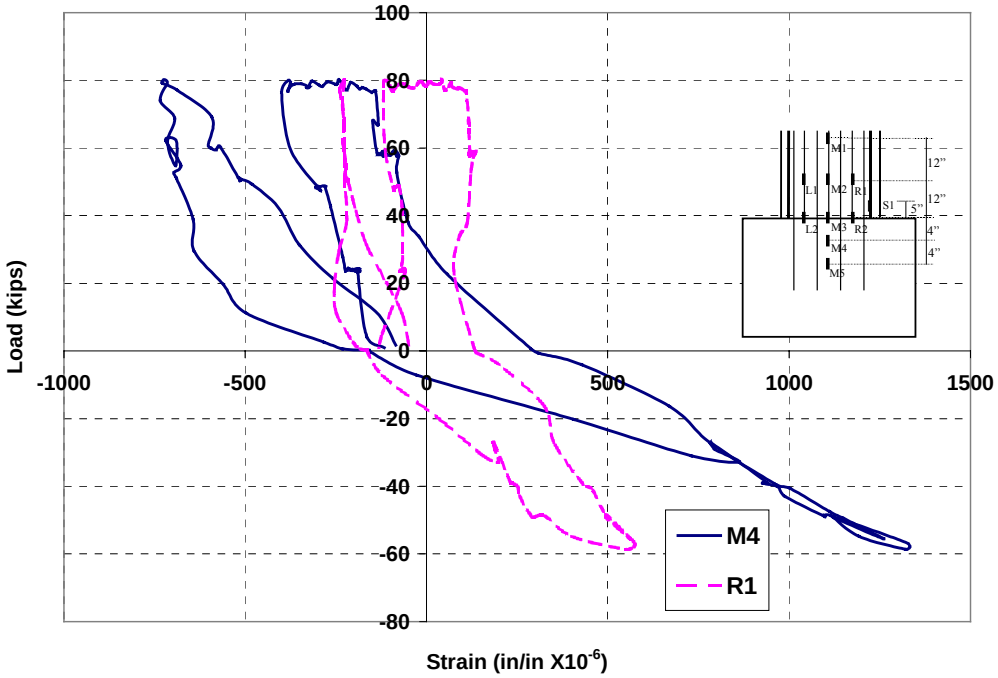


**Figure 4.14.** Measured strains on the north side of Column B2P2.

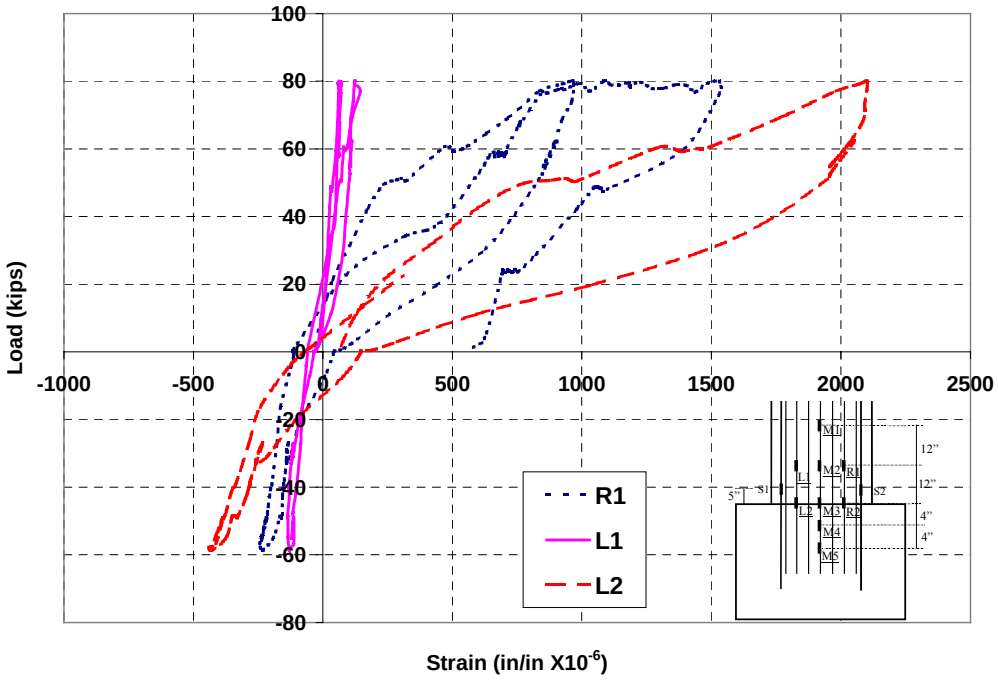


**Figure 4.15.** Measured strains on the south side of Column B2P2.

## 4.3. BENT 3

Prior to testing of the columns of this bent, the decks resting on the bent were jacked up using hydraulic jacks and lubricated steel plates were inserted between the cap beam and the deck slabs to minimize the friction between them. The columns were tested in eight loading cycles. In the first cycle, the maximum applied load was 16.5 kips (73 kN). No significant response was measured on the columns during this cycle. Cycle 7 was terminated prematurely to adjust some of the setup components. These two cycles are not reported herein. Table 4.2 gives the loading condition and the maximum applied load in each cycle.

Failure of column B3P1 was achieved in loading cycle 8. The diagonal bracing was then installed against it. However, due to some technical difficulties, the final loading cycle (cycle 9) was carried out the following day. The results of the final loading cycle are, therefore, reported separately. Only the response of column B3P2 is reported for cycle 9.

**Table 4.2.** Reported Loading Cycles and Maximum Loads for Bent 3.

| Cycle | Type | Max Load kips (kN) |
|---|---|---|
| 2 | pull-in | -21 (-93) |
| 3 | push-out | 20 (89) |
| 4 | pull-in | -29 (-129) |
| 5 | push-out | 31 (138) |
| 6 | pull-in | -43 (-191) |
| 8 | push-out | 51 (227) |

### 4.3.1. Test Results of Column B3P1

#### 4.3.1.1. Displacement and Rotations

The observed behavior of this column during loading cycles 2 and 3 was elastic with small residual deformations measured after the load was removed. The column started to demonstrate instability at higher load levels and the measured displacements and rotations kept increasing without a significant increase in the load capacity. The displacement and rotation of the cap beam relative to the topping deck could be easily detected, as shown in Figures 4.16 and 4.17. Figures 4.18 and 4.19 illustrate the measured displacement at the mid-height and at the top of the column, respectively. Figures 4.20 through 4.22 illustrate the measured rotations at the top, mid-height, and the footing, respectively. From these figures, it can be seen that at load cycle 6 (pull-in) the whole column experienced a rigid body rotation. This indicated that the soil had failed and lost its rotational stiffness. The maximum load achieved in this cycle was 43 kips (191 kN). Relatively, higher residual deformations were measured after the load was removed. The column exhibited similar behavior in the last loading cycle (push-out) and the maximum load at failure was 51 kips (227 kN).

#### 4.3.1.2. Reinforcement Strain

The measured reinforcement strains in the longitudinal direction during the last two loading cycles on the north and south sides are reported in Figures 4.23 and 4.24, respectively. The measured strains were relatively small. However, this strain level is higher than the tensile

strain of concrete at cracking (approximately 130 με) indicating that some cracks could have developed at the base of the column. The measured strains on the composite jacket in the hoop direction were very small and are therefore not reported.


(a) Push-out loading cycle (b) Pull-in loading cycle

**Figure 4.16.** Relative movement of the cap beam.

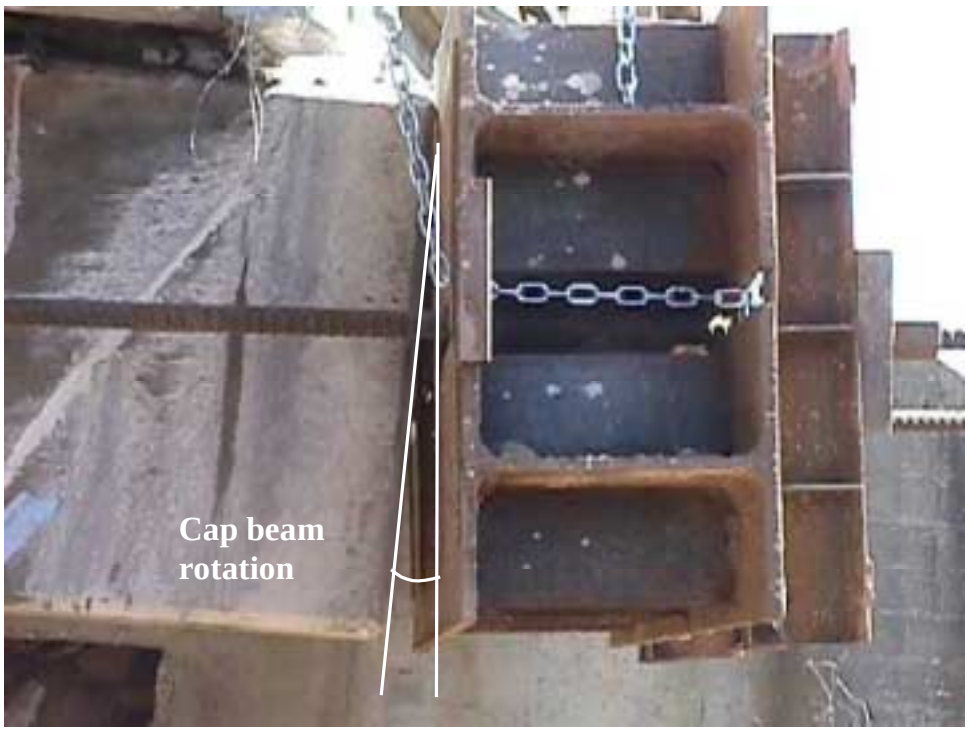


**Figure 4.17.** Cap beam rotation

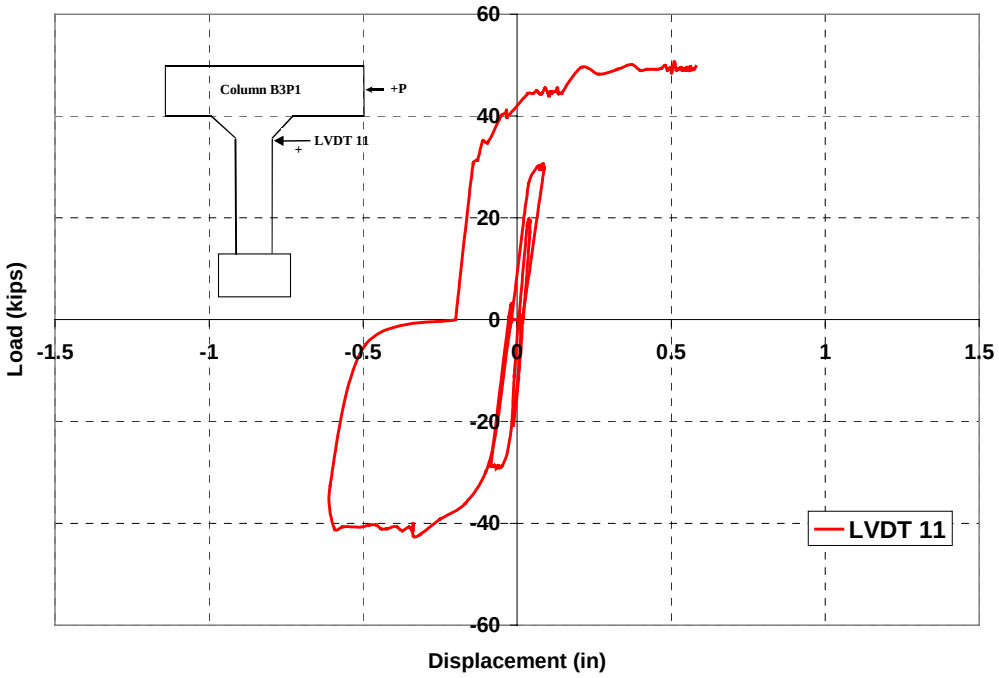


Note: 1 kip = 4.45 kN; 1 in = 25.4 mm

**Figure 4.18.** Displacement at mid-height of Column B3P1.

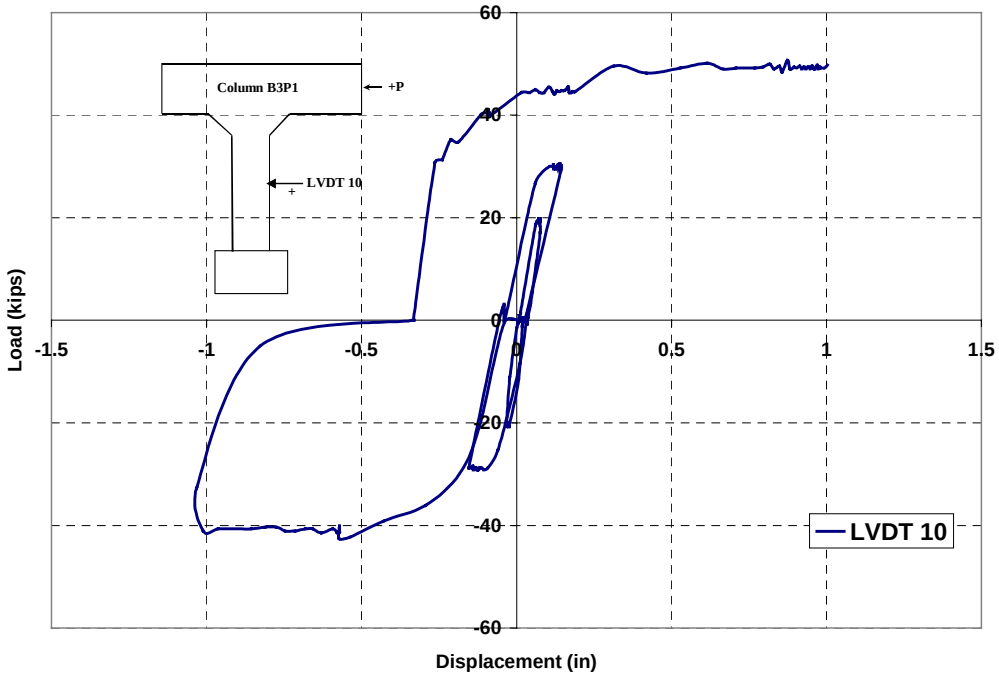


Note: 1 kip = 4.45 kN; 1 in = 25.4 mm

**Figure 4.19.** Displacement at the top of Column B3P1.

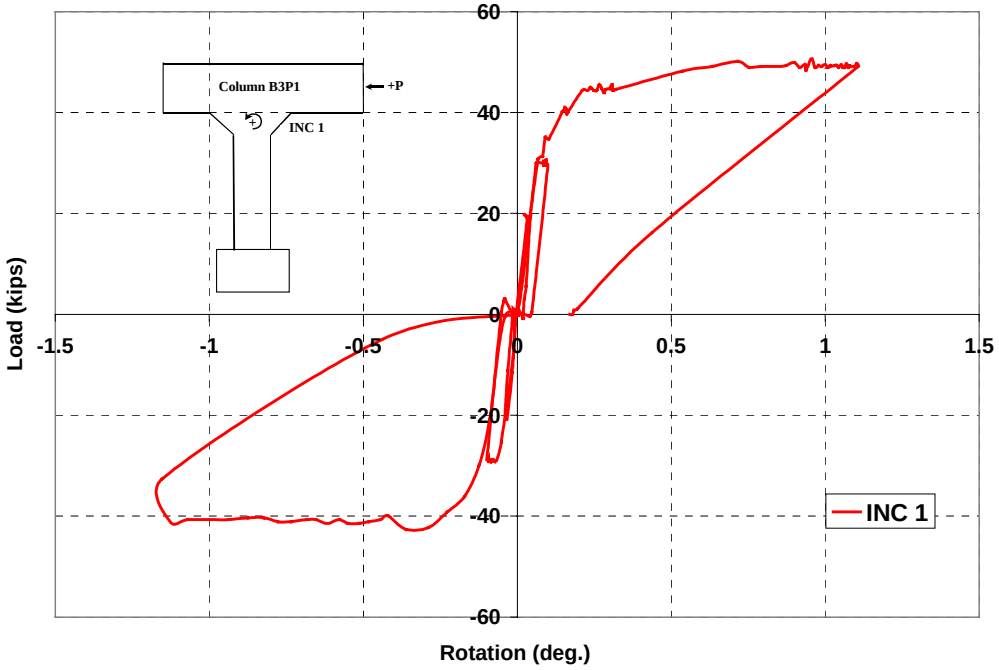


Note: 1 kip = 4.45 kN

**Figure 4.20.** Measured rotation at the top of Column B3P1.

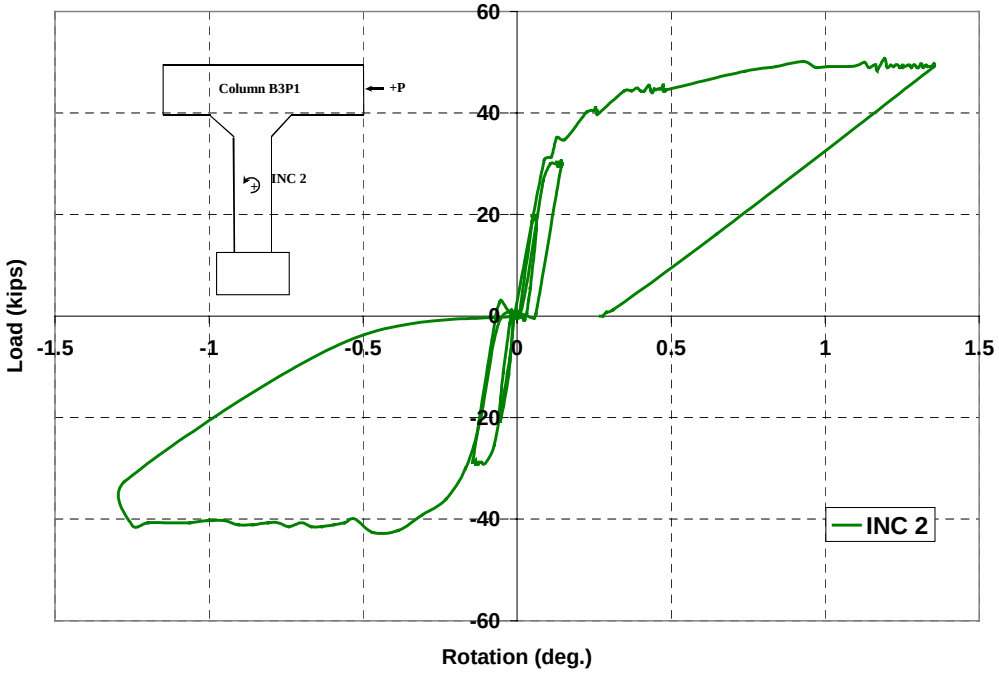


Note: 1 kip = 4.45 kN

**Figure 4.21.** Measured rotation at mid-height of Column B3P1.

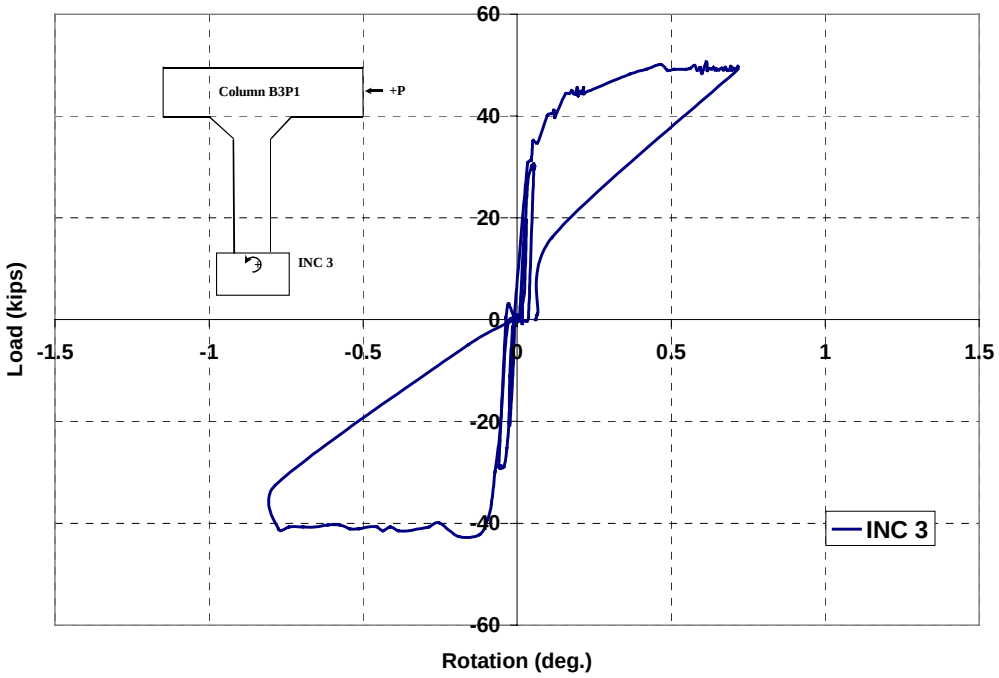


Note: 1 kip = 4.45 kN

**Figure 4.22.** Measured rotation at the footing of Column B3P1.

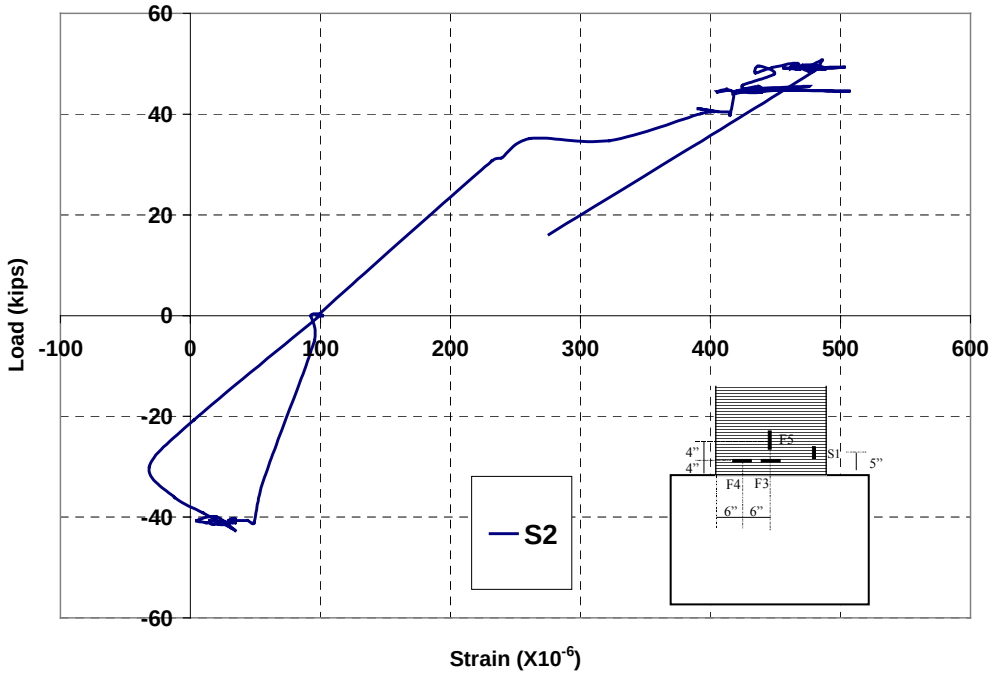


**Figure 4.23.** Measured strain on the north side of Column B3P1.

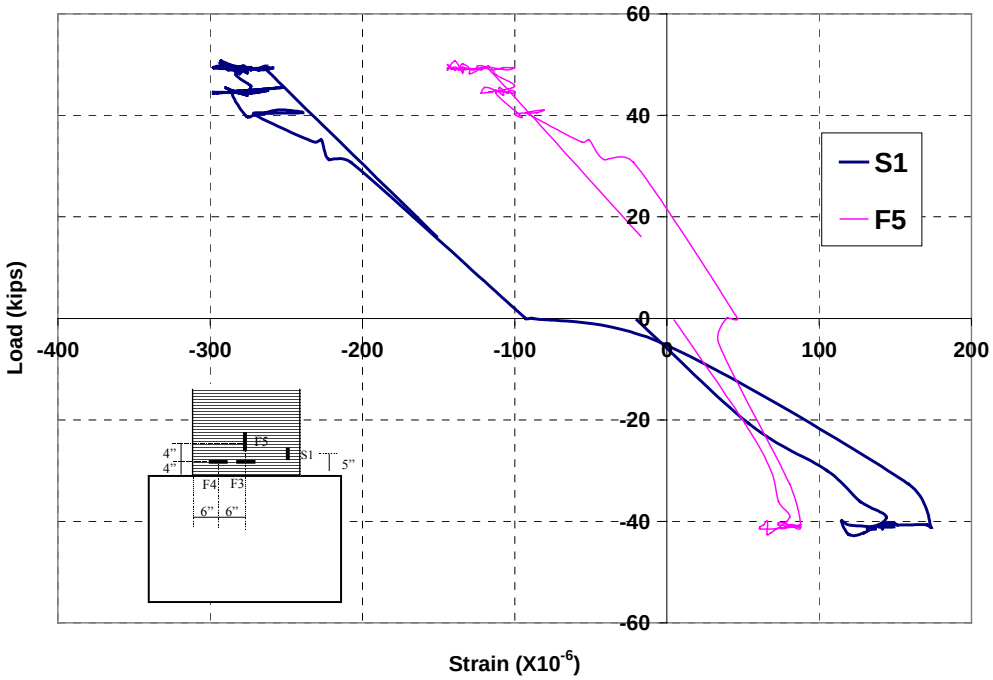


**Figure 4.24.** Measured strain on the south side of Column B3P1.

### 4.3.2. Test Results of Column B3P2

This column was the shortest (6.5 ft or 2 m) amongst the bridge columns and its footing was cast into the bedrock. Figures 4.25 and 4.26 show the measured displacements of this column. Figures 4.27 through 2.29 show the measured rotations. The behavior of the column was elastic up to loading cycle 6 (pull-in), at which a crack was detected at maximum load. The crack was located on the north side of the column at the level of the footing. Small residual deformations were measured on the column after the load was removed. Two additional cracks were detected during loading cycle 8. The cracks occurred at maximum load and were located at the top and the base of the column, locations of maximum moments. The crack at the top occurred on the north side at the end of the haunch and the crack at the column base occurred on the south side at the level of the footing. The behavior of the column was elastic during this load cycle with no residual deformations measured when the column was unloaded. Very small rotations were measured on the footing in during all loading cycles.

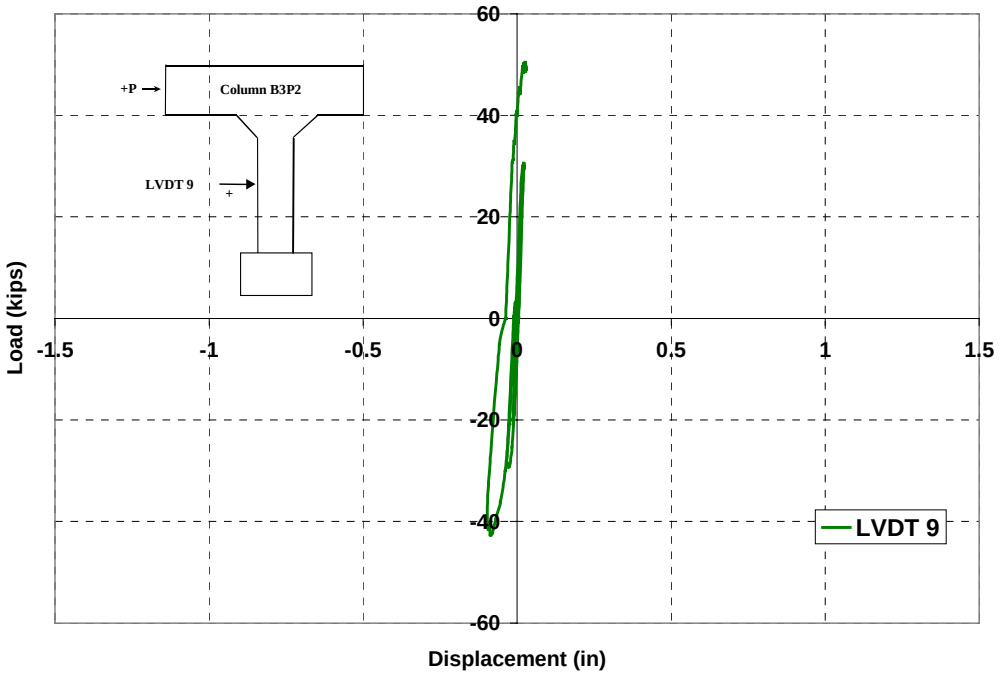


Note: 1 kip = 4.45 kN; 1 in = 25.4 mm

**Figure 4.25.** Displacement at mid-height of Column B3P2.

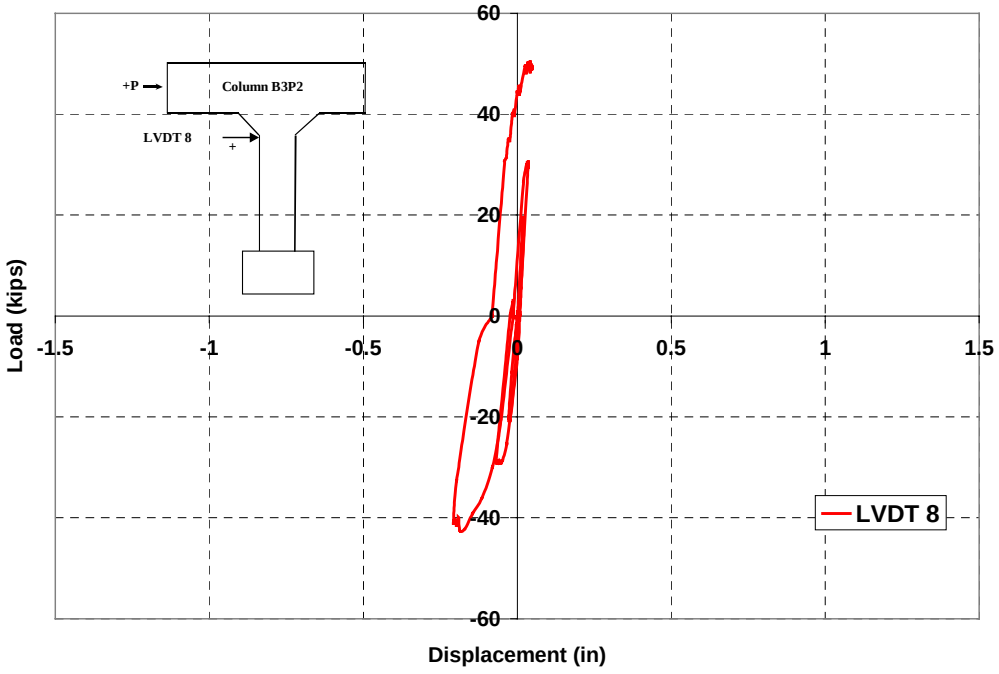


Note: 1 kip = 4.45 kN; 1 in = 25.4 mm

**Figure 4.26.** Displacement at top of Column B3P2.

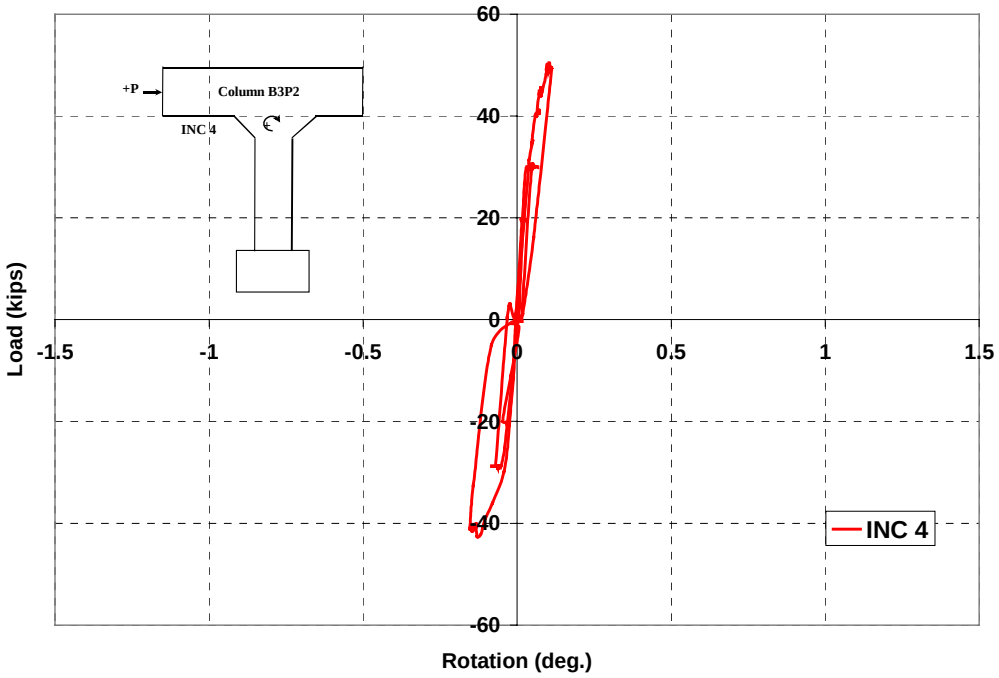


Note: 1 kip = 4.45 kN

**Figure 4.27.** Measured rotation at the top of Column B3P2.

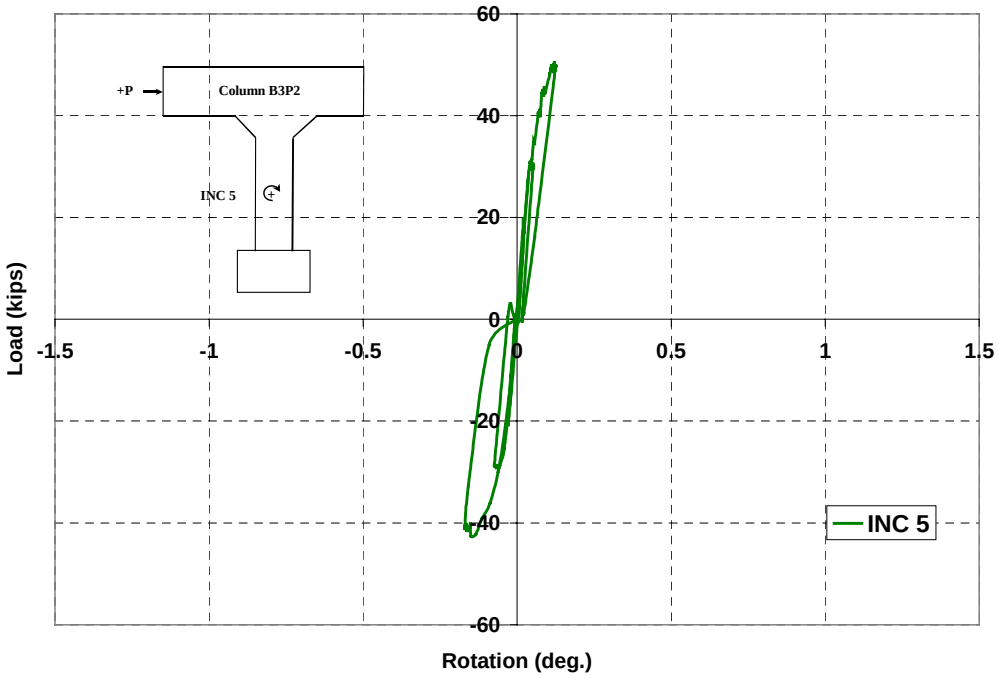


Note: 1 kip = 4.45 kN

**Figure 4.28.** Measured rotation at mid-height of Column B3P2.

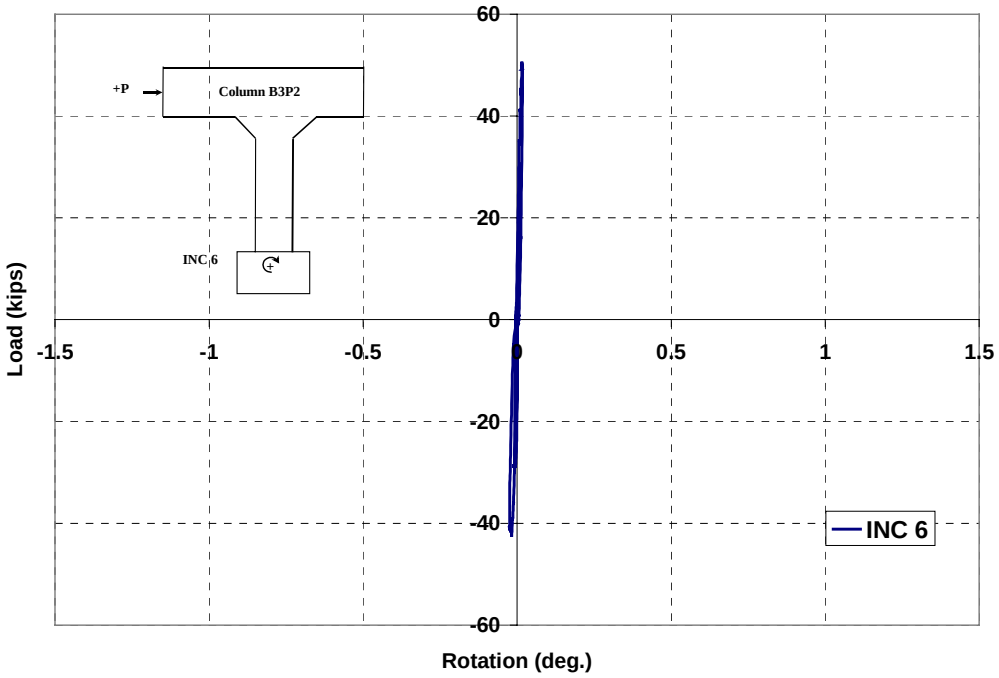


Note: 1 kip = 4.45 kN

**Figure 4.29.** Measured rotation at the footing of Column B3P2.

Figures 4.30 and 4.31 illustrate the measured displacements and rotations during the last loading cycle (push-out). Larger deformations were measured on this loading cycle when compared to the previous cycle and the measured rotation of the footing was very small. As the load was increased, the crack at the top started to open indicating a plastic hinge formation, as shown in Figure 4.32. Due to the large rotation of the cap beam, the vertical force caused by the weight of the deck shifted toward the edge of the cap beam, as shown in Figure 4.33. This behavior resulted in an additional moment that acted at the top of the column. Failure was initiated by the rupture of the FRP rods at the base of the column at 86 kips (382 kN), as shown in Figure 4.34. A larger moment developed at the base of the column due to the plastic hinge that formed at the top of the column and the large rotational stiffness of the footing. Reinforcement Strain. Figures 4.35 and 4.36 show the measured reinforcement strains on the north and south sides of the column. The maximum measured tensile strain at failure was 9300 με while the measured compressive strain was approximately 2700 με.

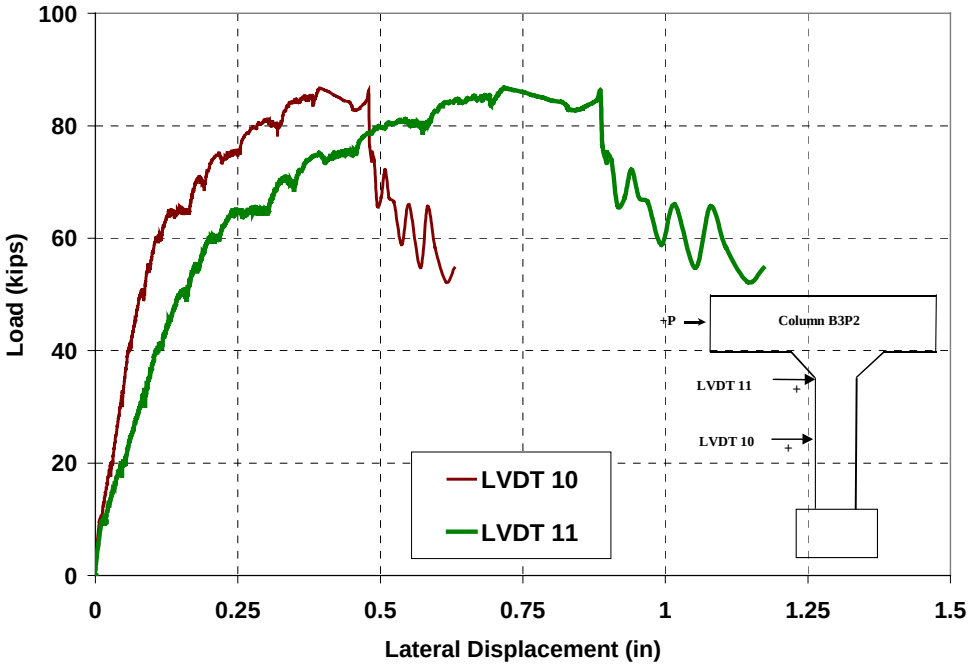


Note: 1 kip = 4.45 kN; 1 in = 25.4 mm

**Figure 4.30.** Measured displacement at final loading cycle of Column B3P2.

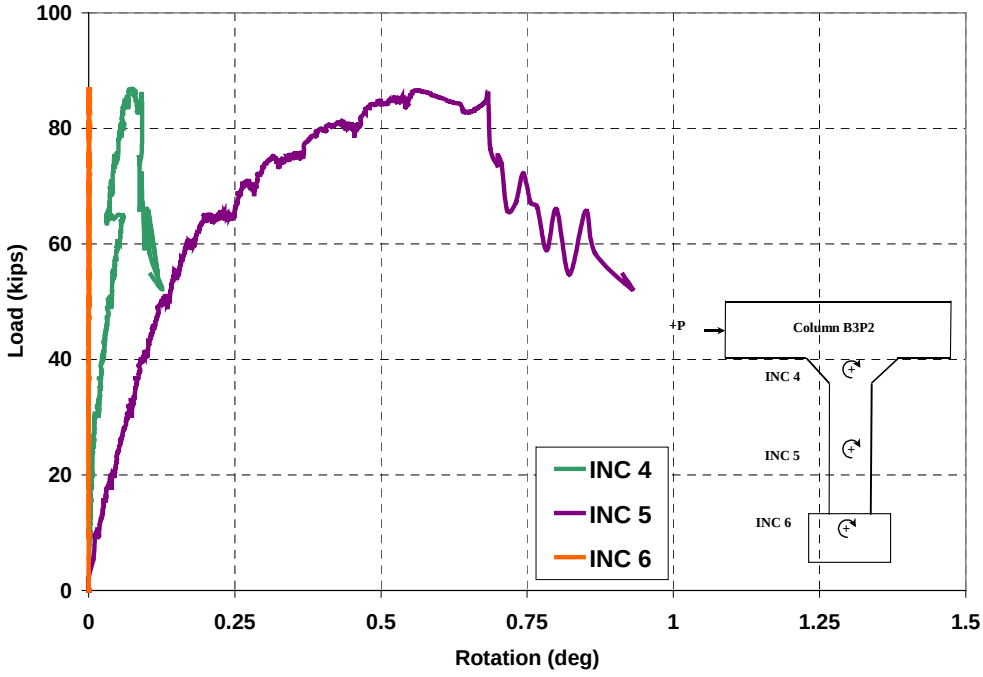


Note: 1 kip = 4.45 kN

**Figure 4.31.** Measured rotation at final loading cycle of Column B3P2.


**Figure 4.32.** Rotation of the cap beam relative to the topping deck.

**Figure 4.33.** Crack at column/haunch intersection at failure.

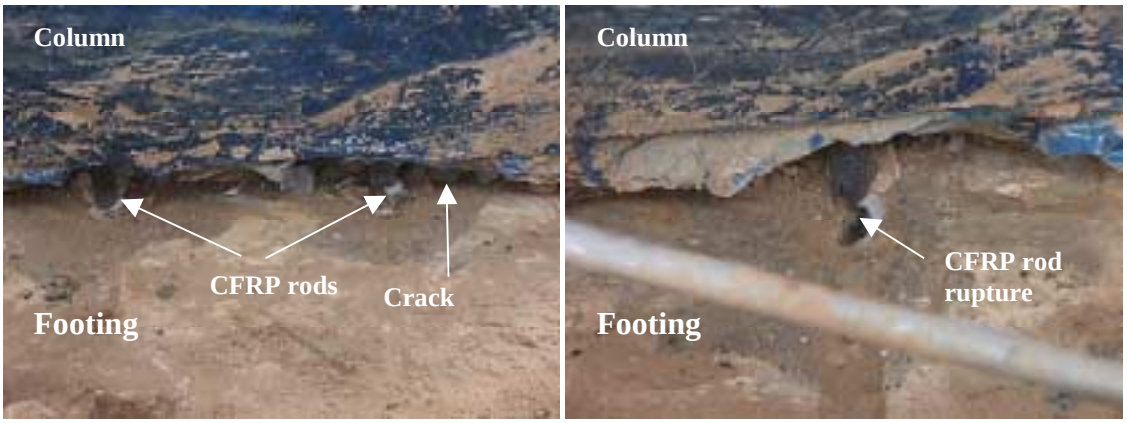


(a) Crack at the base of the column (b) Rupture of the CFRP bar

**Figure 4.34.** Rupture of NSM CFRP rods Column B3P2.

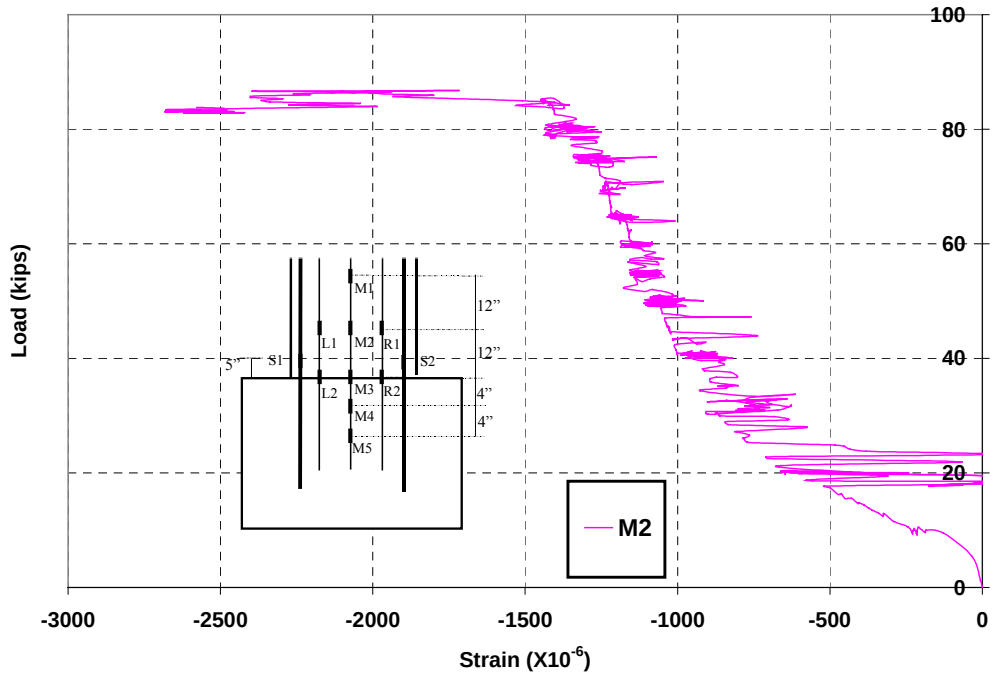


Note: 1 kip = 4.45 kN; 1 in/in = 1 mm/mm

**Figure 4.35.** Measured strain on the north side of Column B3P2 in the final cycle.

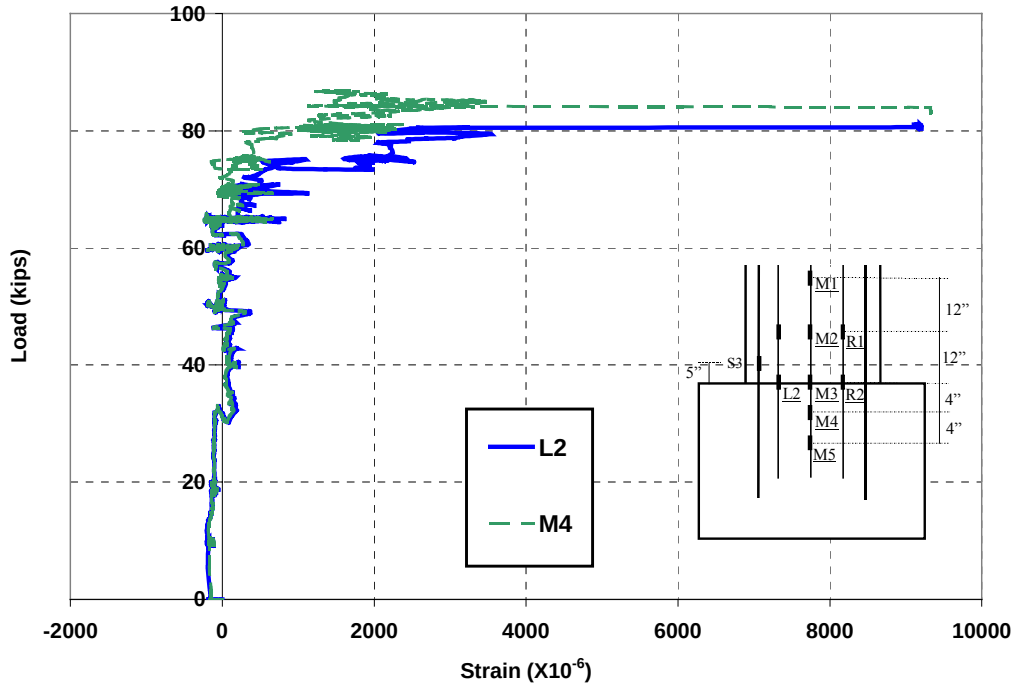


Note: 1 kip = 4.45 kN; 1 in/in = 1 mm/mm

**Figure 4.36.** Measured strain on the south side of Column B3P2 during the final cycle.

# 5. ANALYSIS AND DISCUSSION OF TEST RESULTS

## 5.1. INTRODUCTION

The main objective of this chapter is to determine the effectiveness of NSM FRP strengthening technique for improving the flexural capacity of RC columns. Strength analysis procedure for NSM FRP strengthened columns was presented earlier in chapter 2. The influence of the amount of NSM reinforcement on the axial load-moment interaction for a rectangular column section of given geometry and material properties was investigated. Theoretical capacities of the strengthened columns were calculated based on more representative material properties and results were compared with the experimental ones. The contribution of FRP jacketing was ignored for capacity calculation.

## 5.2. AXIAL LOAD-MOMENT INTERACTION

### 5.2.1. Influence of the Amount of NSM FRP Rods

The complete axial load-moment interaction diagram for a rectangular RC section strengthened with NSM FRP rods can be determined using the design procedure outlined in Appendix A. To achieve this, the axial load is varied from zero axial force to the maximum axial capacity given as follows:

$$P_{max} = 0.85f_c^{'}(A_g - A_s - A_{ft}) + A_s f_y \qquad (5.1)$$

In which $A_g$ is the gross area of the RC concrete section, and $A_{ft}$ is the total area of NSM reinforcement. Due to the lower stiffness modulus of FRP rods, their contribution in compression is minimal and could conservatively be ignored. Initially, the depth of neutral axis, reinforcement strains, and the moment capacity are determined based a maximum concrete strain of 0.003 in./in (or mm/mm), which corresponds to a failure mode governed by concrete crushing. If the FRP strain at failure exceeded its design ultimate strain, then the concrete strain at failure is less than 0.003 in./in (or mm/mm). In this case, the maximum concrete strain at failure is determined through iterations to achieve the design ultimate strain of FRP reinforcement. This behavior represents a failure mode governed by FRP rupture. Figure 5.1 shows the axial load-moment interaction diagram of a RC rectangular column strengthened with different ratios of NSM FRP reinforcement $\rho_{nsm}$ defined as follows:

$$\rho_{nsm} = \frac{A_{ft}}{A_g} \qquad (5.2)$$

Calculations were based on the geometry of a bridge column, concrete strength of 5,000 psi (34.5 MPa), and steel yield strength of 43,333 psi (299 MPa) chosen to reflect the actual material properties as will be discussed later.

Figure 5.1 clearly shows that when the axial load is below the balanced failure load $P_b$, defined as the axial load at which concrete crushing and steel yielding occur simultaneously, NSM FRP rods can significantly improve the moment capacity of the column. Gravity columns

are commonly designed to carry axial loads that are typically less than $P_b$, therefore most of these columns fall into this category. In all the diagrams of Figure 5.1, the failure at zero axial loads is governed by FRP rupture. As the amount of NSM FRP was increased, the failure mode changed from FRP rupture to concrete crushing. The balanced axial load at which concrete crushing and FRP rupture occur simultaneously will be referred to $P_{bf}$. In general, for a given section, $P_{bf}$ is reduced as the amount of FRP is increased. In addition, a local peak moment value is obtained on the axial load-moment diagram at $P_{bf}$. The local peak moment is more evident for larger values of $\rho_{nsm}$. For example, for $\rho_{nsm}$= 0.1, the calculated $P_{bf}$ was 410 kips (1834 kN) and for $\rho_{nsm}$= 0.4, the calculated $P_{bf}$ was 250 kips (1112 kN). These two values are marked on Figure 5.1. The later value can be easily identified on the axial load-moment diagram.

For axial load larger than the balanced load $P_b$, the contribution of NSM rods is reduced. This is because larger portion of the section is in compression and the strain of NSM reinforcement is relatively smaller.

### 5.2.2. Influence of FRP Jacket

Axial compressive load in a RC column causes dilation of the column section that initiates spalling of concrete cover. Unless adequate transverse reinforcement is provided to confine the column section, failure may occur due to loss of strength by excessive dilation as well as buckling of longitudinal compression reinforcement. Confining concrete columns with steel, FRP composites, or concrete jackets acts to provide support to longitudinal reinforcement and restrain the lateral expansion on the core concrete, which enables higher strains to be sustained by the compression concrete prior to failure.

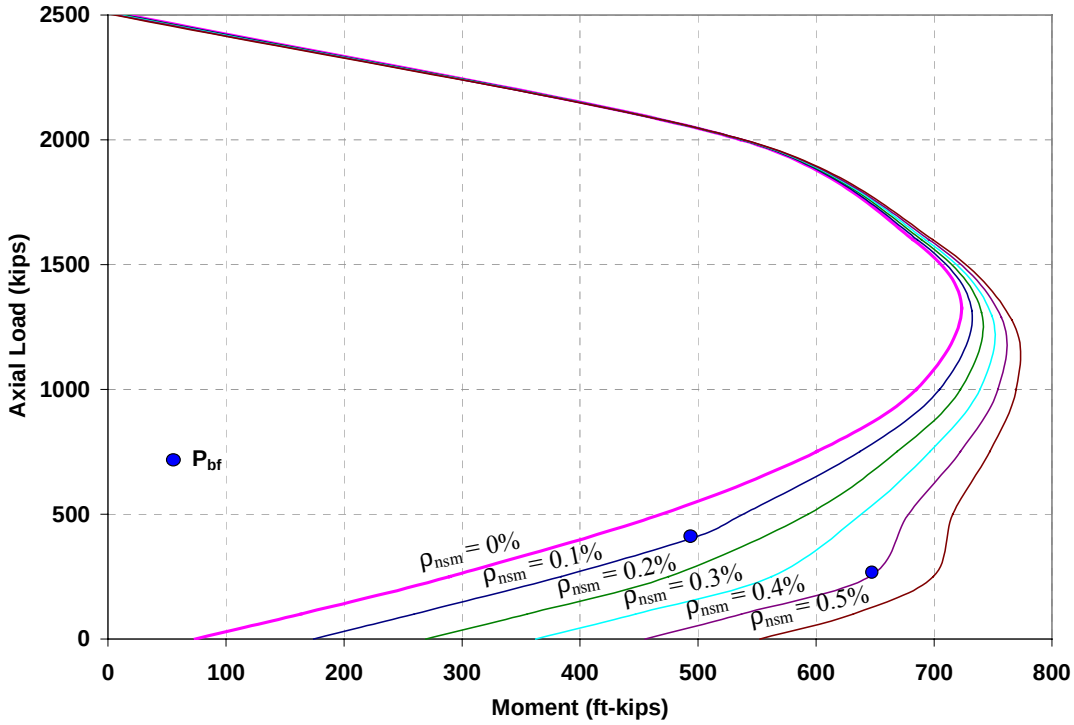


Note: 1 kip = 4.45 kN; 1 ft-kip = 1.356 kN-m

**Figure 5.1.** Theoretical axial load-moment interaction diagrams.

The effect of column confinement is therefore to increase the compression strength and the ultimate strain of concrete. For axially loaded concrete members, confinement effectiveness varies depending on the geometry of the sections. Jacketing a circular column provides it with continuous confining pressure around the circumference and results in increased concrete strength and ultimate strain. Jacketing a square column results in confining pressure that is more dominant at the corners of the section. This is because the sides of the member tend to bend outward due to lower restraint against lateral displacement, which reduces the confinement efficiency. Confining rectangular concrete section results in a small increase in strength while the ultimate strain is significantly increased (Park et al., 1982). Accordingly, fundamentally different stress-strain relationships are exhibited for circular and rectangular sections.

Depending on the geometry of the column section, improving the concrete properties with confinement may result in improved axial load and moment capacities of the column. Determining the axial load-moment interaction for a jacketed column require knowledge of the stress-strain relationship of its confined concrete. The axial load-moment interaction can then be achieved by replacing the stress-strain relationship of the unconfined concrete with that of the confined one.

Many stress-strain relationships have been developed for concrete confined with steel spirals or rectangular hoops (Vellenas et al. 1977, Park and Leslie 1977, Desayi et al. 1978, Sheikh and Uzumeri 1980, Ahmed and Shah, 1982, Dilger et al. 1984, Ahmed and Shah 1985, and Mander et al. 1988). These models are valid only when the confining pressure is provided by jackets made of materials that behave in a plastic manner, such as yielded steel. FRP jackets, on the other hand, are elastic up to failure with no plastic response and will therefore provide continuously increasing confining pressure up to the rupture of the jacket. Currently, many models that been developed for stress-strain relationships of concrete cylinders confined with FRP composites (Samaan et al. 1998, and Spoelstra and Monti 1999). However, no model was sited for rectangular sections confined with FRP composites.

Theoretical investigation of the influence of FRP jacket on the capacity of circular column indicated that this contribution is more significant when the axial load on the columns is larger than the axial load at balanced failure condition $P_b$ (MBT, 1998). This is because the contribution of the confined concrete is more apparent when the capacity is influenced by concrete properties. This usually occurs at higher axial load levels where significant portion of the member is in compression.

Giving the above-mentioned factors and knowing that most gravity piers were designed to carry a small portion of their axial capacity, it could be insinuated that FRP composite jacketing is less effective for flexural strength improvement of rectangular columns. However, jacketing with FRP composites can still improve the ductility of the columns and provide the lateral support to prevent buckling of the longitudinal reinforcement. This postulation has yet to be proven through experiments.

## 5.3. INVESTIGATION OF COLUMN CAPACITIES AND FAILURE MODES

Due to unknown and varying boundary conditions of the columns (e.g., rotational stiffness at supports and lateral resistance at the top of the column), the complete analytical load history behavior of the columns could not be achieved. Investigation of column moment capacities was accomplished by comparing the theoretical and experimental strengths of the columns. Theoretical moments were calculated using the procedure outlined in Appendix A using the material properties stipulated earlier. Experimental column strengths were calculated

using the measured reinforcement strains. At locations where plastic hinge formation was observed, the section was assumed to have developed its predicted capacity.

The main observations from experimental column tests were as follows:

- All tested columns underwent a double-curvature type of behavior.
- The high lateral failure loads indicated that frictional forces existed between the cap beams and the topping decks.
- The decks did not rotate with the cap beam and as the cap beam rotated, it pushed the topping decks upward. As a result, the location of the vertical load from the weight of the decks acting on the columns shifted closer to the cut edge of the cap beam. This resulted in an additional moment at the top of the column caused by the eccentricity of the vertical load.

### 5.3.1. Material Properties for Theoretical Predictions

Preliminary analysis of the flexural capacities of the bridge columns and the design of NSM strengthening was based on conservative material properties. Prior to applying the FRP strengthening, the elastic stiffness modulus of concrete of each column was measured using a pulse velocity tester (James Instruments V-meter MK II). Based on these tests, the actual concrete strengths for column B2P1, B2P2, B3P1, and B3P2 were found to be 4670, 6100, 5860, and 5230 psi (32, 42, 40, and 36 MPa), respectively. No coupons were obtained for laboratory verification of the strength of the steel bars. However, the strength of column steel reinforcement for comparison of theoretical and experimental column strength was assumed to be the same as that of the deck reinforcement of 43,333 psi, which was determined from laboratory testing. Since original drawings of the bridge indicated that the haunch reinforcement extended approximately 3 ft into the column from the end of the haunch, the flexural strength of a section at the top and the at column base was based on 8 #6, and 4 #6 steel bars, respectively.

### 5.3.2. Model for Column Behavior

When the end rotation of a structural column are fully restrained, its shear and bending moment diagrams due to relative lateral displacement of its ends are similar to those given in Figure 5.2. The end moments $M_a$, and $M_b$ are equal and are related to the lateral displacement $\Delta$ by $6EI\Delta/L^2$. The slope of the bending moment diagram at any load level is equal to the applied load P. When end rotations are not fully restrained, the end moments redistribute and the column end with smaller rotation (e.g., higher rotational stiffness) carries larger moment, as shown in Figure 5.3.

The internal equilibrium is always such that column shear is constant and equal to the applied load P (the slope of the moment diagram is equal to P). This is also represented by:

$$M_a + M_b = PL \tag{5.3}$$

By knowing column end moments at any load level the effective lateral force could be calculated using equation (5.3).

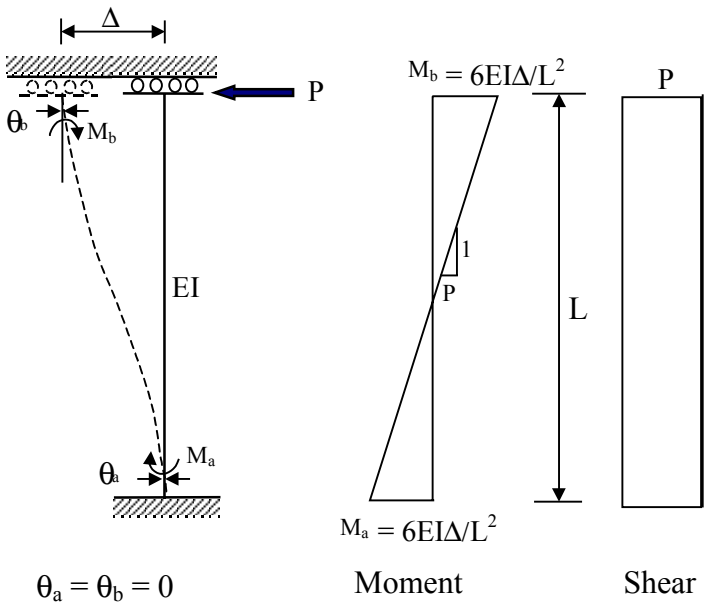


**Figure 5.2.** Theoretical moment and shear diagrams.

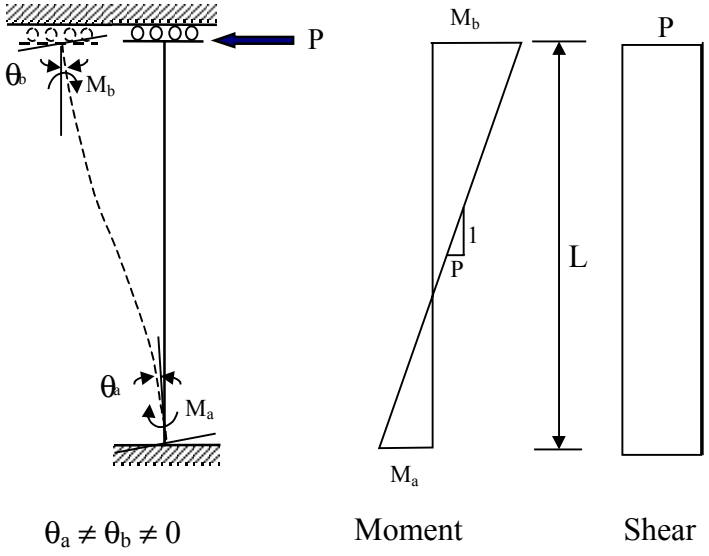


**Figure 5.3.** Theoretical moment and shear diagrams.

### 5.3.3. Bent 2

#### 5.3.3.1. Column B2P1

At the maximum load of the final loading cycle (80 kips or 356 kN), plastic hinges formed at 4 ft (1.2) from the end of the haunch and the base of the column. Knowing that the moment capacity at both locations is approximately 162 ft-k (220 kN-m) (based on 4 #6 steel

bars) and that the distance between these two locations was 7.4 ft (2.3 m), the maximum lateral load at failure was calculated as 44 kips (196 kN). These results indicate that the maximum lateral resistance due to friction was on the order of 36 kips (120 kN) at failure. Considering the axial load due to the dead weight of the deck of approximately 86 kips (385 kN), the friction coefficient at this column was 0.42. However, the actual moment capacity could be higher that the assumed one due to strain hardening of steel reinforcement.

#### 5.3.3.2. Column B2P2

At the final loading cycle (push-out), only column B2P2 was loaded and the failure of this column was achieved at 81 kips (360 kN). At failure of column B2P2, the maximum tensile and compressive strains were 1325 and –440 με, respectively. These strains correspond to a theoretical moment of 192 ft-k (260 kN-m), for which the calculated tensile and compressive FRP strains are 1330 and -428 με, respectively. The full column capacity at the column base could not be achieved because the column failed prematurely due to soil failure. The predicted strength at the base of the column was 433 ft-k (587 kN-m). This indicated that only 44 percent of the capacity of the column was developed.

Assuming that the moment at column top was approximately equal to the nominal moment capacity of 230 ft-k (312 kN-m) (based on 8 #6 steel bars) and using Equation (5.3), the applied lateral load was estimated to be 48 kips (214 kN). This indicated that lateral load resistance was approximately 33 kips (147 kN), which is comparable to that determined for column B2P1. This lateral resistance corresponded to a friction coefficient of 0.38.

### 5.3.4. Bent 3

#### 5.3.4.1. Column B3P1

Experimental results indicated that this column failed prematurely due to soil failure. Accordingly, the flexural capacity of the column could not be achieved.

#### 5.3.4.2. Column B3P2

This column was the shortest (6.5 ft or 2 m) amongst the bridge columns and its footing was cast into the bedrock. Two cracks were detected during the final loading cycle; at the top and at the base of the column, locations of maximum moments. As the load was increased, a plastic hinge formed at the top of the column and the crack started to open. Due to the large rotation of the cap beam, the vertical force caused by the weight of the deck shifted toward the edge of the cap beam, which resulted in an additional moment that acted on the column. Failure was initiated by the rupture of the FRP rods at the base of the column at a load of 86 kips (382 kN).

The maximum measured tensile CFRP rod strain at failure was 9300 με, while the measured compressive strain was approximately 2700 με. Based on this tensile strain and using a concrete strength of 5230 psi (36 MPa), the moment capacity was calculated to be 289 ft-k (392 kN-m) and corresponded to CFRP rods stress of 159 ksi (1075 MPa). This stress level of CFRP rod was larger than the design strength of 144 ksi used in strengthening design. Assuming that the moment at the top of the column at failure is equal to the nominal moment capacity of 229 ft-k (312 kN-m), the effective lateral force at failure was calculated using Equation (5.3) to be 80 kips (356 kN).

To verify this further, the effective lateral force at failure was also calculated considering the equilibrium condition, as shown in Figure 5.4. The vertical load due to the weight of the deck was assumed to act at 1 ft (0.3 m) from the edge of the cap beam. Considering moment summation at the base of the column, the lateral force was calculated as 78 kips (347 kN). These results indicated that the lateral force due to friction was in the order of 6 to 8 kips (27 to 36 kN). This value is significantly lower that those calculated for the columns of bent 2. The average lateral load resistance corresponded to an average friction coefficient of 0.08.

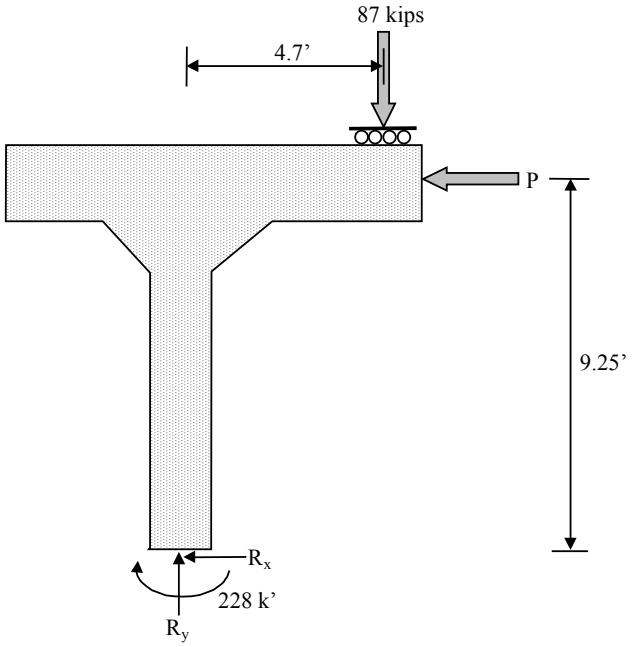


**Figure 5.4.** Equilibrium of Column B3P2 at failure.

# 6. SUMMARY, CONCLUSIONS, AND RECOMMENDATIONS

## 6.1. SUMMARY

The primary purpose for conducting this part of the research program was to verify through full scale testing the feasibility and effectiveness of near-surface mounted (NSM) composites rods for the flexural upgrade/strengthening of rectangular RC columns of gravity piers. The full-scale testing allowed for a better understanding of the performance of the strengthened system as a whole, and therefore the strengthening design requirements. The behavior of the four tested columns was different due to significantly different boundary condition (soil properties) from one column to another. This led to different failure modes that were observed during the destructive load testing, that may not be obtained in a controlled test environment. In the following, a summary of this part of the experimental program is presented.

Seismic evaluation of the bridge columns was performed based on Seismic Performance Category (SPC) B. Seismic evaluation was achieved using a simplified approach based on a single-mode response spectral method and the original geometry of the column columns. Evaluation was based on conservative material properties. Results indicated that the estimated shear capacity of the columns was adequate to resist the seismically induced shear force. The columns were found to be adequate in shear and deficient in flexure.

The initial calculations of strengthening design using NSM CFRP rods were based on conservative material properties. Prior to applying the FRP strengthening, column concrete strengths were determined by measuring their elastic stiffness modulus using a pulse velocity tester (James Instruments V-meter MK II). Due to time constraints, no steel bar coupons were obtained for laboratory verification of the steel yielding strength. The yielding strength was assumed to be the same as that for deck reinforcement, determined from laboratory testing.

Upon excavating, it was found that the columns had significantly larger lengths than provided in the original plans and each column had a different length. A column strengthening design based on the original plans would have resulted in smaller-than-desired flexural strength that would have had different lateral load capacity.

Flexural strengthening was achieved by installing near-surface mounted (NSM) CFRP rods on two opposite sides (north and south) of the columns. Two of the four bridge columns were strengthened for flexure. Column B2P2 was strengthened with 14 NSM rods mounted on two opposite sides, seven on each side. Column B3P2 was strengthened with six NSM rods, three on each side. The rods were anchored into the footings. Columns B2P2 and B3P2 were also wrapped with 4-ply CFRP jackets. Column B3P1 was externally jacketed with six plies of glass FRP sheets. The fourth column B2P1 was left unstrengthened as a benchmark. The columns were tested to failure by applying cyclic lateral loads to their cap beams.

Upgrading the bridge columns was achieved in two days with a crew of three men and without the use of heavy machinery except for the backhoe that was used to excavate around the columns. Application of the FRP materials was rapid due to the lightness of the materials.

For the purpose of testing, a 10-in (0.25 m) strip of the deck was saw-cut along the bridge axis and removed. This was done to minimize the lateral restraint at the top of the columns by allowing for the relative movement of the cap beam and the topping decks. In addition, the central portion of the cap beams was saw-cut and removed. However, this did not reduce the rotational restraint exerted by the decks on the cap beam. As a result, high moments developed at the top of the columns and a double curvature type of behavior was observed.

To reduce friction for testing of bent 3, the bridge decks were jacked up and steel plates greased with heavy-duty lubricant were installed between the deck and the cap beam.

## 6.2. CONCLUSIONS

The following conclusions were drawn based on the experimental observations and interpretation of test results.

1) The spread footing of the columns, which were initially treated as fixed supports, had different flexural capacity and stiffness and three of these footings failed due to soil failure prior to achieving the full capacity of the columns. Upgrading the columns with NSM rods, although improved the flexural capacity, caused the deficiency problem to shift to another structural component. Flexural upgrade of the columns should therefore be accompanied by a comprehensive investigation of the column joints and foundation to ensure adequate performance under improved load capacity.

2) The average friction coefficient between the cap beam and the deck slab was approximately 0.4. Friction could be minimized using assemblies of lubricated steel plates inserted between the cap beam and the topping decks.

3) The approach utilized in this study (based on equilibrium of forces and compatibility of strains) for design/analysis of RC columns strengthened with NSM CFRP rods is satisfactory. It should be noted that since compression properties of a FRP rod are inferior to its tension properties, the effect of compression reinforcement might be ignored for design and analysis purposes.

4) Column B3P2 failed due to rupture of the NSM rods. Test results indicated that the full upgraded flexural capacity was attained at the base of the column with approximately 100% increase in flexural capacity. Therefore, the use of NSM FRP technique for flexural strengthening is considered very effective for such applications.

5) Very small strains were measured on the composite jackets at failure. This indicated that these jackets did not provide significant confinement and that they had no practical contribution to flexural capacity. This was related to the small axial load carried by the columns. However, composite jackets are effective in providing lateral restraint for the NSM rods. This prevents possible instability of the rods under compression and stops splitting cracks of the grout when rods are in tension.

## 6.3. RECOMMENDATIONS FOR FUTURE RESEARCH

In addition to the recommendations regarding NSM strengthening presented in Volume I, the following are recommendations for future research derived from the experimental observations and interpretation of test results for this part of the research program.

1) The short-term behavior of NSM FRP strengthening system was experimentally evaluated. Research addressing long-term performance should be conducted even though FRP materials have demonstrated long life expectancy.

2) Upgrading with CFRP rods will improve the flexural capacity of RC columns. However, this strengthening approach may adversely influence the ductility of the upgraded column. This behavior is related to the perfectly elastic behavior of FRP bars in conjunction with the high stiffness of carbon FRP composites rods. Considering seismic design requirements, this influence may not be desirable. Glass FRP (GFRP) rods and Aramid FRP (AFRP) rods demonstrate higher strain at failure and a lower modulus than that of carbon. Columns upgraded with these materials could demonstrate better deformation behavior (e.g., larger ductility) than those upgraded with CFRP rods. Research into the behavior of RC columns upgraded with GFRP and AFRP rods is needed to verify their behavior and capacity improvement.

3) Upgrading RC columns for flexure may result in larger moment transferred to the base of the column, which is carried to the foundation system. Unless proven to be adequate to resist the additional moment, the foundation system may in turn require upgrading. Research is needed to determine the influence of the flexural upgrade of columns on the behavior and capacity of the bridge foundation system.

4) Columns upgraded with NSM rods may fail due to concrete crushing (compression failure) or FRP bars rupture (tension failure). The two failure modes are different. In addition, the ductility and capacity of an upgraded column for which failure is governed by concrete crushing could be further improved by jacketing with FRP composites. The flexural capacity and ductility improvement of such columns need to be experimentally investigated.

5) The capacity improvement of NSM upgraded columns was investigated. However, the behavior of upgraded columns may be different when subjected to dynamic loading. The reversed loading cycles may cause degradation of bond between the bonded rods and concrete, which may result in premature failure due to rods debonding or anchorage failure. The behavior of upgraded columns under dynamic loading needs to be experimentally verified.

## 7. REFERENCES


AASHTO (1996), Standard Specifications for Highway Bridges, Sixteenth Edition, American Association of State Highway and Transportation Officials, Washington D.C.

ACI Committee 440H, (2000), " Provisional Design Recommendations for Concrete Reinforced with FRP Bars," Draft Document. In print.

Ahmed, S. M. and Shah, S. P. (1982), "Stress-Strain Curves of Concrete Confined by Spiral Reinforcement," American Concrete Institute Journal, Vol. 79, No. 6, pp. 484-490.

Ahmed, S. M., and Shah, S. P. (1985), "Behavior of Hoop Confined Concrete Under High Strain Rates," American Concrete Institute Journal, Vol. 82, No. 5, pp. 634-647.

Almusallam, T.H., Al-Salloum, Y., Alsayed, S., and Amjad, M. (1997) "Behavior of Concrete Beams Doubly Reinforced by FRP Bars," Proceeding of the Third International Symposium on Non-Metallic (FRP) Reinforcement for Concrete Structures (FRPRCS-3), Japan Concrete Institute, Sapporo, Japan, V. 2, pp. 471-478.

Bazant, Z. P., and Bhat, P. D. (1977), "Prediction Hysteresis of Reinforced Concrete Members," Journal of the Structural Division, ASCE, Vol. 103, No. 1, pp. 153-167.

Desayi, P., Iyengar, K. T. S. A., and Reddy, T. S. (1978), "Equations for Stress-Strain Curve of Concrete Confined in Circular Steel Spiral," Materials and Structures, Research and Testing, Paris , France, Vol. 11, No. 65, pp. 339-345.

Dilger, W. H., Koch, R., and Kowalczyk, (1984). "Ductility of Plain and Confined Concrete Under Different Strain Rates," American Concrete Institute Journal, Vol. 81, No. 1, pp. 73-81.

Ehsani, M.R. (1993) "Glass-Fiber Reinforcing Bars," Alternative Materials for the Reinforcement and Prestressing of Concrete, J.L. Clarke, Blackie Academic & Professional, London, England, pp. 35-54.

Hakamada, F. (1997) "Experimental Study on Retrofit of RC Columns Using CFRP Sheets." Proceedings of the Third International Symposium on Non-Metallic (FRP) Reinforcement for Concrete Structures (FRPRCS-3), Japan Concrete Institute, Tokyo, Japan, Vol. 1, pp. 419-426.

Hosotani, M., Kawashima, K., and Hoshikuma J. (1996), "Stress-Strain Relationship of Concrete Wrapped in horizontal Carbon Fiber Sheets," Concrete Engineering Conference, Japan (in Japanese).

Japan Society of Civil Engineers (JSCE) (1997), "Recommendation for Design and Construction of Concrete Structures Using Continuous Fiber Reinforcing Materials," Concrete Engineering Series, No. 23, 325 pp.

Kent, D. C., and Park, R. (1971), " Flexural Members with Confined Concrete," Journal of the Structural Division, ASCE, Vol. 97, No. 7, pp. 1969-1990.

Kobayashi, K., and Fujisaki, T. (1995) "Compressive Behavior of FRP Reinforcement in Non-prestressed Concrete Members," Proceeding of the Second International RILEM Symposium on Non-Metallic (FRP) Reinforcement for Concrete Structures (FRPRCS-2), Ghent, Belgium, pp. 267-274.

Macrae, G. A., Nosho, K., Stanton, J., and Myojo, T. (1997) "Carbon Fiber Retrofit of Rectangular RC Gravity Columns in Seismic Regions," Proceedings, Third Int. Symposium on Non-Metallic (FRP) Reinforcement for Concrete Structures (FRPRCS-3), Japan Concrete Institute, Tokyo, Japan, Vol. 1, pp. 371-386.

Mallick, P.K., (1988). Fiber Reinforced Composites, Materials, Manufacturing, and Design. Marcell Dekker, Inc., New York, New York, 469 pp.

Mander, J.B., Priestly, M.J.N., and Park, R. (1988), " Observed Stress-Strain Behavior of Confined Concrete," Journal of Structural Engineering, ASCE, Vol. 114, No. 8, pp. 1827-1849.

Master Builders Technologies (MBT) (1998), MBrace Composite Strengthening System: Engineering Design Guidelines, Second Edition, Cleveland, Ohio.

MoDOT Bridge Load Rating Manual (1996), Missouri Department of Transportation, Jefferson City, Missouri, 1996, pp. 4.1-4.28.

Nanni, A. (1997), "Carbon FRP Strengthening: New Technology Becomes Mainstream," Concrete International, American Concrete Institute, Vol. 19, No. 6, June, pp. 19-23.

Naval Facilities Engineering Service Center (1998), "Navy Advanced Composite technology in Waterfront Infrastructure," Special Publication Sp-2046-SHR.

Park, R., and Leslie, P. D. (1977), "Curvature Ductility of Circular Reinforced Concrete Columns Confined by the ACI Spiral," 6th Australian Conference on the Mechanic of Structures and Materials, Vol. 1, pp. 342-349.

Park, R., Priestley, M. J. N., and Gill, W. D. (1982), "Ductility of Square-Confined Concrete columns," Journal of Structural Division, ASCE, Vol. 108, No. 4, pp. 929-950.

Park, R., Priestley, M.J.N., Gill, W.D., and Potangarao, R.T. (1980), "Ductility and Strength of Reinforced Concrete Columns with Spiral or Hoop Under Seismic Loading," Proceeding of the Seventh World Conference on Earthquake Engineering, Istanbul, Turkey.

Priestly M.J.N., Seible, F., and Chai, Y.H. (1992), "Design Guidelines for Assessment Retrofit and Repair of Bdidges for Seismic Performance," Report to the National Institute of Standards and Technology, University of California, San Diego, Report No. SSRP-92/01, 266 pp.

Priestly M.J.N., Seible, F., Verma, R., and Xiao, Y. (1993), "Seismic Shear Strengthening of Reinforced Concrete Columns," University of California, San Diego, Report No. SSRP-93/06, 120 pp.

Priestly M.J.N., Seible, F., and Calvi, G. M. (1996). Seismic Design and Retrofit of Bridges. John Wiley and Sons, Inc., New York, New Yourk. 686 pp.

Samaan M., Mirmiran A. and Shahawy M. (1998), " Model of Concrete Confined by Fiber Composites, Journal of Structural Engineering, ASCE, Vol. 124, No. 9, pp. 1827-1849.

Scott, B. D., Park, R., and Priestley, M. J. N. (1982), "Stress-Strain Behavior of Concrete Confined by Overlapping Hoops at Low and High Strain Rates," American Concrete Institute Journal, Vol. 79, No. 1, pp. 13-27.

Seible, F., Hehemier, G.A., Priestly M.J.N., Innamorato, D. and Ho, F. (1995), "Carbon Fiber Jacket Retrofit Test of Rectangular Flexural Column with lap Spliced Reinforcement," Advanced Composites Technology Transfer Consortium Report No. ACTT-95/02UCSD, 53 pp.

Seible, F. and Innamorato, D (1995), "Earthquake Retrofit of Bridge Columns with Continuous Carbon Fiber Jackets," Report to Caltrans, Division of Structures, La Jolla, CA, 56 pp.

Sheikh, S.A., and Uzumeri, S.M. (1980), "Strength and Ductility of Tied Concrete Columns," Proceedings, ASCE, V. 106, ST5, pp. 1079-1102.

Spoelstra M. R. and Monti, G., (1999) "FRP-Confined Concrete Model," Journal of Composites for Construction, ASCE, Vol. 3, No. 3, pp. 143-150.

Todeschini, C., Bianchini, A. C., and Kesler, C. E. (1964), "Behavior of Concrete Columns Reinforced with High Strength Steels," ACI Journal, Proceeding, Vol. 61, No. 6, pp. 701-716.

Vellenas, J., Bertero, V. V., and Popov, E. P. (1977), " Concrete Confined by Rectangular Hoops Subjected to Axial Loads," Report 77/13, Earthquake Engineering Research Center, University of California, Berkeley, California.

Whitman, R.V. (1987) "Thought Re Seismic Building Code Requirements for ENAM," Proceedings: Symposium on Seismic Hazard, Ground Motion, Soil-Liquefaction and Engineering Practice in Eastern North America, technical report NCEER-87-0025, State University of New York at Buffalo, pp. 70-79.

Wu, Wei-Pin (1990), "Thermomechanical Properties of Fiber Reinforced Plastics (FRP) Bars," Ph.D. dissertation, West Virginia University, Morgantown, West Virginia, 292 pp.

Yan, X. (1999). Constructability and Performance of Concrete members Prestressed with CFRP Tendons. Master thesis, University of Missouri-Rolla, Rolla, Missouri.

# APPENDIX A:

DESIGN OF NSM FLEXURAL STRENGTHENING

**Conversion factors**
1 in. =25.4 mm
1 in./in. =1 mm/mm
1 $in^2$ = 645 $mm^2$
1 kip = 4.45 kN
1 psi = 6.895E-3 MPa
1 ksi = 6.895 MPa
1 ft-k/ft = 4.45 kN-m/m

**RC MEMBER UNDER AXIAL LOAD AND BENDING**

The approach discussed hereafter is used to determine the bending moment capacity of RC members strengthened with NSM FRP rods that are subjected to axial load. The strengthening design approach is based on iteration procedure in which a concrete strain at failure is first assumed and the depth of neutral axis is determined by trial and error. The design approach follows the basic assumptions given in Chapter 6 of Volume I. Figure A.1 shows the strain compatibility and force equilibrium conditions used in the design.

Strengthening design is achieved as follows:

1) Assume concrete strain at failure, $\varepsilon_c$
2) The parameters that define the equivalent stress block can be derived using any of the concrete stress-strain relationships available in literature. Using the known parabolic equation, these parameters can be derived as follows.

$$\beta_1 = \frac{4\varepsilon'_c - \varepsilon_c}{6\varepsilon'_c - 2\varepsilon_c} \qquad \text{(A-1)}$$

$$\alpha_1 = \frac{3\varepsilon'_c\varepsilon_c - \varepsilon_c^{\,2}}{3\beta_{1c}\varepsilon'^{\,2}_c} \qquad \text{(A-2)}$$

In which $\varepsilon'_s$ is the concrete strain at peak stress, $f'_c$, is defined as follows (Todeschini et al., 1982):

$$\varepsilon'_c = \frac{1.71\, f'_c}{E_c} \qquad \text{(A-3)}$$

3) The strain of steel and FRP reinforcement are determined utilizing compatibility of the section as follows:

$$\varepsilon_s = \varepsilon_c \frac{d - c}{c} \qquad \text{(A-4)}$$

$$\varepsilon'_s = \varepsilon_c \frac{c - d'}{c} \qquad \text{(A-5)}$$

$$\varepsilon_f = \varepsilon_c \frac{d_n - c}{c} \qquad \text{(A-6)}$$

$$\varepsilon'_f = \varepsilon_c \frac{c - d_n'}{c} \quad \text{(A-7)}$$

4) The stress of steel and FRP reinforcement is determined from the constitutive laws of the materials, as follows:

$$f_s = E_s \varepsilon_s \le f_y \quad \text{(A-8)}$$

$$f'_s = E_s \varepsilon'_s \le f_y \quad \text{(A-9)}$$

$$f_f = E_f \varepsilon_f \le f_{fy} \quad \text{(A-10)}$$

$$f'_f = E_f \varepsilon'_f \le f_{fy} \quad \text{(A-11)}$$

5) The depth is then determined utilizing equilibrium and accounting for the axial load, P, as follows:

$$c = \frac{P + A_s f_s - A'_s f'_s + A_f f_f - A'_s f'_f}{\alpha_1 \beta_1 f'_c b} \quad \text{(A-12)}$$

6) For symmetrically reinforced section (as in the current case), this latest equation can be simplified to the following:

$$c = \frac{P + A_s (f_s - f'_s) + A_f (f_f - f'_f)}{\alpha_1 \beta_1 f'_c b} \quad \text{(A-13)}$$

7) If the calculated value of the neutral axis, c, does not match the assumed one, another value is assumed and the process is continued until the two values converge. The moment capacity of the section is determined as follows:

$$M = \alpha_1 f'_c \beta_1 cb\left(\frac{h}{2} - \frac{\beta_1 c}{2}\right) + A'_s f'_s \left(\frac{h}{2} - d'\right) + A_s f_s \left(d - \frac{h}{2}\right) + A'_f f'_f \left(\frac{h}{2} - d'_n\right) + A_f f_f \left(\frac{h}{2} - d'_n\right)$$

8) A final check can be made to ensure equilibrium of forces as follows:

$$P = \alpha_1 f'_c \beta_1 cb + A'_s f'_s + A_s f_s + A'_f f'_f + A_f f_f \quad \text{(A-15)}$$

Based on this approach the strengthening design of the bridge piers is determined considering two cased: the first using 3 CFRP rods mounted on each side of the pier and the second based on 7 CFRP rods mounted an each side of the column. Previous laboratory testing of the carbon rods indicated the strength of the rods varies between 144 and 183 ksi (993 and 1262 MPa). Both limits were considered in the strengthening design.

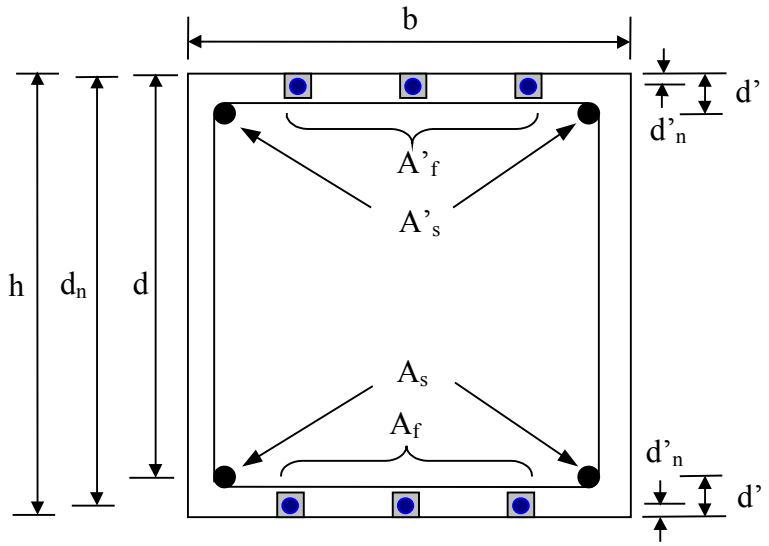


(a) details of cross-section

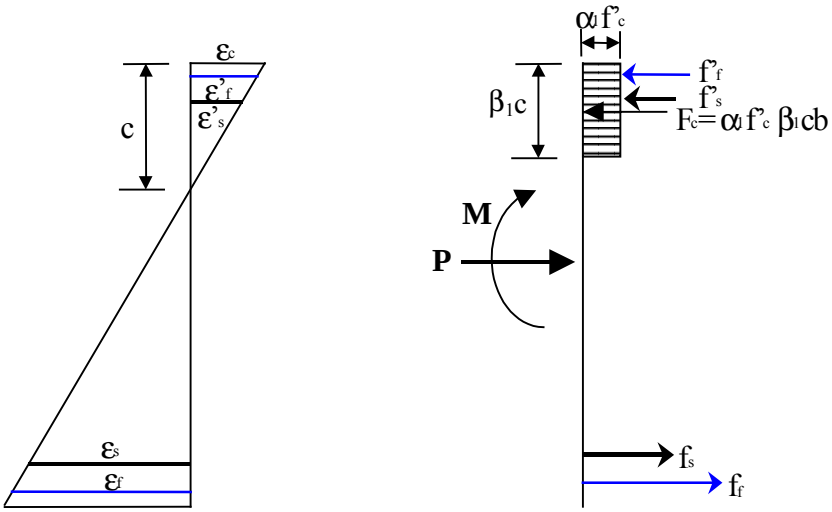


(b) strain compatibility (c) force equilibrium

**Figure A.1.** Strain and stress condition of RC section strengthened with NSM FRP rods.

Case 1: 3 CFRP rods on two opposite sides of the pier

The sectional and material properties considered next are listed below.

| | | | |
|---|---|---|---|
| H | = | 24 | in. |
| b | = | 24 | in. |
| d | = | 22 | in. |
| d’ | = | 2 | in. |
| $d_n$ | = | 23.5 | in. |
| $d'_n$ | = | 0.5 | $in^2$ |
| $f'_c$ | = | 2500 | psi |
| $A_s$ | = | 0.88 | $in^2$ |
| $A'_s$ | = | 0.88 | $in^2$ |
| $f_y$ | = | 33 | ksi |
| $E_s$ | = | 29 | ksi |
| $A_f$ | = | 0.45 | $in^2$ |
| $A'_f$ | = | 0.45 | $in^2$ |
| $f_{fu}$ | = | 144 | ksi |
| $E_f$ | = | 17.2 | ksi |

After few iterations, assume $\varepsilon_c$ = **0.00168**

$$\beta_1 = \frac{4*0.0015 - 0.00168}{6*0.0015 - 2*0.00168} = 0.766$$

$$\alpha_1 = \frac{3*0.0015*0.00168 - 0.00168^2}{3*0.766*0.0015^2} = 0.916$$

Assuming c = **4.03** in., the strain and stress of steel and FRP reinforcement are determined as follows:

$$\varepsilon_f = 0.00168 * \frac{23.5 - 4.03}{4.03} = 0.0084$$

$$f_f = 17200 * 0.0084 \le 183 = 144$$

$$\varepsilon'_f = 0.00168 * \frac{4.03 - 0.5}{4.03} = 0.0015$$

$$f'_f = 17200 * 0.0015 \le 183000 = 0.0$$

$$\varepsilon_s = 0.00168 * \frac{22 - 4.03}{4.03} = 0.0077$$

$$f_s = 29000 * 0.0077 \le 33 \qquad = 33$$

$$\varepsilon'_s = 0.00168 * \frac{4.03 - 2}{4.03} \qquad = 0.00087$$

$$f'_s = 29000 * 0.00087 \le 33000 \qquad = 25.3$$

These results indicate that the stress in FRP reaches its ultimate strength before the concrete. Failure is, therefore, governed by the rupture of FRP reinforcement.
For P = 100 kips, the depth of neutral axis is determine as follows:

$$c = \frac{100 + 0.88(33.00 - 25.3) + 0.45(144 - 0)}{0.921 * 0.771 * 2500 * 24} \qquad = 4.03$$

Which is the same as the assumed value of 4.03 in. The moment capacity is determined as follows:

$$M_n = \begin{array}{l} 0.921 * 2500 * 0.771 * 4.03 * 24(24/2 - 0.771 * 4.03/2) + 0.88 * 25.3(24/2 - 2) \\ + 0.88 * 33.00(22 - 24/2) + 0.45 * 144(24/2 - 0.5) \end{array}$$

$M_n$ = 254 ft-k

Case 2: 7 CFRP rods on two opposite sides of the pier

In this case $A_f = A'_f = 1.05$ in$^2$. The sectional and material properties are the same as those considered earlier. Using the same approach outlined earlier, the results of the strengthening designs are as follows:

**Table A.1.** Results of Strengthening Design Using 7 NSM CFRP Rods.

| $\varepsilon_c$ | $f_f$ | $f_f'$ | $f_s$ | $f_s'$ | c | $M_n$ |
|---|---|---|---|---|---|---|
| 0.00273 | 144 | 0.0 | 33.00 | 33.00 | 5.78 | 393 |

# APPENDIX B:

STRAIN GAGE LOCATIONS FOR STRENGTHENED COLUMNS

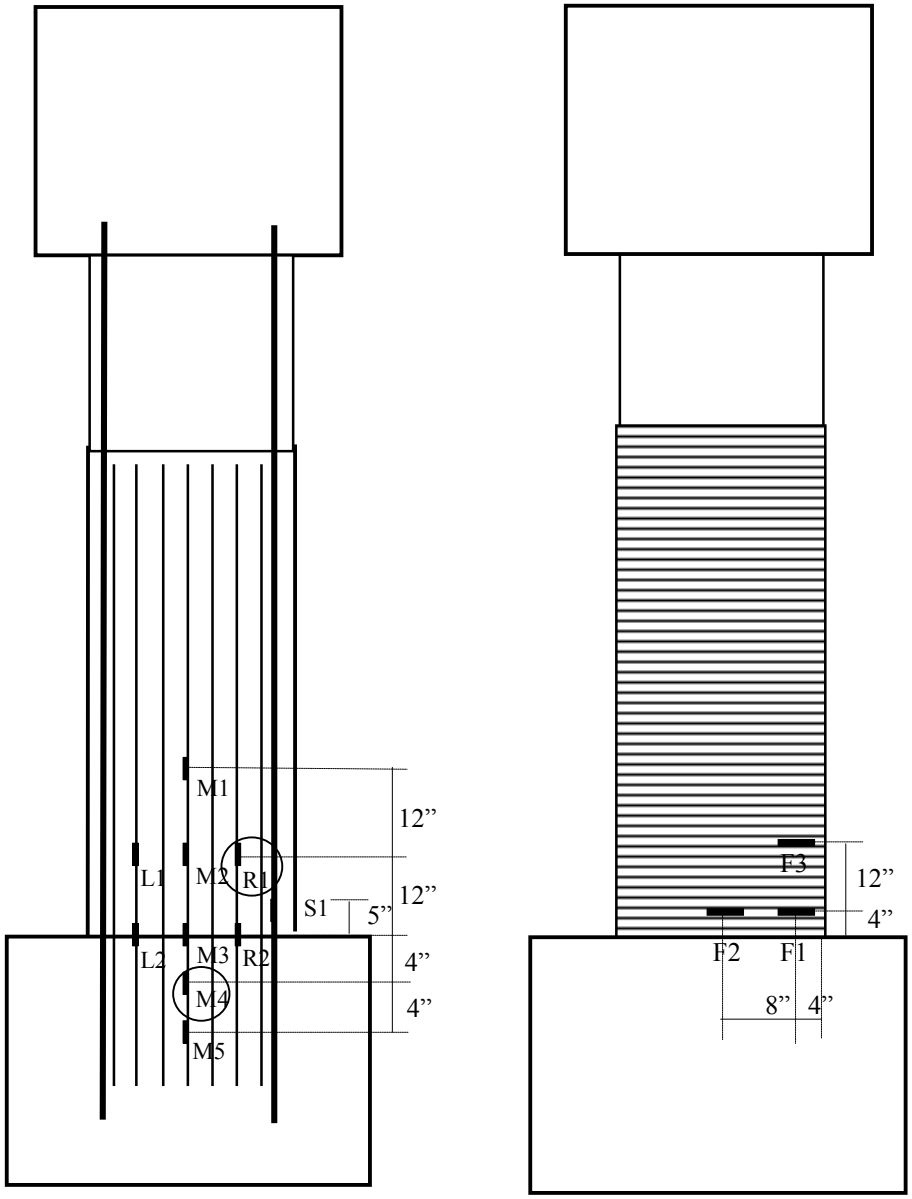


(a) Strain gages on steel and FRP

(b) Strain gages on FRP Jacket

**Figure B.1.** Strain gages on the north side of column B2P2.

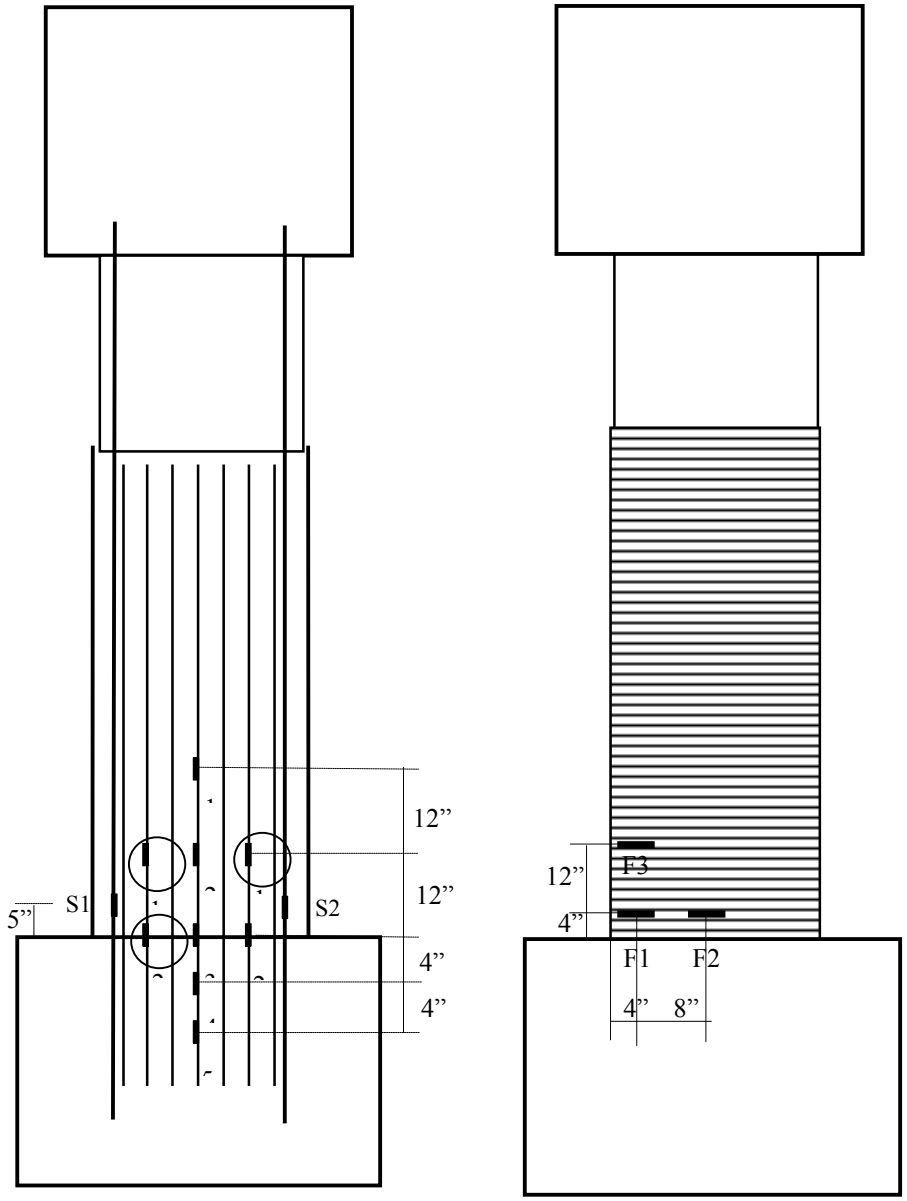


(a) Strain gages on steel and FRP (b) Strain gages on FRP Jacket

**Figure B.2.** Strain gages on the south side of column B2P2.

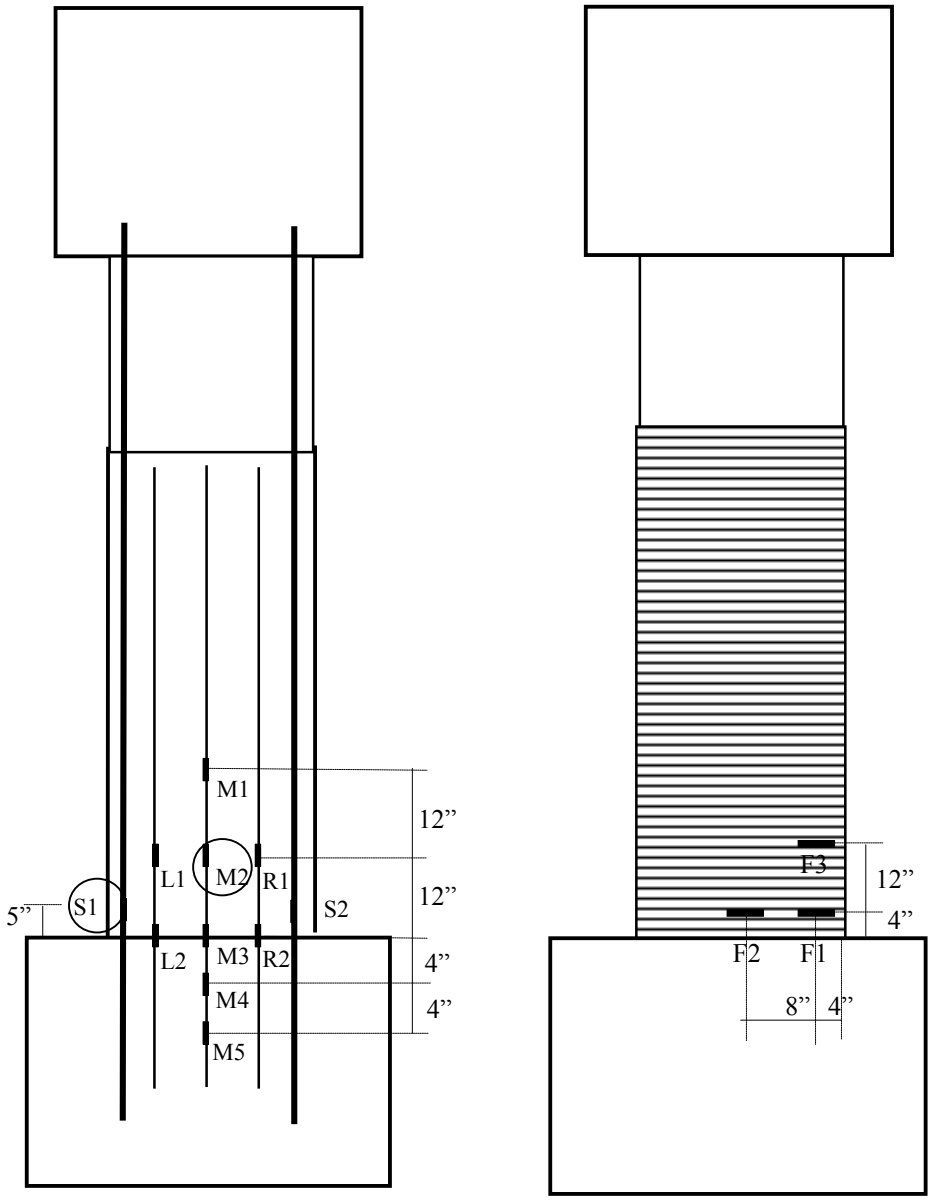


(a) Strain gages on steel and FRP

(b) Strain gages on FRP Jacket

**Figure B.3.** Strain gages on the north side of column B3P2.

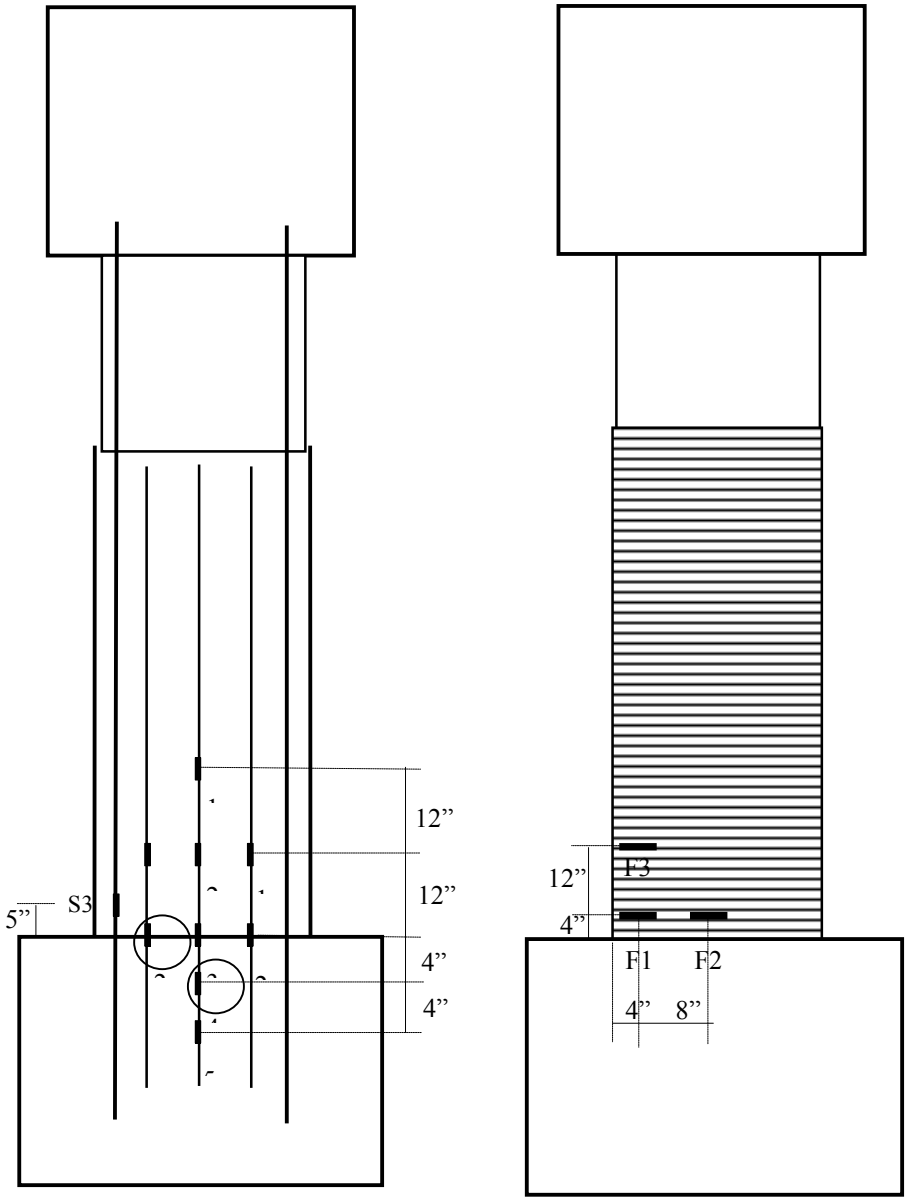


(a) Strain gages on Steel and FRP (b) Strain gages on FRP Jacket

**Figure B.4.** Strain gages on the south side of column B3P2.

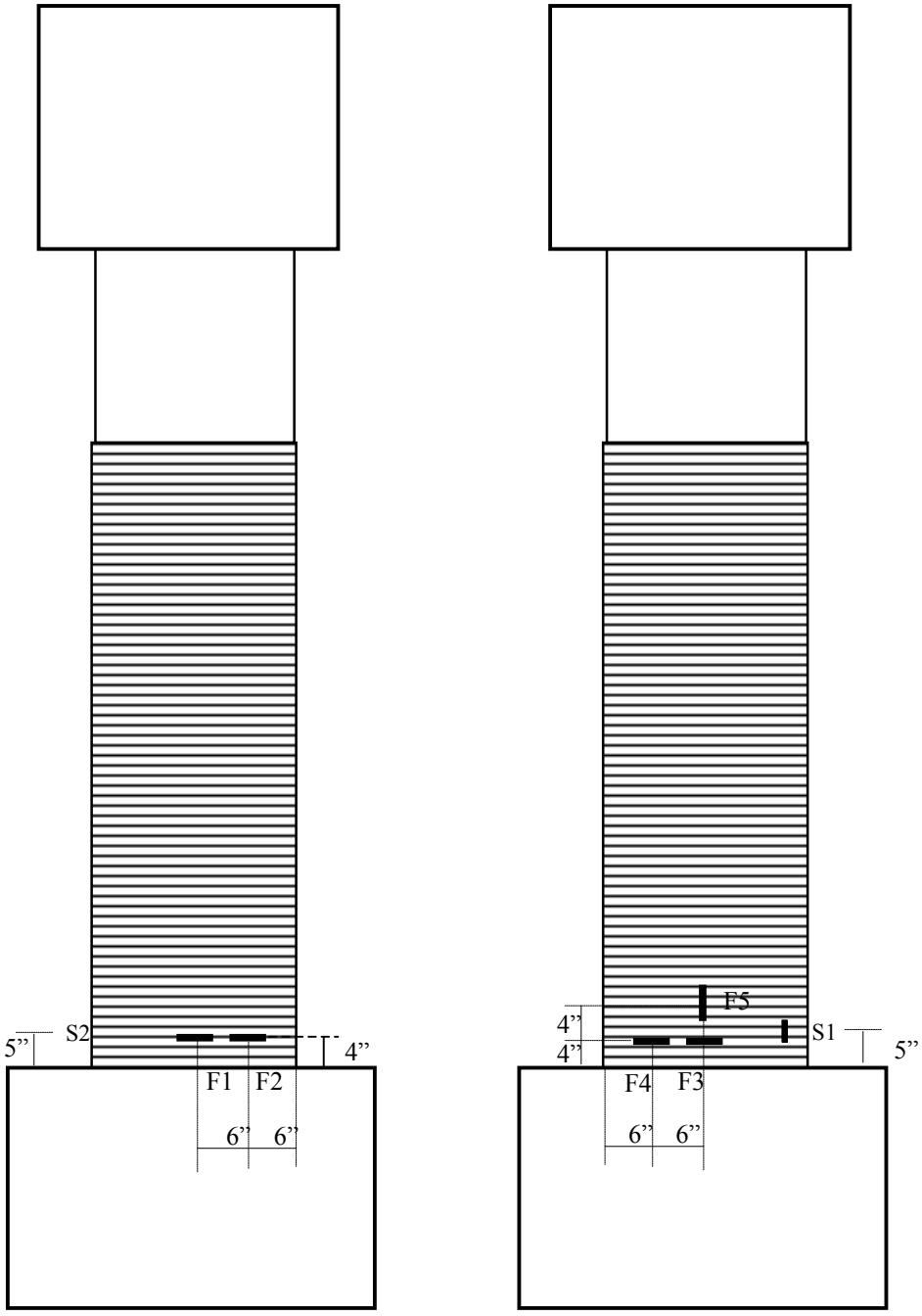


(a) Strain gages on the north side

(b) Strain gages on the south side

**Figure B.5.** Strain gages on column B3P1.